




2018

DESIGN, SYNTHESIS AND BIOLOGICAL EVALUATION OF INHIBITORS AGAINST BOTH HUMAN AND MOUSE MICROSOMAL PROSTAGLANDIN E₂ SYNTHASE-1 ENZYMES

Kai Ding

University of Kentucky, kai.adrian.ding@gmail.com

Author ORCID Identifier:

 <https://orcid.org/0000-0002-5216-669X>

Digital Object Identifier: <https://doi.org/10.13023/etd.2018.395>

[Right click to open a feedback form in a new tab to let us know how this document benefits you.](#)

Recommended Citation

Ding, Kai, "DESIGN, SYNTHESIS AND BIOLOGICAL EVALUATION OF INHIBITORS AGAINST BOTH HUMAN AND MOUSE MICROSOMAL PROSTAGLANDIN E₂ SYNTHASE-1 ENZYMES" (2018). *Theses and Dissertations--Chemistry*. 102.

https://uknowledge.uky.edu/chemistry_etds/102

This Doctoral Dissertation is brought to you for free and open access by the Chemistry at UKnowledge. It has been accepted for inclusion in Theses and Dissertations--Chemistry by an authorized administrator of UKnowledge. For more information, please contact UKnowledge@lsv.uky.edu.

STUDENT AGREEMENT:

I represent that my thesis or dissertation and abstract are my original work. Proper attribution has been given to all outside sources. I understand that I am solely responsible for obtaining any needed copyright permissions. I have obtained needed written permission statement(s) from the owner(s) of each third-party copyrighted matter to be included in my work, allowing electronic distribution (if such use is not permitted by the fair use doctrine) which will be submitted to UKnowledge as Additional File.

I hereby grant to The University of Kentucky and its agents the irrevocable, non-exclusive, and royalty-free license to archive and make accessible my work in whole or in part in all forms of media, now or hereafter known. I agree that the document mentioned above may be made available immediately for worldwide access unless an embargo applies.

I retain all other ownership rights to the copyright of my work. I also retain the right to use in future works (such as articles or books) all or part of my work. I understand that I am free to register the copyright to my work.

REVIEW, APPROVAL AND ACCEPTANCE

The document mentioned above has been reviewed and accepted by the student's advisor, on behalf of the advisory committee, and by the Director of Graduate Studies (DGS), on behalf of the program; we verify that this is the final, approved version of the student's thesis including all changes required by the advisory committee. The undersigned agree to abide by the statements above.

Kai Ding, Student

Dr. Dong-Sheng Yang, Major Professor

Dr. Mark Lovell, Director of Graduate Studies

DESIGN, SYNTHESIS AND BIOLOGICAL EVALUATION OF INHIBITORS
AGAINST BOTH HUMAN AND MOUSE MICROSOMAL PROSTAGLANDIN E₂
SYNTHASE-1 ENZYMES

DISSERTATION

A dissertation submitted in partial fulfillment of the
requirements for the degree of Doctor of Philosophy in the
College of Arts and Sciences
at the University of Kentucky

By

Kai Ding

Lexington, Kentucky

Co- Directors: Dr. Dong-Sheng Yang, Professor of Chemistry
and Dr. Chang-Guo Zhan, Professor of Pharmaceutical Sciences

Lexington, Kentucky

2018

Copyright © Kai Ding 2018
<https://orcid.org/0000-0002-5216-669X>

ABSTRACT OF DISSERTATION

DESIGN, SYNTHESIS AND BIOLOGICAL EVALUATION OF INHIBITORS AGAINST BOTH HUMAN AND MOUSE MICROSOMAL PROSTAGLANDIN E₂ SYNTHASE-1 ENZYMES

As the principal pro-inflammatory prostanoid, prostaglandin E₂ (PGE₂) serves as mediator of pain and fever in inflammatory reactions. The biosynthesis of PGE₂ starts from arachidonic acid (AA). Cyclooxygenase (COX)-1 and/or COX-2 converts AA to prostaglandin H₂ (PGH₂), and PGE₂ synthases transform PGH₂ to PGE₂. Current mainstream approach for treating inflammation-related symptoms remains the application of traditional non-steroidal anti-inflammatory drugs (tNSAIDs) and selective COX-2 inhibitors (coxibs). As both categories shut down the biosynthesis of all downstream prostanoids, their application renders several deleterious effects including gastrointestinal ulceration and cardiovascular risk. Microsomal prostaglandin E₂ synthase-1 (mPGES-1) inhibitors, specifically blocking the production of inflammation-related PGE₂, are expected to reduce the adverse effects while retain the anti-inflammation activity. Although several compounds have been reported, only a few have entered clinical trials and none was on the market. Particularly, most of the reported human mPGES-1 inhibitors were not active for wild-type mouse/rat mPGES-1 enzymes, which prevents using the well-established mouse/rat models of inflammation in preclinical studies. Therefore, we expect our designed inhibitors to also be potent against mouse mPGES-1 and thus is suitable for preclinical testing in wild-type mice.

KEYWORDS: anti-inflammatory drugs, mPGES-1 inhibitors, selectivity, isatin derivatives, benzyldenebarbituric acid, carrageenan air-pouch.

Kai Ding

10/15/2018

Date

DESIGN, SYNTHESIS AND BIOLOGICAL EVALUATION OF INHIBITORS
AGAINST BOTH HUMAN AND MOUSE MICROSOMAL PROSTAGLANDIN
E₂ SYNTHASE-1 ENZYMES

By
Kai Ding

Dr. Dong-Sheng Yang

Co-Director of Dissertation

Dr. Chang-Guo Zhan

Co-Director of Dissertation

Dr. Mark Lovell

Director of Graduate Studies

10/15/2018

Date

DEDICATION

To my wife Ms. Li-Jun Shen and daughter Beiyuan Breanna Ding.

ACKNOWLEDGMENTS

I would like to express my appreciation to Dr. Dong-Sheng Yang (director of my graduate studies in the Ph.D. program of chemistry) at Department of Chemistry and Dr. Chang-Guo Zhan (co-director of my graduate studies in the Ph.D. program of chemistry and my Ph.D. thesis research advisor) at Department of Pharmaceutical Sciences. They gave me valuable suggestions in taking courses, conducting research projects and writing manuscripts for publication. Moreover, they set good examples of scientists. Their dedication to science and great passion for their research will always be a precious treasure for me. In addition, I sincerely appreciate my other committee members Drs. Robert Grossman and Yinan Wei, and my outside examiner Dr. Charles Loftin, for keeping tracking my research progress, sharing their knowledge and experience and proofreading my dissertation.

My current group members, graduate students Shuo Zhou, Xirong Zheng, Ting Zhang, Kyungbo Kim, Yingting Cai, Huimei Wei, Jing Deng and Alex Williams, postdocs Drs. Jianzhong Chen, Zhenyu Jin and Chunhui Zhang, provided me a lot of help and create an excellent environment for everyday work. I also need to thank former group members who also actively participated in my research projects. They are Drs. Yaxia Yuan, Ziyuan Zhou, Shurong Hou, Xiabin Chen, Lei Fang, Jianzhuang Yao, Yuxin Zhang, Adel Hamza, Xiaoqin Huang, Yan Qiao, Aibin Wu, and Wenpeng Cui, Mr. Haifeng Huang and Mr. Xiaozhi Yang.

I am deeply grateful to Dr. Hsin-Hsiung Tai for providing protocol and materials of PGE₂ quantitative assays, Dr. Sean Parkin for single-crystal diffraction study and Dr.

Yonsoo Bae for formulation development. I also have to thank ladies and gentlemen working for Department of Chemistry, Department of Pharmaceutical Sciences and UK Division of Laboratory Animal Resources (DLAR). Their efforts helped building a friendly climate suitable for learning and research.

I would like to thank the National Science Foundation, the National Institute of Health, and Molecular Modeling and Biopharmaceutical Center (MMBC) at UK College of Pharmacy for the financial supporting of my research projects. I also acknowledge the Computer Center at University of Kentucky for supercomputing time on a Dell Supercomputer Cluster consisting of 338 nodes or 4,816 processors.

Last but not least, I would like to extend my deepest gratitude to my parents, Mr. Jianqiu Ding and Ms. Yasu Dai couple, Mr. Rong-Gen Shen and Ms. Shui-Juan Shen couple, my wife Lijun Shen, and my daughter Beiyuan Breanna Ding. The greatest love they give me is the most important thing I possess.

TABLE OF CONTENTS

ACKNOWLEDGMENTS	iii
LIST OF TABLES	x
LIST OF FIGURES	xi
LIST OF SCHEMES.....	xiii
LIST OF ABBREVIATIONS	xiv
Chapter 1 Introduction	1
1.1 Prostaglandin E ₂ : mediator in inflammation	1
1.2 The biosynthetic pathway of PGE ₂	1
1.3 Anti-inflammatory strategies.....	3
1.3.1 Traditional non-steroidal anti-inflammatory drugs (tNSAIDs)	3
1.3.2 Coxibs	3
1.3.3 Potent mPGES-1 inhibitors.....	4
1.4 Structure of mPGES-1.....	6
1.5 Recent progress in the development of potent mPGES-1 inhibitors.....	8
1.5.1 Early unselective inhibitors.....	8
1.5.2 MK-886, MF-63 and their analogs by Merck.....	9
1.5.3 Oxicam and benzoxazole derivatives by Pfizer	11
1.5.4 Dual mPGES-1/5-LO inhibitors	12
1.5.5 Inhibitors discovered by virtual screening.....	14

1.5.6	Other synthetic compounds as potent mPGES-1 inhibitors.....	14
1.5.7	Natural products as potent mPGES-1 inhibitors.....	16
1.6	Summary	17
Chapter 2 Structure-based discovery of substituted benzylidenebarbituric acid derivatives as mPGES-1 inhibitors suitable for preclinical testing in wild-type mice.....		
2.1	mPGES-1 as a more promising anti-inflammation target	19
2.2	Design of dual inhibitors of human and mouse mPGES-1 enzymes	20
2.3	Chemistry and SAR study	23
2.3.1	SAR on the central benzene ring	23
2.3.2	SAR on the barbituric acid moiety.....	25
2.3.3	SAR on the side chain.....	26
2.4	<i>In vitro</i> activities and selectivity	28
2.5	Enzyme-inhibitor binding modes	30
2.6	<i>In vivo</i> anti-inflammatory activity.....	33
2.7	Acute toxicity/safety of 25b	34
2.8	Conclusion.....	35
Chapter 3 (Z)-5-(2-oxoindolin-3-ylidene)thiazolidine-2,4-dione derivatives as potent inhibitors against both human and mouse mPGES-1 enzymes: rational design, synthesis, <i>in vitro</i> assays and <i>in vivo</i> evaluation.....		
3.1	Dual human/mouse mPGES-1 inhibitors enabling preclinical testing in wild-type mice	38

3.2	Design of the (Z)-5-(2-oxoindolin-3-ylidene)thiazolidine-2,4-dione (isati-thiazolidine-2,4-dione backbone) derivatives	39
3.3	Chemistry and SAR study	40
3.3.1	SAR on 1-substituted isatin derivatives	40
3.3.2	SAR on 1,5-disubstituted isatin derivatives	44
3.4	Structural analysis	46
3.5	<i>In vitro</i> assays	47
3.6	Enzyme-inhibitor binding modes	48
3.7	<i>In vivo</i> anti-inflammatory efficacy	50
3.8	Conclusions	52
Chapter 4 Experimental Section		54
4.1	Computational studies	54
4.1.1	Trimer structure of human mPGES-1	54
4.1.2	Trimer structure of mouse mPGES-1	54
4.1.3	Molecular docking	54
4.2	Chemistry	55
4.2.1	General	55
4.2.2	Preparation of tosylates 23 and 35	55
4.2.3	Preparation of the chlorides 32a–32c	56
4.2.4	Preparation of the aldehyde intermediates 24a–24q, 30, 33a–33c and 36a–	

4.2.5	Preparation of the benzylidenenbarbituric acid derivatives 25a–25q, 27a–27c, 29a–29c, 31, 34a–34c and 37a–37f.....	66
4.2.6	Preparation of 2-(2,4-dioxothiazolidin-3-yl)acetic acid (40).....	80
4.2.7	Preparation of 1-substituted isatins 43a–43m.....	81
4.2.8	Preparation of (Z)-5-(2-oxoindolin-3-ylidene)thiazolidine-2,4-dione derivatives 42 and 44a–44m.....	87
4.2.9	Preparation of 2-(2,3-dioxoindolin-1-yl)acetic acid (46) from isatin (41) .	95
4.2.10	Preparation of N-substituted thiazolidine-2,4-dione 47a–47b.....	96
4.2.11	Preparation of (Z)-5-(2-oxoindolin-3-ylidene)thiazolidine-2,4-dione derivatives 48a–48b.....	97
4.2.12	Preparation of 1,5-disubstituted isatins (50, 54a–54d) through N-substitution	99
4.2.13	Preparation of 1,5-disubstituted isatins (51a–51e and 53) through Suzuki and Sonogashira coupling.....	101
4.2.14	Preparation of (Z)-5-(2-oxoindolin-3-ylidene)thiazolidine-2,4-dione derivatives 52a–52e, 54 and 55a–55d.....	105
4.2.15	Preparation of the meglumine salt of 52e (52e-MEG).....	110
4.3	Crystallographic studies.....	111
4.4	<i>In vitro</i> experimental tests.....	112
4.4.1	Preparation of mPGES-1 enzymes.....	112

4.4.2	Activity assays using a recombinant mPGES-1.....	113
4.4.3	Activity assays of COX-1/2.....	113
4.5	<i>In vivo experiments</i>	113
4.5.1	Animals.....	113
4.5.2	Wild-type mice based air-pouch model of inflammation	114
Chapter 5 Concluding Remarks		115
5.1	Overall conclusion.....	115
5.2	Future directions.....	115
References.....		117
Vita.....		123

LIST OF TABLES

Table 2-1. Variation on the Central Benzene Ring.....	24
Table 2-2. SAR on the barbituric acid moiety.....	26
Table 2-3. SAR on the aliphatic side chain.....	28
Table 2-4. Inhibition against COX-1/2 of selected compounds.....	30
Table 3-1. SAR on 1-Substituted isatin derivatives.....	42
Table 3-2. SAR on 1,5-Diubstituted isatin derivatives.....	45
Table 3-3. Inhibition against COX-1/2 of selected compounds.....	48
Table 4-1. Crystallographic data for compound 42.....	111

LIST OF FIGURES

Fig. 1-1. Structures of selected tNSAIDs: ibuprofen and indomethacin.	3
Fig. 1-2. Structures of selected coxibs: celecoxib and rofecoxib.	4
Fig. 1-3. Unselective mPGES-1 inhibitors.	9
Fig. 1-4. MK-886 and structurally related indole-2-proponionic acid derivatives.	10
Fig. 1-5. Molecular structures of the lead azaphenanthrenone, designed inhibitor MF-63 and structurally related inhibitors 3–5.	11
Fig. 1-6. The molecular structures of compound derived from oxicam template 6, benzoxazole derivatives PF-0469362, and 7–8.	12
Fig. 1-7. Molecular structures of dual mPGES-1/5-LO inhibitors: benzo[g]indol-3-carboxylate derivative 9, triazole-based compound 10, indomethacin derivative 11 and lonazolac derivative 12.	13
Fig. 1-8. Structures of compounds 13–14 identified from virtual screening.	14
Fig. 1-9. Structures of carbazole derivative AF-3442, imidazolequinoline derivative 15, dihydropyrimidin-2(1 <i>H</i>)-one derivative 16–17 and pyrazolone derivative 18.	15
Fig. 1-10. Structures of natural products active against human mPGES-1 enzyme: curcumin, mytucommulone, garcinol, hyperforin and arzanol.	17
Fig. 2-1. Molecular structures of ligand structure 19, scaffold structures 20–21, and their binding with human mPGES-1. (A) Ligand structures; (B) binding with the lead 19; (C) binding complex (B) with surface representation of human mPGES-1; (D) binding with 20; (E) binding with 21.	22
Fig. 2-2. Concentration-dependent curves of compound 25b against human and mouse mPGES-1 enzymes. (A) Concentration-dependent inhibition of human mPGES-1 (n = 3); (B) Concentration-dependent inhibition of mouse mPGES-1 (n = 3).	29
Fig. 2-3. Molecular structures of 25b and MF63 and their binding with human and mouse mPGES-1 enzymes. (A) Ligand structures of 25b and MF63; (B) binding of 25b with human mPGES-1; (C) binding of 25b with mouse mPGES-1; (D) binding of MF63 with human mPGES-1; (E) hypothetical binding structure of mouse mPGES-1 with MF63 after human mPGES-1 structure in panel D is replaced by mouse mPGES-1 structure.	32
Fig. 2-4. Data from <i>in vivo</i> assays using the mouse carrageenan air-pouch model of inflammation (n = 4 each group) with 25b or celecoxib dosed orally. (A) the effectiveness of 25b in reducing PGE ₂ level in air-pouch fluid; (B) the effectiveness of 25b in reducing PGE ₂ level in kidney (assayed for PGE ₂ by ELISA and expressed as Mean ± SEM). Statistical results from the one-way ANOVA analysis of the data in panel A with post hoc tests: <i>p</i> = 0.0003 for Vehicle Control vs 20 mg/kg 25b (p.o., bid); <i>p</i> < 0.0001 for Vehicle Control vs 10 mg/kg 25b (p.o., bid); and <i>p</i> < 0.0001 for Vehicle Control vs 50 mg/kg celecoxib (p.o., pid). Statistical results from the one-way ANOVA analysis of the data in panel A with post hoc tests: <i>p</i> < 0.0001 for Vehicle Control vs 20 mg/kg 25b (p.o., bid); <i>p</i> < 0.0001 for Vehicle Control vs 10 mg/kg 25b (p.o., bid); and <i>p</i> < 0.0001 for Vehicle Control vs 50 mg/kg celecoxib (p.o., pid).	33
Fig. 2-5. Representative images of stomach tissues collected from mice at 24 h after oral administration of (A) vehicle (oil) or (B) 25b (1 g/kg in oil) or (C) celecoxib (50 mg/kg in oil). For all mice in the vehicle and 25b groups, we did not find any bleeding spot on the	

inner side of stomach samples. Meanwhile, for each mouse in the celecoxib group, we were able to clearly see at least one bleeding spot; the bleeding points are labeled in red circles.35

Fig. 3-1. Molecular structures of the lead 19, designed inhibitor 44d and their binding with human mPGES-1. (A) Ligand structures; (B) binding with the lead 19; (C) binding with 44d.....40

Fig. 3-2. Crystal structure of 42. Crystals of 42 were non-merohedric twins and crystallized as a DMSO solvate. For the sake of clarity, the DMSO, which was disordered over two orientations, is not shown.47

Fig. 3-3. Molecular structures of 52e and 55c and their binding with human and mouse mPGES-1 enzymes. (A) Ligand structures; (B) binding of 52e with human mPGES-1; (C) surface representation of human mPGES-1 using the same orientation as in (B); (D) binding of 52e with mouse mPGES-1; (E) surface representation of mouse mPGES-1 using the same orientation as in (D); (F) binding of 55c with human mPGES-1; (G) surface representation of human mPGES-1 using the same orientation as in (F); (H) binding of 55c with mouse mPGES-1; (I) surface representation of mouse mPGES-1 using the same orientation as in (H).50

LIST OF SCHEMES

Scheme 1-1. Biosynthetic pathway of prostaglandin E ₂	2
Scheme 1-2. Biosynthetic pathway of PGE ₂ and anti-inflammatory roles of tNSAIDs, coxibs and mPGES-1 inhibitors.....	5
Scheme 1-3. Functional coupling of PGES with COXs.	6
Scheme 1-4. Suggested mechanism of mPGES-1 catalyzed isomerization of PGH ₂ to PGE ₂	7
Scheme 2-1. Synthetic protocol of substituted benzylidenebarbituric acid derivatives with various substitution patterns on the central benzene ring.	23
Scheme 2-2. Synthetic protocol of substituted benzylidenebarbituric acid derivatives with variation on the barbituric acid moiety.	26
Scheme 2-3. Synthetic protocol of substituted benzylidenebarbituric acid derivatives with various aliphatic side chains.	27
Scheme 3-1. Synthesis of 1-substituted isatin derivative.....	41
Scheme 3-2. Synthesis of 1-substituted isatin derivatives with reversed polarity.	43
Scheme 3-3. Synthesis of 1,5-disubstituted isatin derivatives.....	46
Scheme 3-4. Preparation of meglumine salt of 52e.	51

LIST OF ABBREVIATIONS

PLA₂, phospholipase A₂
PGE₂, prostaglandin E₂
LPS, lipopolysaccharide
IL-1 β , interleukin-1 β
AA, arachidonic acid
PLA₂, phospholipase A₂
PGG₂, prostaglandin G₂
PGH₂, prostaglandin H₂
PGD₂, prostaglandin D₂
PGI₂, prostacyclin
TXA₂, thromboxane A₂
COX, cyclooxygenase
PGES, prostaglandin E₂ synthases
mPGES-1, microsomal prostaglandin E₂ synthase-1
mPGES-2, microsomal prostaglandin E₂ synthase-2
cPGES, cytosolic prostaglandin E₂ synthase
MAPEG, membrane-associated protein involved in eicosanoid and glutathione metabolism
tNSAIDs, traditional non-steroidal anti-inflammatory drugs
KO, knock-out
GI, gastrointestinal
KI, knock-in
PGF_{2 α} , prostaglandin F_{2 α}
FLAP, 5-lipoxygenase-activating protein
5-LO, 5-lipoxygenase
mGST-1, microsomal glutathione S-transferase-1
5-HPETE, 5-hydroperoxyeicosatetraenoic acid
LTA₄, leukotriene A₄
LTB₄, leukotriene B₄
LTC₄, leukotriene C₄
LTD₄, leukotriene D₄
LTE₄, leukotriene E₄
SAR, structure–activity relationship
GSH, glutathione
DMF, *N,N*-dimethylformamide
DMSO, Dimethyl sulfoxide
rt, room temperature
equiv., equivalence
DCM, dichloromethane

ELISA, Enzyme-linked immunosorbent assay
SD, standard deviation
SEM, standard error of the mean
PDB, protein data bank
TFA, trifluoroacetic acid
DIPEA, *N,N*-diisopropylethylamine
PK, pharmacokinetic
HWB, human whole blood
CDCl₃, chloroform-*d*₁
IC₅₀, the half maximal inhibitory concentration

Chapter 1 Introduction

1.1 Prostaglandin E₂: mediator in inflammation

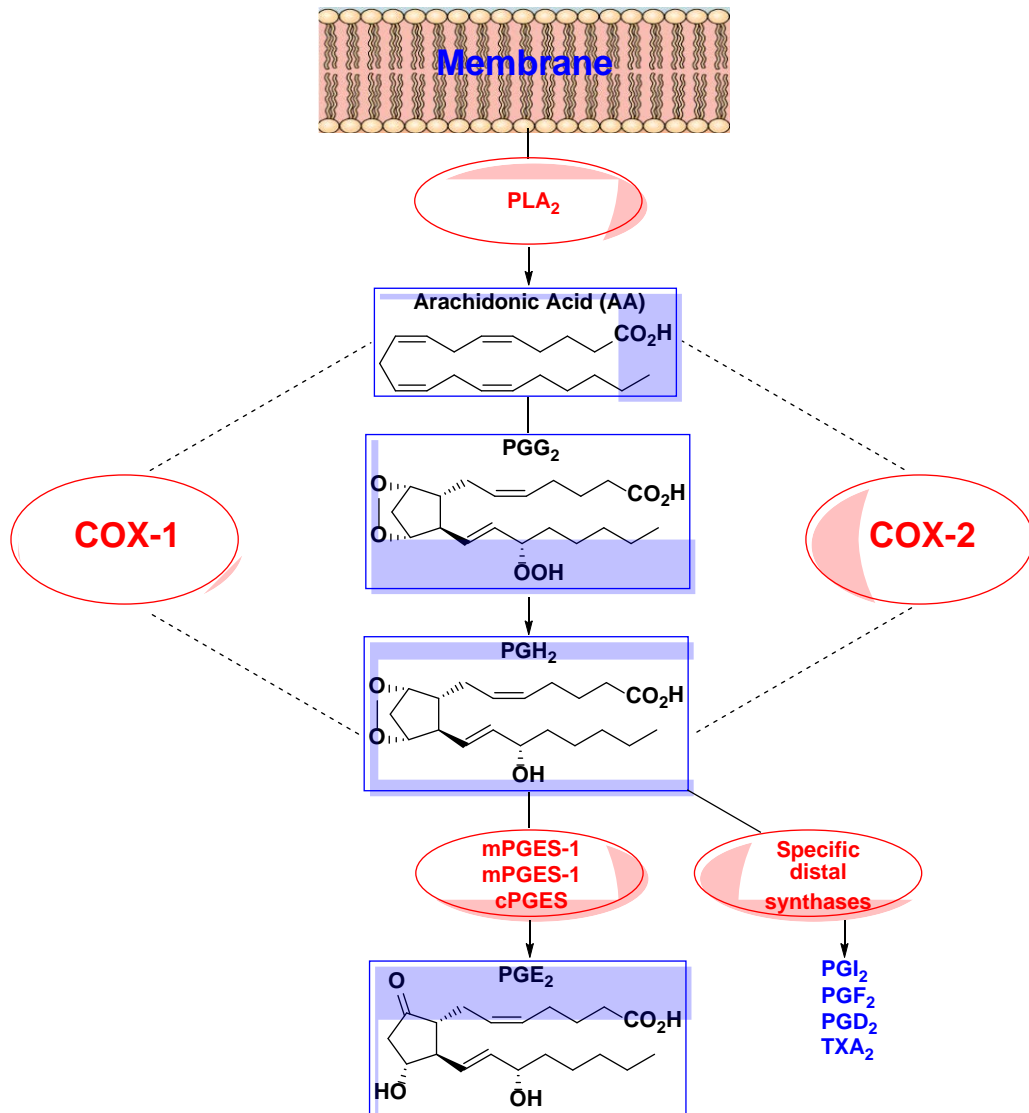
The prostaglandins are biologically active lipids released from phospholipid membranes by the action of phospholipase A₂ (PLA₂). Structurally, prostaglandins are derivatives of arachidonic acid and other polyunsaturated fatty acids. Among various prostaglandins, prostaglandin E₂ (PGE₂) is widely recognized as a pro-inflammatory mediator. It tends to be over-produced at pathological sites of inflammation; it triggers two prominent characteristics of inflammation: fever and pain,^[2] and its production can be largely induced by pro-inflammatory stimuli such as lipopolysaccharide (LPS) and interleukin-1 β (IL-1 β).^[3] Moreover, recent research revealed that PGE₂ could be closely involved in many types of cancers as it was believed to regulate crucial steps in tumorigenesis by stimulating cancer cell proliferation, enhancing angiogenesis, preventing apoptosis and inducing metastasis.^[4]

However, the physiological functions as the positive sides of PGE₂ should not be ignored, especially its protective function of gastrointestinal system in the promotion of duodenal bicarbonate secretion and in the suppression of gastric acid production.^[5]

1.2 The biosynthetic pathway of PGE₂

PGE₂ is biosynthesized from arachidonic acid (AA) liberated by phospholipase A₂ (PLA₂) from membrane phospholipids, followed by several enzymatic transformations known as one of the pathways of arachidonic cascade,^[6] as shown in Scheme 1-1. In the first step, AA is converted into prostaglandin H₂ (PGH₂) by the action cyclooxygenases (COX-1 and COX-2) that are also known as PGH₂ synthases. COX isozymes catalyze both of the two successive steps in the formation of PGH₂: the foregoing cyclooxidation at the cyclooxygenase site to generate the endoperoxide prostaglandin G₂ (PGG₂), and the subsequent reduction of the unstable intermediate PGG₂ at the peroxidase site of COXs to form PGH₂.^[7]

PGH₂ acts as the common precursor for various prostanoids such as PGD₂, PGE₂, PGF_{2α}, prostacyclin (PGI₂) and thromboxane A₂ (TXA₂), depending on the action of specific distal synthases. Among these terminal synthases, PGE₂ synthases are responsible for the final step in the biosynthesis of PGE₂: the isomerization COXs-derived peroxide PGH₂ to PGE₂.^[8] Three distinct PGE₂ synthases have been cloned and characterized in recent decades: microsomal prostaglandin E₂ synthase-1 (mPGES-1), microsomal prostaglandin E₂ synthase-2 (mPGES-2) and cytosolic prostaglandin E₂ synthase (cPGES).



Scheme 1-1. Biosynthetic pathway of prostaglandin E₂.

1.3 Anti-inflammatory strategies

1.3.1 Traditional non-steroidal anti-inflammatory drugs (tNSAIDs)

For decades, traditional non-steroidal anti-inflammatory drugs (tNSAIDs), including ibuprofen and indomethacin (structures shown in Fig. 1-1), have been the mainstay to diminish inflammation and to treat inflammation-related symptoms by non-selectively inhibiting either COX-1 or COX-2 or both.^[9] However, COX-1 and COX-2, despite their similarities in molecular weights and 3D structures,^[10] behave and function distinctly. COX-1 is ubiquitous and constitutively expressed with a relatively stable concentration in the body, whereas COX-2 is absent from most cell types. The expression of COX-2 is highly inducible in response to inflammatory stimuli.^[11] COX-1 primarily produces prostanoids for “housekeeping” homeostatic functions such as stomach mucosal protection and kidney water excretion, while COX-2, on the other hand, is responsible for the prostanoids associated with inflammation, fever and pain.^[12] The application of tNSAIDs is believed to exert anti-inflammatory activity through the inhibition of only COX-2. However, the unwanted adverse effects of tNSAID application, including ulcers and bleeding within the gastrointestinal (GI) tract^[13] are believed to result from the interference of COX-1-derived protective function in GI tract as homeostatic PGE₂ produced by COX-1 promotes duodenal bicarbonate secretion and suppresses gastric acid production.^[5]

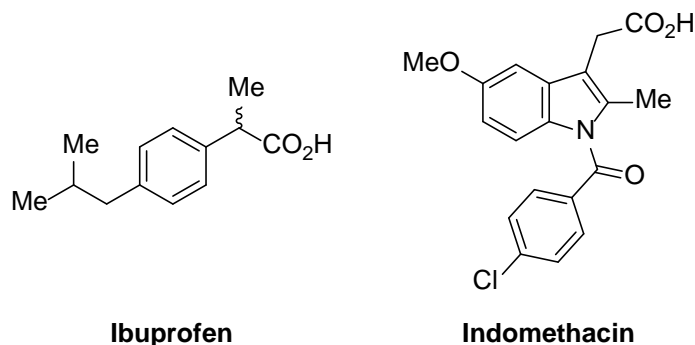


Fig. 1-1. Structures of selected tNSAIDs: ibuprofen and indomethacin.

1.3.2 Coxibs

Due to the adverse effects associated with the application of non-selective tNSAIDs, a major effort has been deployed in the development of selective COX-2 inhibitors^[14] so as

to preserve the regular housekeeping function of COX-1. While tNSAIDs are considered as the 1st generation, selective COX-2 inhibitors, also known as coxibs, represent the 2nd generation of non-steroidal anti-inflammatory drugs. Indeed, celecoxib and rofecoxib (structures shown in Fig. 1-2) did exhibit comparable anti-inflammatory efficacy with enhanced gastrointestinal tolerance as compared to non-selective tNSAIDs. Unexpectedly, coxib application were later observed with increased risk of cardiovascular events, including myocardial infarction, stroke, pulmonary hypertension and congestive heart failure.^[15] These severe deleterious effects eventually resulted in the withdrawal of rofecoxib from the US market in 2004, leaving celecoxib the only FDA-approved selective COX-2 inhibitor on US market with the warning of cardiovascular risk.

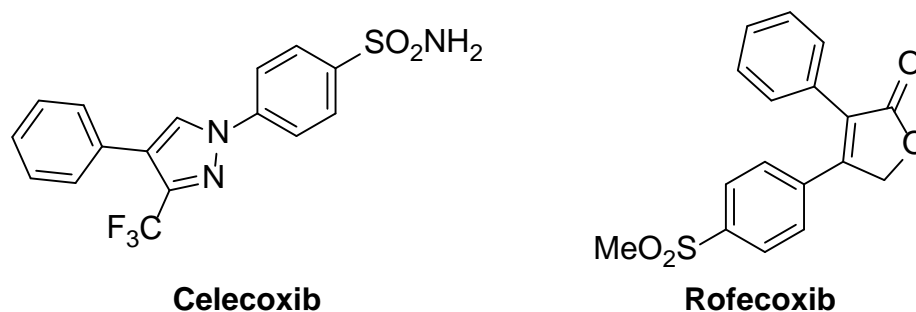


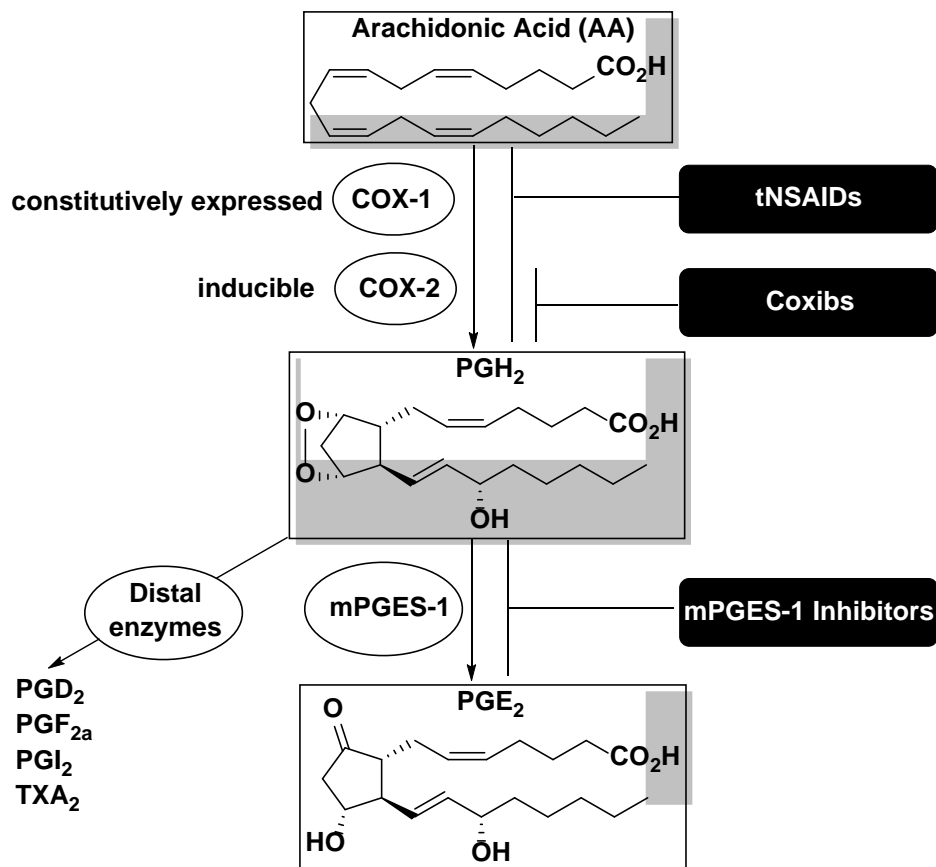
Fig. 1-2. Structures of selected coxibs: celecoxib and rofecoxib.

The biological mechanism behind the cardiovascular consequences associated with coxib application may result from the disruption of the crucial balance between COX-1 derived TXA₂ and COX-2 produced PGI₂, in which the former is vasoconstrictive and pro-thrombotic while the latter is vasodilative and anti-platelet.^[16] For example, celecoxib was discovered to suppress PGI₂ synthesis (from COX-2) without simultaneous blocking the TXA₂ production (from COX-1), from which the cardiovascular effects arise.^[17]

1.3.3 Potent mPGES-1 inhibitors

From the biosynthetic pathway of PGE₂ as shown in Scheme 1-1, the terminal step of the isomerization of PGH₂ to PGE₂ is catalyzed by three distinct PGE₂ synthases, including two microsomal enzymes, mPGES-1 and mPGES-2, and a cytosolic enzyme cPGES. Recent reports indicated the specific inhibition of mPGES-1, which only blocks the yield

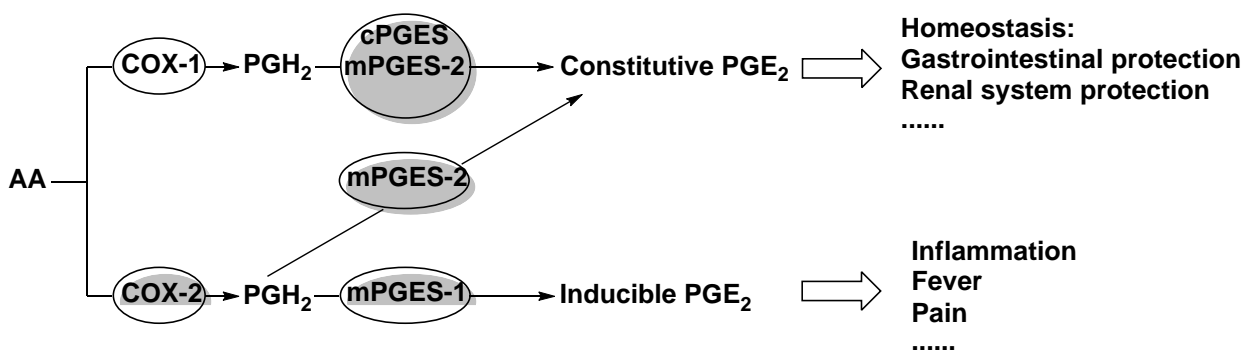
of inflammation-related PGE₂ without affecting the normal production of other prostanoids and homeostatic PGE₂ downstream COX-2 (as shown in Scheme 1-2), provides promising perspective in the exploration of a next generation of drugs in the treatment of inflammation-associated symptoms.^[18]



Scheme 1-2. Biosynthetic pathway of PGE₂ and anti-inflammatory roles of tNSAIDs, coxibs and mPGES-1 inhibitors.

First, both cPGES and mPGES-2 are constitutively expressed enzymes in which cPGES is functionally coupled with COX-1 and mPGES-2 with both COX-1 and COX-2. Specifically, cPGES receives the substrate PGH₂ from COX-1 and mPGES-2 receives PGH₂ from either COX-1 or COX-2 without selectivity, and they together provide basal level of PGE₂ for physiological homeostasis.^[19] However, mPGES-1, first identified in 1999,^[20] is pro-inflammatory stimuli-dependent and preferentially uses COX-2-derived PGH₂ as a substrate to produce PGE₂ related to inflammation, fever, and pain, as shown in Scheme 1-3.^[19]

In addition, the knockout (KO) studies in various animal models of diseases including collagen-induced arthritis,^[21] atherosclerosis,^[22] LPS-stimulated pyresis^[23] and pain hypersensitivity^[24] confirmed the involvement of mPGES-1 enzyme. Specifically, ischemic stroke induced in mPGES-1 knockout mice showed significantly reduced infarct size and volume^[25] and a decrease in inflammation response was observed in a collagen-induced arthritis model. In human, enhanced mPGES-1 expression and PGE₂ production have been observed in several pathologies such as rheumatoid arthritis,^[26] myositis,^[27] atherosclerosis,^[28] inflammatory bowel disease,^[29] cancer^[30] and Alzheimer's disease.^[31] Altogether, these encouraging findings provided a firm rationale for targeting this enzyme in the development of new generation of anti-inflammatory drugs.



Scheme 1-3. Functional coupling of PGES with COXs.

1.4 Structure of mPGES-1

Several crystal structures of human mPGES-1 enzyme have been disclosed in recent years. The first two-dimensional (2D) low resolution crystal structure (PDB ID: 3DWW)^[32] derived from transmission electron microscope represents the closed conformation. Our group proposed an mPGES-1 model in the open conformation derived from the crystal structures of microsomal glutathione S-transferase-1 (mGST-1) and ba3-cytochrome c oxidase.^[33] The first three-dimensional (3D) high resolution structure provided by X-ray experiments (PDB ID: 4AL0)^[34] and the first crystal structure of this enzyme in complex with an inhibitor (PDB ID: 4BPM)^[35] were disclosed recently. These crystal structures, especially the last two with high crystallographic resolution, provide detailed structural information of human mPGES-1 enzyme, which is of great importance in the rational

This thiolate anion nucleophilically attack one of the endoperoxide oxygen atom at C-9 carbon of PGH₂, producing the mixed sulfide intermediate. (2) D49 is responsible for the proton attraction at C-9 carbon, facilitating the S-O bond cleavage. The bidentate complex of D49 with R126 promotes the basicity of carboxylate of D49, which increases the effectiveness of proton transfer. (3) PGE₂ is produced and the reactive thiolate anion is regenerated.

The suggested mechanism of the isomerization of PGH₂ to PGE₂ by the action of mPGES-1 including a nucleophilic attack of the thiolate anion of GSH at one of the peroxide oxygen atoms to form a mixed sulfide, followed by the deprotonation on C-9 and the cleavage of S-O bond. The hydroxyl group of S127 is suggested to promote the formation and stabilization of the GSH thiolate anion, facilitating the nucleophilic attack in the first step. D49 is the residue considered acting as base to deprive the proton on C-9. The putative role of R126 is the alteration of the *pKa* of D49 to promote the proton abstraction in the second step and to prevent the reduction of the intermediate. The plausible mechanism of mPGES-1 catalyzed isomerization of PGH₂ to PGE₂ is suggested in Scheme 1-4.

1.5 Recent progress in the development of potent mPGES-1 inhibitors

1.5.1 Early unselective inhibitors

A number of coxibs including celecoxib (IC₅₀ = 22 μM) and lumiracoxib (IC₅₀ = 33 μM),^[38] and PGH₂ structural analogs such as arachidonic acid (IC₅₀ = 0.3 μM)^[39] and 15-Δ^{12,14}-PGJ₂ (IC₅₀ = 0.3 μM)^[39] were among the first bunch of compounds identified to be potent against mPGES-1 enzyme, although these compounds were rather not selective for mPGES-1.^[39] The structures of these early inhibitors are shown in Figure 1-3.

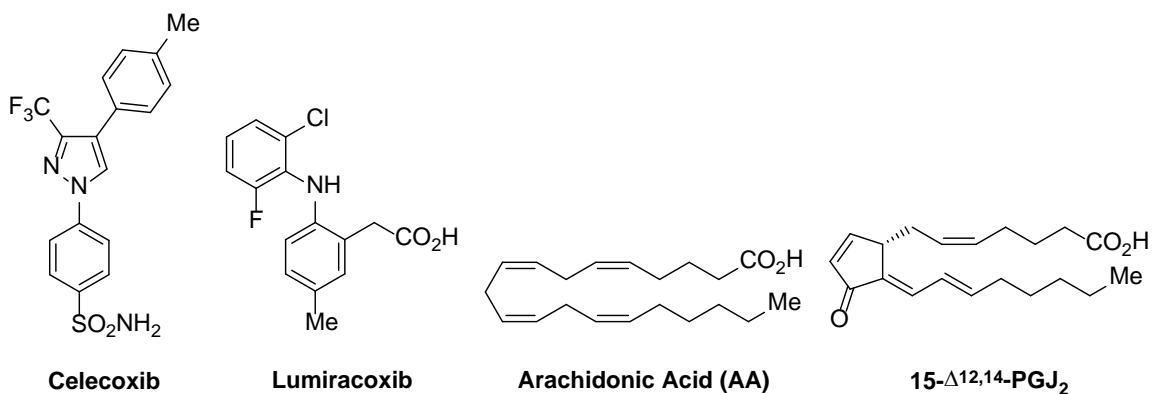


Fig. 1-3. Unselective mPGES-1 inhibitors.

1.5.2 MK-886, MF-63 and their analogs by Merck

Merck Frosst Centre for Therapeutic Research has been a productive leading group in the discovery of potent mPGES-1 inhibitors in the recent decades. A 5-lipoxygenase-activating protein (FLAP) inhibitor,^[40] MK-886, was identified to inhibit human recombinant mPGES-1 enzyme with low micromolar potency ($IC_{50} = 2.4 \mu M$).^[41] MK-886 was then used as the lead structure for the design of a series of potent and selective mPGES-1 inhibitors with the scaffold of indole-2-propionic acid.^[42] The introduction of biphenyl substituent at indole-5-position led to the discovery of inhibitors **1** ($IC_{50} = 7 \text{ nM}$) and **2** ($IC_{50} = 3 \text{ nM}$) with low nanomolar potencies. The molecular structures of MK-886 and its analogs **1** and **2** are outlined in Fig. 1-4. Both **1** and **2** showed negligible activity toward FLAP (target enzyme of the lead MK-886) and acceptable selectivity for mPGES-1 over mPGES-2 ($IC_{50} > 1 \mu M$) and TXA₂ synthase ($IC_{50} = 1 \mu M$). However, the remarkable loss of inhibitory efficacy in both cell-based assays and human whole blood (HWB) assays prohibited these series of compounds from entering preclinical evaluation.

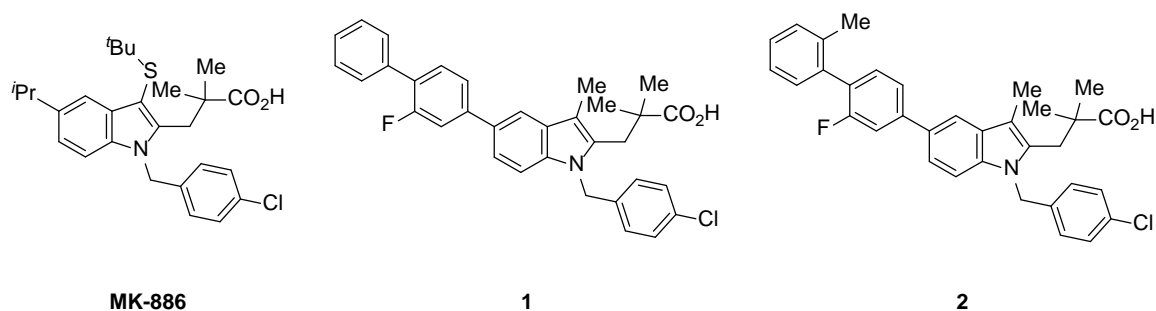


Fig. 1-4. MK-886 and structurally related indole-2-proponionic acid derivatives.

Unsatisfied with the poor whole cell potency of indole carboxylic acid compounds mentioned above, Merck scientists developed a novel class of phenanthreneimidazoles and their heterocyclic derivatives from the lead compound azaphenanthrenone,^[43] a JAK kinase inhibitor also suppressing mPGES-1 ($IC_{50} = 0.14 \mu M$). MF-63 was obtained through the replacement of azaphenanthrenone by phenanthrene with a 2,6-dicyanophenyl substituent at 2-position and alternation of 6-fluoro by chorine.^[44] MF-63 not only exhibited excellent activity in cell-free assays ($IC_{50} = 1 \text{ nM}$), but also showed markedly better inhibitory efficacy in whole cells and ($IC_{50} = 0.05\text{-}0.42 \mu M$) with high selectivity for mPGES-1 over other recombinant prostanoid synthases and isolated JAK isoenzymes. However, MF-63 was active against neither mouse nor rat mPGES-1 enzyme, which prevents using well-established mouse and rat models of inflammation in preclinical studies. Therefore, human mPGES-1 knock-in (KI) mice and guinea pigs were used as the alternatives ($IC_{50} = 0.9 \text{ nM}$ against guinea pig mPGES-1). Using these animal models, MF-63 was observed to suppress LPS-induced thermal hyperalgesia, iodoacetate-induced osteoarthritis pain, and LPS-induced pyresis.^[45]

Further structural modification generated the disubstituted phenanthreneimidazole derivatives **3** and **4** with IC_{50} value of 1 nM each. These compounds showed comparably potency as compared to MF-63, but were much more potent in human whole blood ($IC_{50} = 0.20 \mu M$ and $0.14 \mu M$, respectively). Compound **4**, with a rat half-life of 2.3 h, was encouragingly observed anti-analgesic effect in an LPS-stimulated guinea pig hyperalgesia model.^[46]

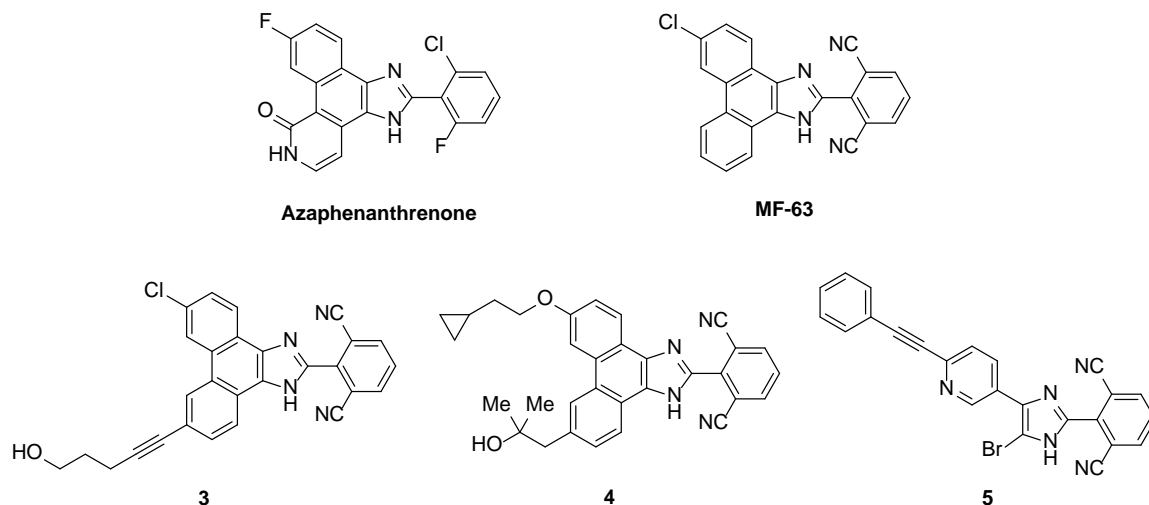


Fig. 1-5. Molecular structures of the lead azaphenanthrenone, designed inhibitor MF-63 and structurally related inhibitors **3–5**.

Residing in the structure of MF-63, a new biarylimidazole scaffold was then reported by Merck. The extensive SAR studies led to the discovery of **5**, a highly potent mPGES-1 inhibitor with an IC_{50} value of 1 nM in cell-free assay. Compound **5** was also active in A549 cells and HWB assays ($IC_{50} = 13\sim 160$ nM and 1.6 μ M, respectively). The rat pharmacokinetic study with this compound gave a clinical relevant half-life of 4.8 h and a bioavailability of 127%.^[47] The structures of azaphenanthrenone, MF-63, and other structural analogs **3–5** are shown in Fig. 1-5.

1.5.3 Oxicam and benzoxazole derivatives by Pfizer

A series of compounds with oxicam template were identified as human mPGES-1 inhibitors by high throughput screening of Pfizer chemical files. The subsequent extensive SAR studies led to the discovery of **6**, a low nanomolar ($IC_{50} = 0.016$ μ M) inhibitor against mPGES-1 with desired selectivity for mPGES-1 over COX-2 (>238 folds).^[48]

Pfizer scientists also developed a class of potent inhibitors with a benzoxazole scaffold. Based on detailed synthesis and the first round of SAR study, PF-0469362 ($IC_{50} = 3.0$ nM) was discovered as a promising mPGES-1 inhibitor with low nanomolar potency.^[49] Unsatisfied with the poor aqueous solubility and non-detectable half-life, Pfizer scientists conducted a new round of SAR study, from which compounds **7** ($IC_{50} = 8.3$ nM) and **8**

($IC_{50} = 19$ nM) were identified as comparably potent human mPGES-1 inhibitors with improved water solubility and longer rat half-life (4.5 h and 17 h, respectively). The molecular structures of **6**, PF-0469362, and **7–8** are shown in Fig. 1-6.

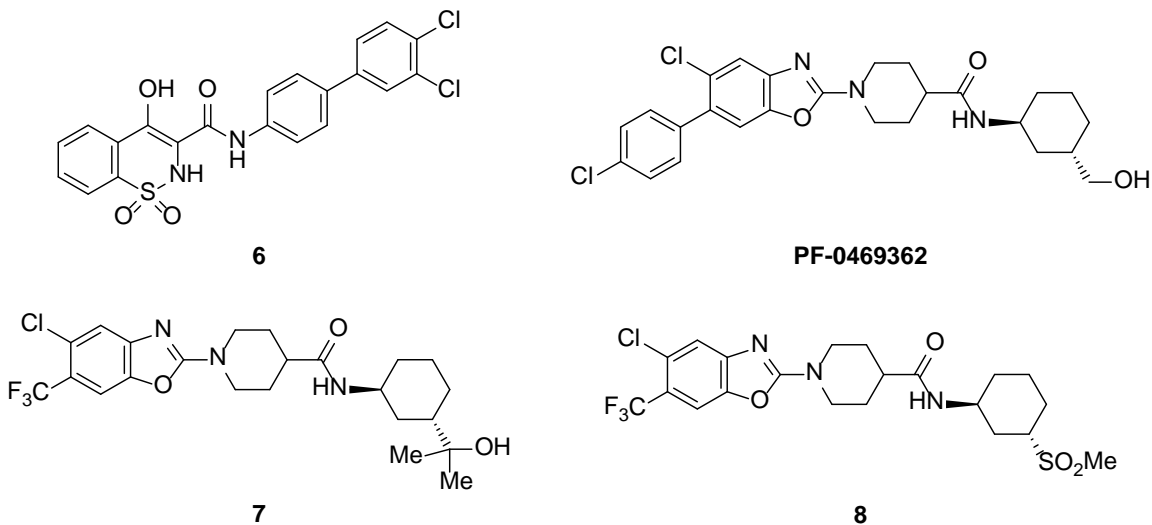


Fig. 1-6. The molecular structures of compound derived from oxicam template **6**, benzoxazole derivatives PF-0469362, and **7–8**.

1.5.4 Dual mPGES-1/5-LO inhibitors

As part of arachidonic acid cascade, AA released by PLA₂ is transferred to 5-lipoxygenase (5-LO) *via* FLAP. Enzyme 5-LO converts AA into arachidonic acid 5-hydroperoxide (5-HPETE), which is then further metabolized to leukotriene A₄ (LTA₄). LTA₄ is converted into a series of cysteinyl-leukotrienes (LTC₄, LTD₄ and LTE₄) and is hydrolyzed into LTB₄.^[11,50] Leukotrienes are also important lipid mediators in inflammation that play a role in cancers and cardiovascular diseases.^[51] Dual 5-LO and mPGES-1 inhibitors, blocking the biosynthesis of both PGE₂ and leukotrienes, might be more efficient in diminishing inflammation while less afflicted with GI and cardiovascular deleterious effects.^[50]

Werz group from University of Tuebingen, Germany discovered a series of benzo[g]indol-3-carboxylate derivatives as potent dual mPGES-1/5-LO inhibitors.^[52] Compound **9** was identified to inhibit both mPGES-1 ($IC_{50} = 0.6$ μ M) and 5-LO ($IC_{50} = 0.086$ μ M) with submicromolar potencies in cell-free assays.^[52] The low percentages of inhibition against

both COX-1 and COX-2 at a concentration of 10 μM of compound **9** (12% and 33%, respectively) demonstrated the high selectivity for mPGES-1 over COX isozymes. *In vivo* intraperitoneal administration of **9** significantly reduced PGE₂ levels in pleural exudates of carrageenan-treated rats.^[53]

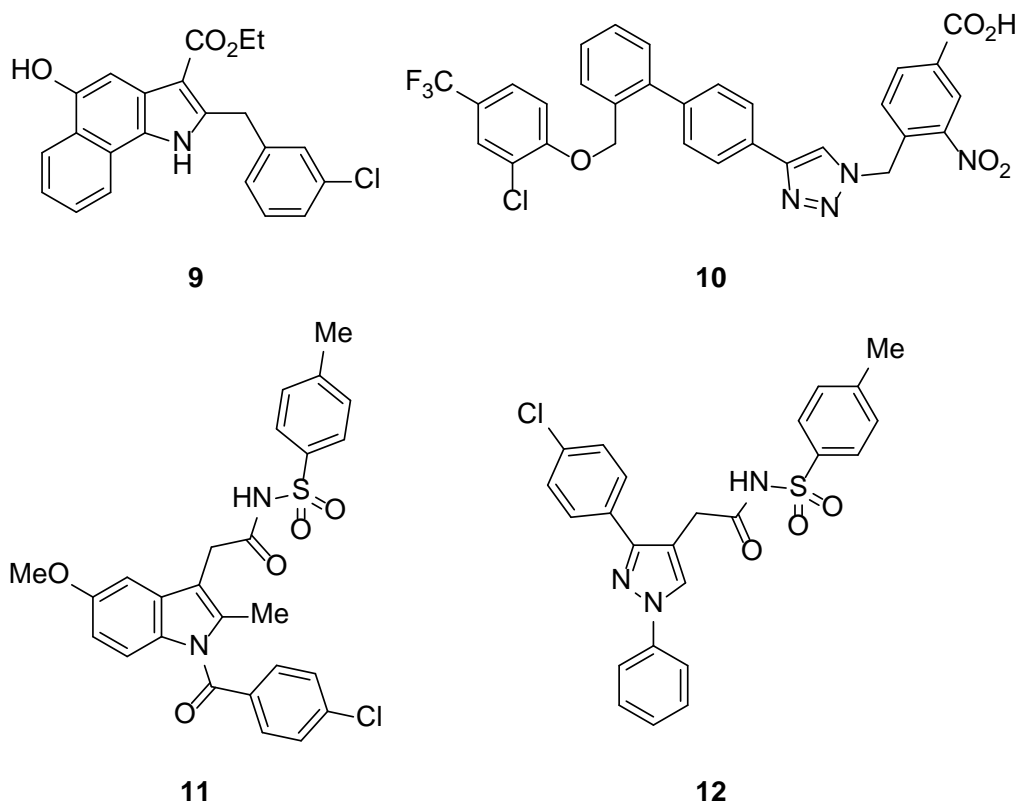


Fig. 1-7. Molecular structures of dual mPGES-1/5-LO inhibitors: benzo[g]indol-3-carboxylate derivative **9**, triazole-based compound **10**, indomethacin derivative **11** and lonazolac derivative **12**.

As continued effort, Werz group designed, synthesized and biologically evaluated another series of triazole-based compounds.^[54] Several compounds, including **10** ($\text{IC}_{50} = 1.2 \mu\text{M}$ and $2.0 \mu\text{M}$ against mPGES-1 and 5-LO, respectively), were identified as low micromolar inhibitors against both mPGES-1 and 5-LO.

By structurally modifying acidic NSAIDs, Werz *et al.* also identified several potent dual mPGES-1/5-LO inhibitors among a variety of synthetic molecules.^[55] Compounds **11** ($\text{IC}_{50} = 6.4 \mu\text{M}$ against mPGES-1 and $\text{IC}_{50} = 2.9 \mu\text{M}$ against 5-LO) and **12** ($\text{IC}_{50} = 3.4 \mu\text{M}$ against

mPGES-1 and $IC_{50} = 2.5 \mu\text{M}$ against 5-LO), derived from indomethacin and lonazolac, respectively, were identified to inhibit both enzymes with comparable low micromolar potency. The structures of these dual mPGES-1/5-LO inhibitors are depicted in Fig. 1-7.

1.5.5 Inhibitors discovered by virtual screening

Although high-throughput screening has been used to identify new leads in drug discovery for decades, it remains an expensive and time-consuming procedure. Virtual screening has emerged as an alternative approach widely used in modern rational drug design. Using the structural model of the active conformation derived from newly disclosed crystal structures of MAPEG family proteins, Lai group (Peking University, China) identified highly potent mPGES-1 inhibitors *via* virtual screening.^[56] Some of the molecules, with novel scaffolds, such as compounds **13** and **14** (Fig. 1-8) exhibited submicromolar inhibitory potencies against mPGES-1 in both cell-free assays ($IC_{50} = 0.0040 \mu\text{M}$ and $0.0093 \mu\text{M}$ for compounds **13** and **14**, respectively) and HWB assays ($IC_{50} = 0.3 \mu\text{M}$ and $0.7 \mu\text{M}$, respectively).

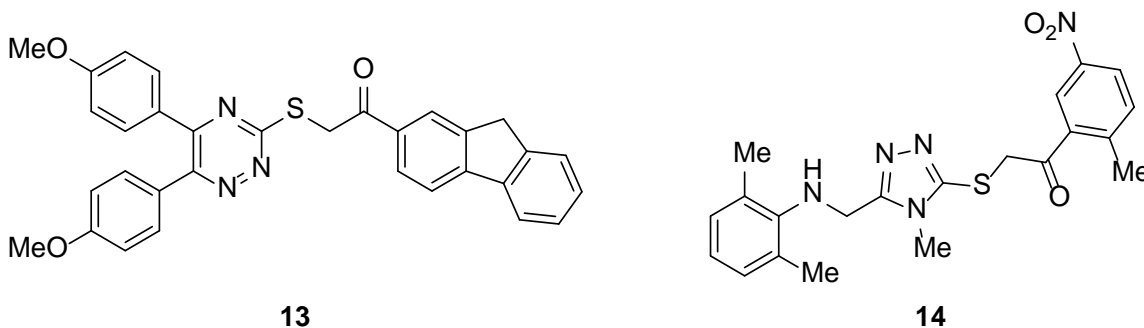


Fig. 1-8. Structures of compounds **13–14** identified from virtual screening.

1.5.6 Other synthetic compounds as potent mPGES-1 inhibitors

Bruno *et al.* characterized the function of mPGES-1 toward PGH_2 metabolism in LPS-treated human monocytes and human whole blood by analyzing the biosynthesis of prostanoids downstream PGES and expression of COXs in the presence of inhibition by the novel selective mPGES-1 inhibitor AF-3442 they prepared.^[57] Compound AF-3442 is a carbazole derivative with an IC_{50} value of $0.06 \mu\text{M}$ against human recombinant mPGES-

1. This compound was reported to suppress PGE₂ biosynthesis in LPS-stimulated human monocyte with an IC₅₀ value of 0.41 μM although it was not quite potent in HWB assays (IC₅₀ = 29 μM).

A novel class of compounds based on imidazolequinoline core, which was structurally analogous with phenanthreneimidazole series,^[44] were reported by Shiro *et al.* as potent mPGES-1 inhibitors. Compound **15**, as an example, was identified as an mPGES-1 inhibitor with low nanomolar potency (IC₅₀ = 9.1 nM) and a 1000-fold selectivity for mPGES-1 over COX isoenzymes.^[58]

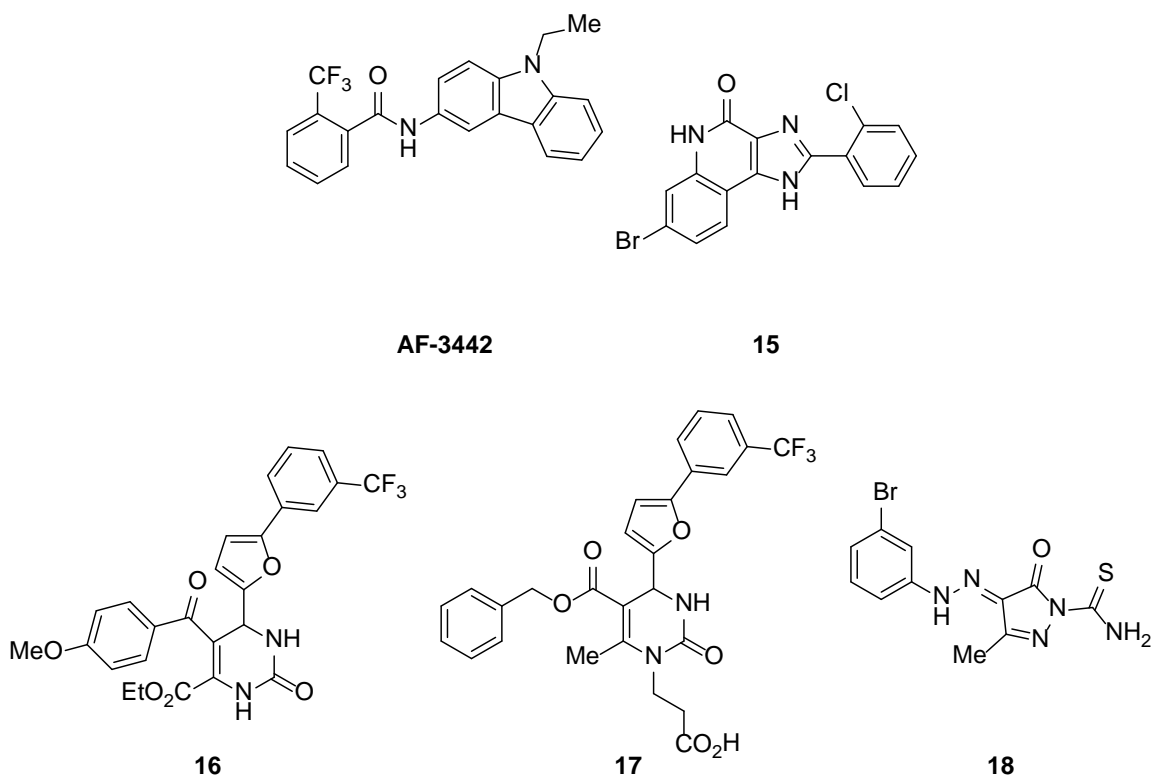


Fig. 1-9. Structures of carbazole derivative AF-3442, imidazolequinoline derivative **15**, dihydropyrimidin-2(1H)-one derivative **16–17** and pyrazolone derivative **18**.

Terracciano *et al.* reported the rational structural optimization of dihydropyrimidin-2(1H)-one lead compound **16** (IC₅₀ = 4.16 μM) based on the simulated binding mode of **16** with recently disclosed crystal structure of human mPGES-1 (PDB ID: 4BPM).^[35] By introducing hydrophilic group and altering the dimensions of hydrophobic moiety, compound **17** was designed and synthesized, with a 10-fold improved potency against

human mPGES-1 ($IC_{50} = 0.41 \mu\text{M}$).^[59]

Although several compounds have been reported to inhibit human mPGES-1 with low nanomolar activity, these compounds were either inactive or insignificantly active for mouse or rat mPGES-1 enzyme. The lack of mouse/rat animal models often precluded preclinical study. Leclerc group from Karolinska Institute, Sweden characterized the pyrazolone derivative **18** as dual human/rat mPGES-1 inhibitor ($IC_{50} = 1.8$ and $0.62 \mu\text{M}$, for human and rat mPGES-1 enzymes, respectively).^[60] A number of *in vivo* studies were conducted to evaluate PGE_2 production in rat peritoneal macrophages and rat carrageenan air-pouch, which supported the effectiveness of **18** in these rat models. For example, in rat carrageenan air-pouch model, treatment of rats with **18** at 75 mg/kg intraperitoneally reduced PGE_2 production by 62% relative to vehicle control. The structures of AF-3442 and **15–18** are shown in Fig. 1-9.

1.5.7 Natural products as potent mPGES-1 inhibitors

Curcumin, an antioxidant polyphenolic β -diketone from turmeric with anti-carcinogenic and anti-inflammatory activities, is a major component of the curry spice turmeric. Werz group identified mPGES-1 as a predominant target of curcumin in the mechanism of suppressing PGE_2 biosynthesis.^[61] Curcumin was observed to reversibly inhibit the isomerization of PGH_2 to PGE_2 by mPGES-1 in microsomes of IL-1 β -stimulated A549 lung carcinoma cells ($IC_{50} = 0.2\text{--}0.3 \mu\text{M}$). In addition, neither isolated ovine COX-1 nor human recombinant COX-2 was inhibited by curcumin at a concentration as high as $30 \mu\text{M}$. In addition, curcumin was also identified to inhibit 5-LO with an IC_{50} value of $0.7 \mu\text{M}$.

A few other natural products such as mytucommulone (from myrtle),^[62] hyperforin (from St. John's wort),^[63] garcinal (from the rind of guttiferae)^[64] and arzanol (from *Helichrysum italicum*)^[65], sharing no structural similarities except an acylphloroglucinol, were identified as dual mPGES-1 ($IC_{50} = 0.3\text{--}1.3 \mu\text{M}$) and 5-LO ($IC_{50} = 1\text{--}3 \mu\text{M}$) inhibitors. At higher concentrations, these natural products also showed inhibitory potency against COX-1 ($IC_{50} > 12 \mu\text{M}$). The structures of these natural products are described in Fig. 1-10.

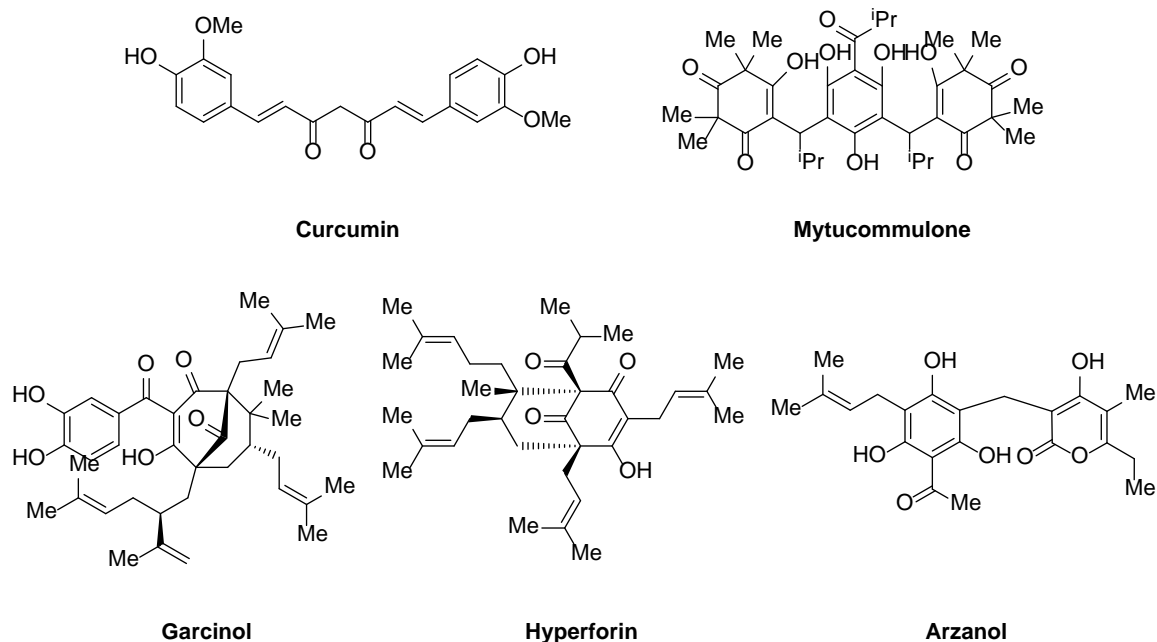


Fig. 1-10. Structures of natural products active against human mPGES-1 enzyme: curcumin, mytucommulone, garcinol, hyperforin and arzanol.

1.6 Summary

Human mPGES-1 has emerged as prospective target in the exploration of a next-generation of anti-inflammatory drugs, as specific mPGES-1 inhibitors are expected to discriminatively suppress the production of induced PGE₂ without blocking the normal biosynthesis of other prostanoids including homeostatic PGE₂. Therefore, this therapeutic approach is believed to reduce the adverse effects associated with the application of tNSAIDs and selective COX-2 inhibitors (coxibs). Although great effort has been deployed in the exploration of mPGES-1 inhibitors, be it from virtual screening, synthesis and natural products,^[42, 44-49, 52, 54, 57-58, 59, 66] only a few have entered clinical trials^[67] and none has made it to market so far. In particular, most of the reported human mPGES-1 inhibitors are not active for wild-type mouse or rat mPGES-1 enzyme, which prevents using the well-established mouse/rat models of inflammation in preclinical studies. Therefore, we expect that our designed inhibitors to be potent for both human and mouse mPGES-1 enzymes and thus can be preclinically evaluated using mouse models of inflammation, such as carrageenan air-pouch and paw edema models. In the following chapters, the strategies for the design and structural optimization, the chemical synthesis and the biological evaluation

of two series of compounds are described in detail.

Chapter 2 Structure-based discovery of substituted benzylidenebarbituric acid derivatives as mPGES-1 inhibitors suitable for preclinical testing in wild-type mice

Part of the results described in this chapter has been published (“Structure-based discovery of mPGES-1 inhibitors suitable for preclinical testing in wild-type mice as a new generation of anti-inflammatory drugs” *Sci. Rep.* **2018**, 8, 5205).

2.1 mPGES-1 as a more promising anti-inflammation target

The first generation of nonsteroidal anti-inflammatory drugs (tNSAIDs) used to treat pain and reduce fever or inflammation, such as ibuprofen, inhibit both COX-1 and COX-2 without selectivity, and the second generation of NSAIDs (Coxibs), including celecoxib (Celebrex), rofecoxib (Vioxx) and valdecoxib (Bextra), selectively inhibit COX-2. The COX-2 specific inhibitors still have a number of serious side effects, such as increasing the risk of fatal heart attack or stroke and causing stomach or intestinal bleeding. The serious side effects led to the withdrawal of rofecoxib and valdecoxib, although celecoxib still remains in clinical use. The serious side effects are due to the fact that the synthesis of all physiologically needed prostaglandins downstream of PGH₂ are inhibited by the action of the COX-1/2 inhibitors. For example, blocking the production of PGI₂ will cause significant cardiovascular problems.^[68]

The mPGES-1 expression in most tissues including heart and brain is low, but abundant in a limited number of organs including kidney^[69] and reproductive organs.^[70] Enzyme mPGES-1 in human is related to various diseases associated with inflammation. For example, up-regulation of mPGES-1 was detected in heart tissue after myocardial infarction and in Alzheimer’s disease tissues.^[31, 71] Unlike the COX-1/2 inhibition, inhibition of terminal mPGES-1 will only block the production of PGE₂ without affecting the normal production of other prostaglandins including PGI₂. Therefore, mPGES-1, an inducible enzyme, is a more promising target for anti-inflammatory drugs. Reported knock-out studies identified mPGES-1 as an essential central switch in pyresis.^[72] The mPGES-1 knock-out studies also revealed a decrease in inflammatory response in a collagen-induced arthritis model.^[73] In contrast to COX-2, mPGES-1-deficient mice were reported to be viable, fertile and have normal phenotype.^[73] Ischemic stroke induced in mPGES-1 null

mice was reported to show significant reduction in the infarct size and volume.^[74] Thus, mPGES-1 inhibitors are expected to retain the anti-inflammatory effect of COX-1/2 inhibitors, but without the side effects caused by the COX-1/2 inhibition. For development of a next generation of anti-inflammatory drugs, various mPGES-1 inhibitors have been reported in the literature.^[42, 44, 46-49, 52, 54, 57-59, 66-67, 75]

Unfortunately, none of the reported potent inhibitors of human mPGES-1 has shown to be also a potent inhibitor of mouse or rat mPGES-1, which prevents using the well-established mouse/rat models of inflammation-related diseases for preclinical studies. Here we present the discovery of a novel type of mPGES-1 inhibitors potent for both human and mouse mPGES-1 enzymes through structure-based rational design. These inhibitors are also highly selective for mPGES-1 over COX-1/2 and orally bioavailable, enabling preclinical testing using the well-established wild-type mouse models of inflammation-related diseases through oral administration.

2.2 Design of dual inhibitors of human and mouse mPGES-1 enzymes

Our rational design of novel mPGES-1 inhibitors started from molecular modeling of various human mPGES-1 inhibitors, including MF63,^[75] **19**^[76] and its scaffold structure (**20**) depicted in Fig. 2-1A and Fig. 2-2A, for their binding with human and mouse mPGES-1 enzymes, and aimed to design a modified, novel compound which can favorably bind with both human and mouse mPGES-1 enzymes at the active site. To design a compound which can favorably bind with both human and mouse mPGES-1 enzymes, our strategy was to identify a scaffold structure which can bind in the conserved region of the active site, ensuring that the scaffold structure can bind with both of the enzymes in a similar binding mode. For this purpose, molecular docking was performed to understand the binding of known mPGES-1 inhibitors with both human and mouse mPGES-1 enzymes based on an X-ray crystal structure (PDB ID: 4BPM)^[35] of human mPGES-1 and a homology model of mouse mPGES-1 developed by using the human mPGES-1 structure as a template.

As seen in Fig. 2-1B and Fig. 2-1C, compound **19** (identified from virtual screening),^[76]

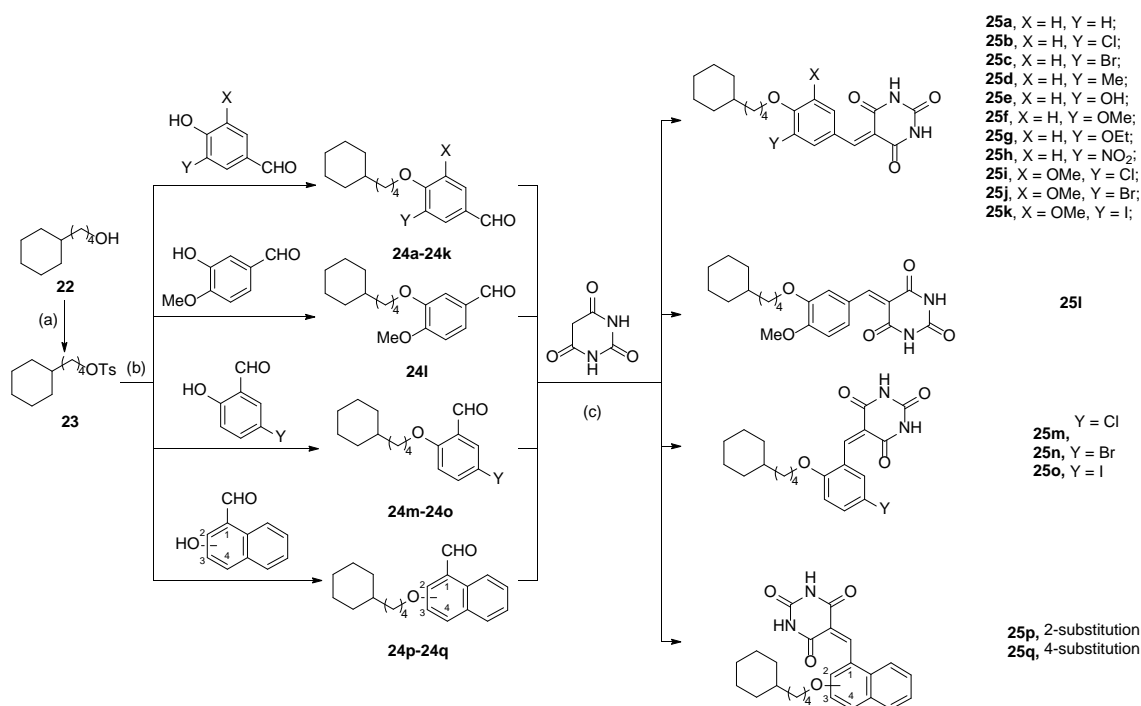
which has a unique scaffold structure (**20**), binds in a conserved region of the active site in the human and mouse mPGES-1 enzymes, although **19** has a low binding affinity with human mPGES-1 ($IC_{50} = 3.5 \mu M$).^[76] The conserved region is nearby S127 and has a mainly hydrophobic pocket surrounded by Y28, I32, G35, L39, S127, Y130, T131, L135, and A138 for human mPGES-1. In comparison, mouse mPGES-1 differs from human mPGES-1 only in residues #32 (which is V32), #131 (which is V131), and #138 (which is F138). In Fig. 2-1B, D and E, we mainly highlight the residues of human mPGES-1 that are different in mouse mPGES-1, in addition to the most important residues (such as S127) for binding.

On the basis of the scaffold structure **20**, we designed a modified scaffold structure (**21**, see Fig. 2-1A) which can more favorably bind in the conserved region of the active site. Depicted in Fig. 2-1B to E are the binding structures of human mPGES-1 with **19**, **20**, and **21**, respectively. The overall binding complex with surface representation of human mPGES-1 is shown in Fig. 2-1C. As seen in Fig. 2-1D and E, compared to **20**, **21** is a more favorable scaffold structure, as a carbonyl oxygen on the barbituric acid head group of **21** forms a hydrogen bond with the hydroxyl group of S127 side chain. The same hydrogen bond is expected to exist in mouse mPGES-1 binding with **21**. By using this novel scaffold (**21**), a series of potentially promising new compounds were designed, synthesized, characterized and assayed for their *in vitro* inhibitory activities against human and mouse mPGES-1 enzymes.

2.3 Chemistry and SAR study

2.3.1 SAR on the central benzene ring

The initial SAR study was the impacts of the substitution pattern of the central benzene ring on the inhibitory efficacy. The synthetic protocol is outlined in Scheme 2-1. The tosylate **23** derived from commercially available 4-cyclohexyl-1-butanol (**22**) was reacted with various substituted hydroxybenzaldehyde in the presence of excess potassium carbonate as acid capturer, yielding aldehyde intermediates (**24a–24q**). These aldehyde intermediates were then condensed with barbituric acid in reflux mixture of EtOH and H₂O to produce the final products, a series of substituted benzylidenebarbituric acid derivatives (**25a–25q**).



Scheme 2-1. Synthetic protocol of substituted benzylidenebarbituric acid derivatives with various substitution patterns on the central benzene ring. Reagents and conditions: (a) *p*-Toluenesulfonyl chloride (1.20 equiv.), 50% KOH aq., DCM, 0 °C→rt, 95%; (b) K₂CO₃ (2.0 equiv.), DMF, 80 °C, 74–93%; (c) EtOH/H₂O (4:1, v/v), reflux, 71–95%.

As shown in Table 2-1, we first investigated the impact of substitution on the central benzene ring on the inhibitory potency with fixed 4-cyclohexyl-1-butyl group as the

hydrocarbon tail. Without a substituent, as for **25a** (X = H, Y = H), the inhibitory potency of the compound against both human and mouse mPGES-1 enzymes was greatly impaired.

Table 2-1. Variation on the Central Benzene Ring.

Compound	Inhibition of mPGES-1	
	IC ₅₀ (human, nM) ^a	IC ₅₀ (mouse, nM)
25a	622±121	7087±627
25b	33±3	157±31
25c	45±8	917±321
25d	82±10	n.d. ^b (25) ^c
25e	116±17	2900±293
25f	121±20	1458±209
25g	186±26	2410±339
25h	67±20	698±97
25i	22±7	360±56
25j	69±16	292±47
25k	54±12	359±50
25l	155±23	727±109
25m	87±27	n.d. (28)
25n	96±14	n.d. (38)
25o	135±18	n.d. (54)
25p	154±18	n.d. (46)
25q	171±34	3699±562

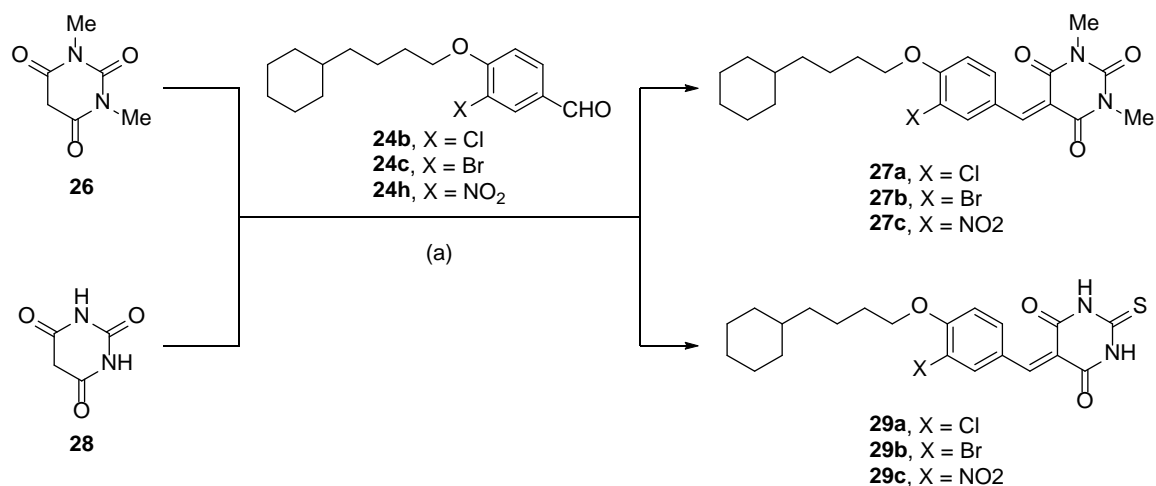
^aData are expressed as means ± SD of single determinations obtained in triplicate. ^bn.d. = not detected. ^cThe % inhibition of the compound at a concentration of 10 μM against mPGES-1. The IC₅₀ values were determined if the compound cause significant inhibition at 10 μM (≥ 70%).

Secondly, both electro-withdrawing and electro-donating groups were tolerated, although the former resulted in greater inhibition. Di-substitution on the central benzene ring, as investigated in the structures of **25i–25k**, resulted in compounds with comparable inhibitory efficacy as those mono-substituted. The central benzene ring of **25l** was

originated from isovanillin. As compared with the vanillin derivative **25f**, compound **25l** was comparably potent against human mPGES-1 ($IC_{50} = 121$ nM and 155 nM for **25f** and **25l**, respectively) whereas 2-fold more potent against the mouse enzyme ($IC_{50} = 1458$ nM and 727 nM for **25f** and **25l**, respectively). In compound group **25m–25o**, the central benzene ring was originated from salicylaldehyde with chlorine, bromine and iodine substituted at 5-position. These compounds were active against human mPGES-1 with submicromolar potencies ($IC_{50} = 87$ nM, 96 nM and 135 nM for **25m**, **25n** and **25o**, respectively) but surprisingly not effective against the mouse enzyme. Naphthalene, instead of benzene, was used to form the “linker” in compounds **25p–25q**. Compared with the most potent compound **25b**, the inhibition against mouse mPGES-1 was markedly decreased while that against the human enzyme was mostly retained ($IC_{50} = 154$ nM and 171 nM for **25p** and **25q**, respectively).

2.3.2 SAR on the barbituric acid moiety

In the next round of SAR study, variations were made on the barbituric acid “head”. We fixed the substitution on the central benzene ring as electro-withdrawing groups (Cl, Br and NO_2) and the aliphatic “tail” as 4-cyclohexyl-1-butyl group. Instead of barbituric acid, 1,3-dimethylbarbituric acid and 2-thiobarbituric acid were introduced to the structure as polar “head”, respectively. As shown in Scheme 2-2, the aldehyde intermediates **24b**, **24c** and **24h** (with Cl, Br and NO_2 substituted, respectively) were condensed with either 1,3-dimethylbarbituric acid (**26**) or 2-thiobarbituric acid (**28**). The final products 1,3-dimethylbarbituric acid derivatives **27a–27c** and 2-thiobarbituric acid derivatives **29a–29c**, were thus prepared. Compared with the normal barbituric acid “head” (**25b**, **25c** and **25h**), the substitution of methyl group (as in compounds **27a–27c**) significantly impaired the inhibitory efficacy against human mPGES-1 with 8, 9 and 9 folds. The inhibitory potency against the mouse enzyme was also decreased. However, the replacement of O with S (as in compounds **29a–29c**) generally slightly improved the inhibition for human mPGES-1.



Scheme 2-2. Synthetic protocol of substituted benzylidenebarbituric acid derivatives with variation on the barbituric acid moiety. Reagents and conditions: (a) EtOH/H₂O (4:1, v/v), reflux, 83–95%.

Table 2-2. SAR on the barbituric acid moiety.

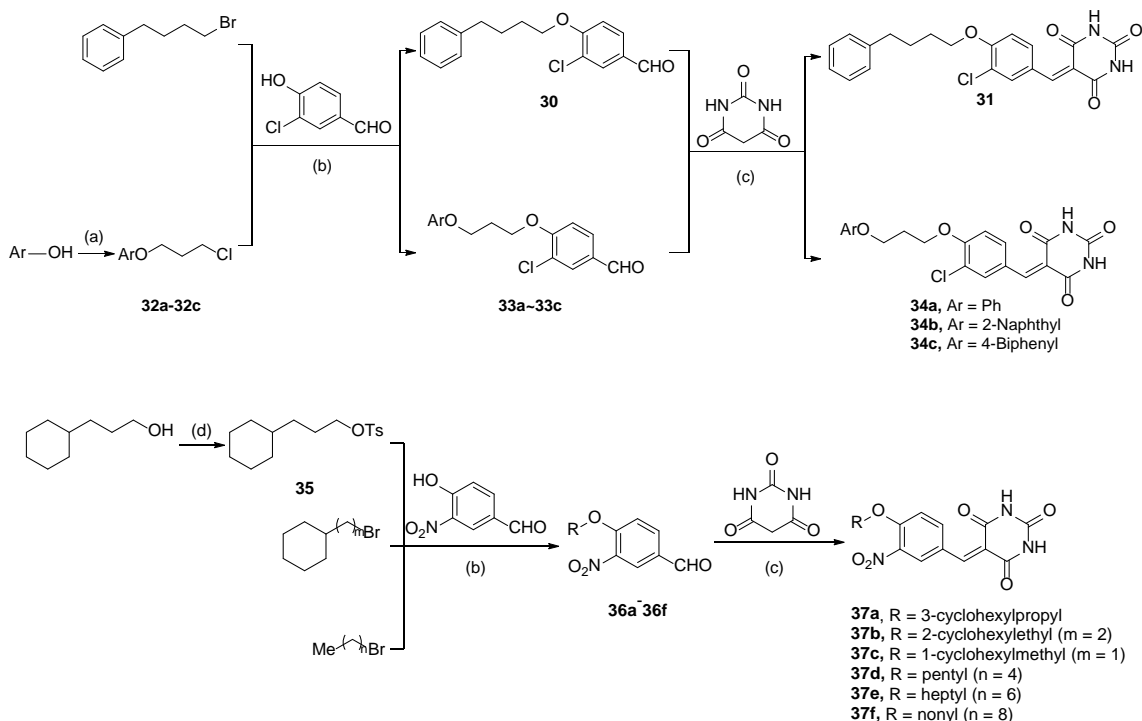
Compound	Inhibition of mPGES-1	
	IC ₅₀ (human, nM) ^a	IC ₅₀ (mouse, nM)
27a	272±30	n.d. ^b (8) ^c
27b	427±55	n.d. (24)
27c	561±55	n.d. (15)
29a	28±3	239±72
29b	20±5	415±21
29c	53±14	n.d. (49)

^aData are expressed as means ± SD of single determinations obtained in triplicate. ^bn.d. = not detected. ^cThe data in the parentheses refer to the % inhibition of the compound at a concentration of 10 μM against mPGES-1. The IC₅₀ values were determined if the compound cause significant inhibition at 10 μM (≥ 70%).

2.3.3 SAR on the side chain

The length, shape and the substitution pattern of the aliphatic side chain were also investigated. The terminal cyclohexyl or cyclohexylmethyl group in **25b** was replaced by phenyl (**31**) and aryloxy groups (**34a–34c**). Compound **31** remained active against human mPGES-1 but lost the potency against the mouse enzyme by 18 folds. The presence of

terminal aryloxy groups on the side chain was remarkably detrimental to the maintenance of the inhibitory activity. A plausible explanation is that the presence of oxygen atom on the side chain impairs the hydrophobic interaction of the compound with the enzyme, as discussed later in the computational part. The impact of “tail” length on the mPGES-1 inhibition was investigated in compound group of **25h** and **37a–37c** ($IC_{50} = 67$ nM, 156 nM, 517 nM and 1114 nM for compounds **25h**, **37a**, **37b** and **37c** respectively). One methylene group (CH_2) was “cut off” from the former on the side chain of each compound. The rank order of potency was in accordance with the length of the “tail”: greater inhibition favored longer “tail”. Similarly, compounds with linear side chains (**37d–37f**) also followed the rank order, as shown Table 2-3. The synthetic protocol of these compounds with a range of side chains are described in Scheme 2-3.



Scheme 2-3. Synthetic protocol of substituted benzylidenebarbituric acid derivatives with various aliphatic side chains. Reagents and conditions: (a) K_2CO_3 (2.0 equiv.), acetone, reflux, 89–92%; (b) K_2CO_3 (2.0 equiv.), DMF, 80 °C, 71–96%; (c) EtOH/H₂O (4:1, v/v), reflux, 78–95%; (d) *p*-Toluenesulfonyl chloride (1.20 equiv.), 50% KOH aq., DCM, 0 °C→rt, 67%.

Table 2-3. SAR on the aliphatic side chain.

Compound	Inhibition of mPGES-1	
	IC ₅₀ (Human, nM) ^a	IC ₅₀ (Mouse, nM)
31	73±10	2788±525
34a	349±40	n.d. ^b (52) ^c
34b	337±34	n.d. (17)
34c	365±59	n.d. (19)
37a	156±30	373±51
37b	517±68	2395±425
37c	1114±104	n.d. (42)
37d	460±64	n.d. (62)
37e	232±54	734±119
37f	188±43	1303±163

^aData are expressed as means ± SD of single determinations obtained in triplicate. ^bn.d. = not detected. ^cThe data in the parentheses refer to the % inhibition of the compound at a concentration of 10 μM against mPGES-1. The IC₅₀ values were determined if the compound cause significant inhibition at 10 μM (≥ 70%).

2.4 *In vitro* activities and selectivity

All the synthesized compounds were first screened at a single concentration of 10 μM for the calculation of percentage of inhibition against both human and mouse mPGES-1 enzymes. Compounds caused significant inhibition (≥ 70%) were further tested for their IC₅₀ values. MK-886, a well-recognized human mPGES-1 inhibitor, was used as a reference compound for which we obtained IC₅₀ = 2.6 ± 0.6 μM, which is close to the previously reported IC₅₀ values (IC₅₀ = 1.6 μM,^[42] and 2.4±0.3 μM^[66a]) without significant inhibition of mouse mPGES-1. The concentration-dependent curves of compound **25b** against human and mouse mPGES-1 enzymes are shown in Fig. 2-2.

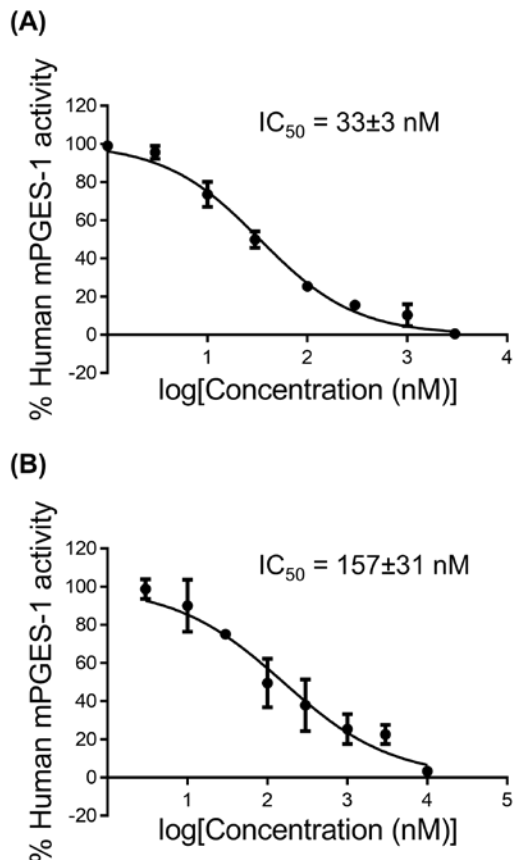


Fig. 2-2. Concentration-dependent curves of compound **25b** against human and mouse mPGES-1 enzymes. (A) Concentration-dependent inhibition of human mPGES-1 ($n = 3$); (B) Concentration-dependent inhibition of mouse mPGES-1 ($n = 3$).

Next we wanted to know whether these compounds have significant inhibitory activities against either COX-1 or COX-2. For this purpose, some of the more potent compounds with IC_{50} values less than 100 nM) were assayed for their potential inhibitory activities against mixed COX-1 and COX-2 (denoted as COX-1/2) with equal amounts of COX-1 and COX-2 in terms of the enzyme activities. The protein preparation and purification and the protocol for *in vitro* activity assays followed our previous reports.^[76-77] The data shown in Table 2-4 demonstrated that among all the 14 compounds tested, only **25c**, **25m**, **25n**, **29d**, **29e** and **31** caused an inhibition greater than 50% at a concentration as high as 100 μ M, most of these compounds caused less than 50% inhibition, including the most potent compounds **25b** (4.3%) and **25i** (2.6%).

Table 2-4. Inhibition against COX-1/2 of selected compounds.

Compound	% Inhibition at 100 μM^a
25b	4 \pm 6
25c	63 \pm 1
25d	9 \pm 7
25h	43 \pm 3
25i	3 \pm 7
25j	17 \pm 5
25k	15 \pm 3
25m	56 \pm 4
25n	71 \pm 5
29d	93 \pm 2
29e	79 \pm 3
29f	18 \pm 1
31	53 \pm 4

^aThe % inhibition of the compound at a concentration of 100 μM against the COX-1/2 (mixed COX-1 and COX-2). The enzyme mixture contained equal amounts of COX-1 and COX-2 in terms of their enzyme activities. In this way, when a compound can significantly inhibit either COX-1 or COX-2, it will show significant inhibitory effects against the mixed COX-1 and COX-2. The error bars were given by the program of GraphPad Prism 7.

2.5 Enzyme-inhibitor binding modes

To further elucidate the SAR of this series of compounds, we performed molecular docking study of **25b**, one of the most potent barbituric acid derivative inhibiting both human and mouse mPGES-1 enzymes with nanomolar potencies without significant inhibition against COX isozymes, using the AutoDock 4.2 program.^[78] The binding modes of **25b** with both human and mouse mPGES-1 enzymes were investigated, as depicted in Fig. 2-3B and Fig. 2-3C, respectively. As predicted, compound **25b** binds in a conserved region of the active site of both human and mouse mPGES-1 enzymes. For human mPGES-1 (PDB ID: 4BPM), the conserved region is nearby S127 and has a hydrophobic pocket surrounded by Y28, I32, G35, L39, Y130, T131, L135, and A138. Only a few amino acid residues in mouse

mPGES-1 differentiate from the human enzyme in this conserved region, where V32, V131, and F138 take over I32, T131, and A138 respectively. The hydrogen bonding interaction between the barbituric acid carbonyl group and the hydroxyl groups of S127 is crucial for the compound to maintain the inhibitory potency. As discussed in the SAR study, replacement of the amide hydrogens on the barbituric acid with two methyl groups significantly lowers the inhibitory potency, which might result from the impairment of hydrogen bonding. The substituted alkoxy on the side chain occupies the hydrophobic groove where the long hydrocarbon “tail” of PGH₂ locates. The longer and bulkier side chains are favored as they match the size and shape of the hydrophobic pocket better. Aryloxy substitution on the side chain greatly lowers the inhibition not only because of oxygen atom that impairs the hydrophobic interaction, but also the rigidity of aryl groups that hampers structural complementarity.

In addition, we obtained $IC_{50} = 1.5$ nM for MF63 against human mPGES-1 and MF63 at 10 μ M had no significant inhibition against mouse mPGES-1, which is consistent with the previously reported data showing that MF63 potently inhibited human mPGES-1 ($IC_{50} = 1.3$ nM) without significant activity against the mouse or rat enzyme.^[45] For comparison, we also investigated the binding of MF63 with mPGES-1 and tried to propose a plausible explanation of this selectivity. As predicted in Fig. 2-3D, the NH group on the imidazole ring of H53 of human mPGES-1 forms a hydrogen bond with one aromatic nitrogen atom on MF63. As we transferred the structure of MF63 from Fig. 2-3D to mouse mPGES-1 (Fig. 2-3E), the same hydrogen bond between H53 and MF63 does not exist as amino acid residue R53 in mouse mPGES-1 (which is H53 in the human enzyme) almost overlap with the ligand structure. The binding of MF63 with unique residue in human mPGES-1 makes it inactive against the mouse enzyme.

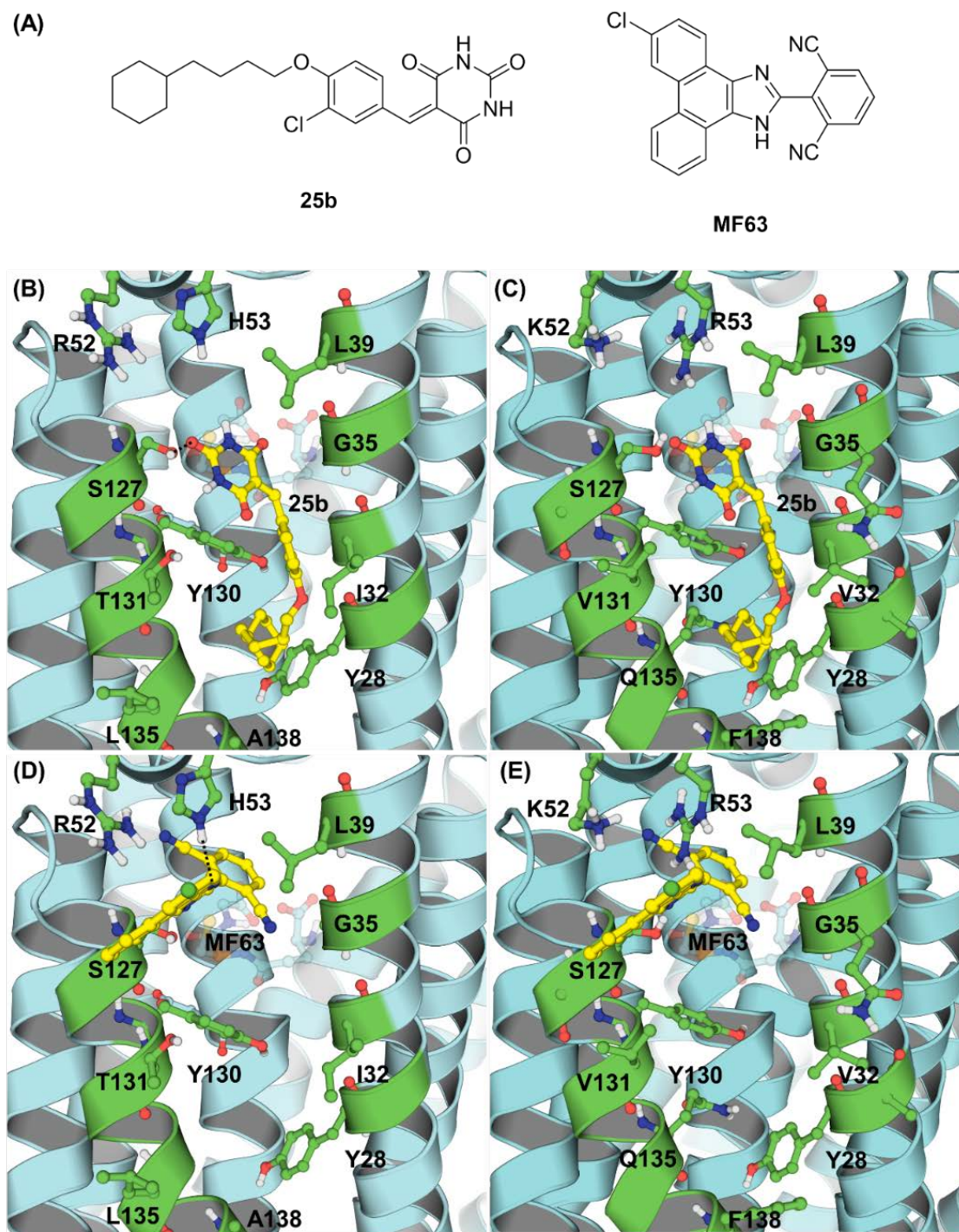


Fig. 2-3. Molecular structures of **25b** and MF63 and their binding with human and mouse mPGES-1 enzymes. (A) Ligand structures of **25b** and MF63; (B) binding of **25b** with human mPGES-1; (C) binding of **25b** with mouse mPGES-1; (D) binding of MF63 with human mPGES-1; (E) hypothetical binding structure of mouse mPGES-1 with MF63 after human mPGES-1 structure in panel D is replaced by mouse mPGES-1 structure.

2.6 *In vivo* anti-inflammatory activity

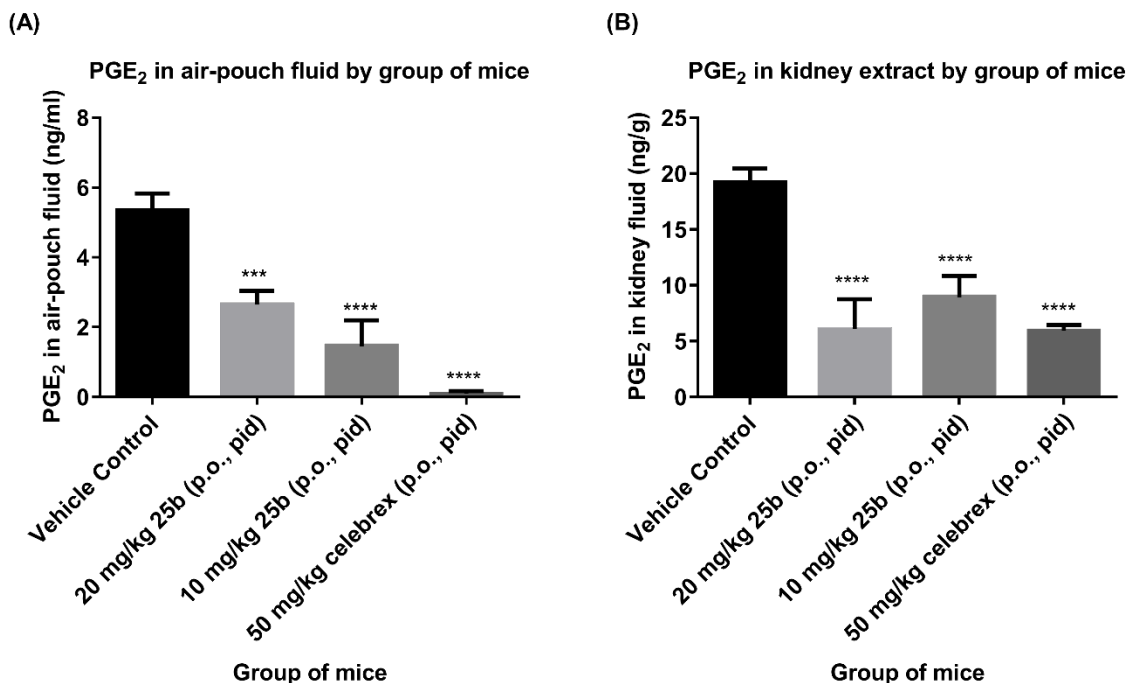


Fig. 2-4. Data from *in vivo* assays using the mouse carrageenan air-pouch model of inflammation (n = 4 each group) with **25b** or celecoxib dosed orally. (A) the effectiveness of **25b** in reducing PGE₂ level in air-pouch fluid; (B) the effectiveness of **25b** in reducing PGE₂ level in kidney (assayed for PGE₂ by ELISA and expressed as Mean ± SEM). Statistical results from the one-way ANOVA analysis of the data in panel A with *post hoc* tests: $p = 0.0003$ for Vehicle Control vs 20 mg/kg **25b** (p.o., bid); $p < 0.0001$ for Vehicle Control vs 10 mg/kg **25b** (p.o., bid); and $p < 0.0001$ for Vehicle Control vs 50 mg/kg celecoxib (p.o., pid). Statistical results from the one-way ANOVA analysis of the data in panel B with *post hoc* tests: $p < 0.0001$ for Vehicle Control vs 20 mg/kg **25b** (p.o., bid); $p < 0.0001$ for Vehicle Control vs 10 mg/kg **25b** (p.o., bid); and $p < 0.0001$ for Vehicle Control vs 50 mg/kg celecoxib (p.o., pid).

To examine the anti-inflammatory potential of **25b**, we determined the *in vivo* effectiveness of **25b** in the most popularly used mouse air-pouch model of inflammation in comparison with celecoxib. The air-pouch model of inflammation is widely used for determining the *in vivo* effectiveness of inhibitors of prostaglandin synthesis. Air pouches were produced by duplicate injections of 3 mL of sterile air under the skin on the back of mice. After the formation of the air-pouch, a single injection of the inflammatory reagent λ -carrageenan into the pouch resulted in the recruitment of inflammatory cells and the production of a fluid exudate containing significant levels of PGE₂ (an inflammatory marker) produced

primarily by activities of COX-2 and mPGES-1. Then, the mice were orally administered with a single dose of **25b**, celecoxib, or vehicle for 24 hours prior to collection of air-pouch fluid and the kidney samples. The air-pouch fluid and kidney samples were analyzed for PGE₂ by the same ELISA method used in the *in vitro* enzyme activity assay mentioned above. As mPGES-1 is more abundant in kidney, we examined the effects of **25b** and celecoxib on the PGE₂ level in kidney. Depicted in Fig. 2-4A and Fig. 2-4B are the measured PGE₂ levels in air-pouch fluid samples and kidney extract samples.

As shown in Fig. 2-4A, compound **25b** administered p.o. at each dose (20 or 10 mg/kg) condition significantly decreased the PGE₂ levels in the mouse air-pouch fluid samples ($p = 0.0003$, $p < 0.0001$, and $p < 0.0001$, respectively), although the effectiveness was not as good as 50 mg/kg celecoxib with the same dosing method. Further, according to Fig. 2-4B, compound **25b** was also capable of reducing the PGE₂ levels in kidney ($p < 0.0001$, $p < 0.0001$, and $p < 0.0001$, respectively) as compared to vehicle control. Although the dose-dependence was not quite obvious, no significant difference was observed between 20 mg/kg **25b** with 50 mg/kg celecoxib and between 10 mg/kg **25b** with 50 mg/kg celecoxib, respectively ($p = 0.9994$ and $p = 0.2244$).

2.7 Acute toxicity/safety of **25b**

Finally, we also tested acute toxicity/safety of **25b** in comparison with celecoxib. In fact, 50 mg/kg celecoxib administered p.o. were very toxic for stomach and other issues of mice, and bleeding ulcer was observed at gastric mucosa. In comparison, a high dose (up to 1 g/kg) of **25b** administered p.o. did not cause any toxic sign in mice during our observation for 14 days. Depicted in Fig. 2-5 are representative images of the stomach tissues collected from mice at 24 hour after the PO administration of vehicle or **25b** or celecoxib. For all mice in the vehicle, the stomach samples were used as standard for comparison with **25b** dosed and celecoxib dosed groups. In the 2nd group dosed with a high dose of **25b** (1 g/kg), we did not detect any bleeding spot on the inner side of stomach samples. Meanwhile, for each mouse in the celecoxib group, we were able to clearly see at least one bleeding spot, as labeled in red circles.

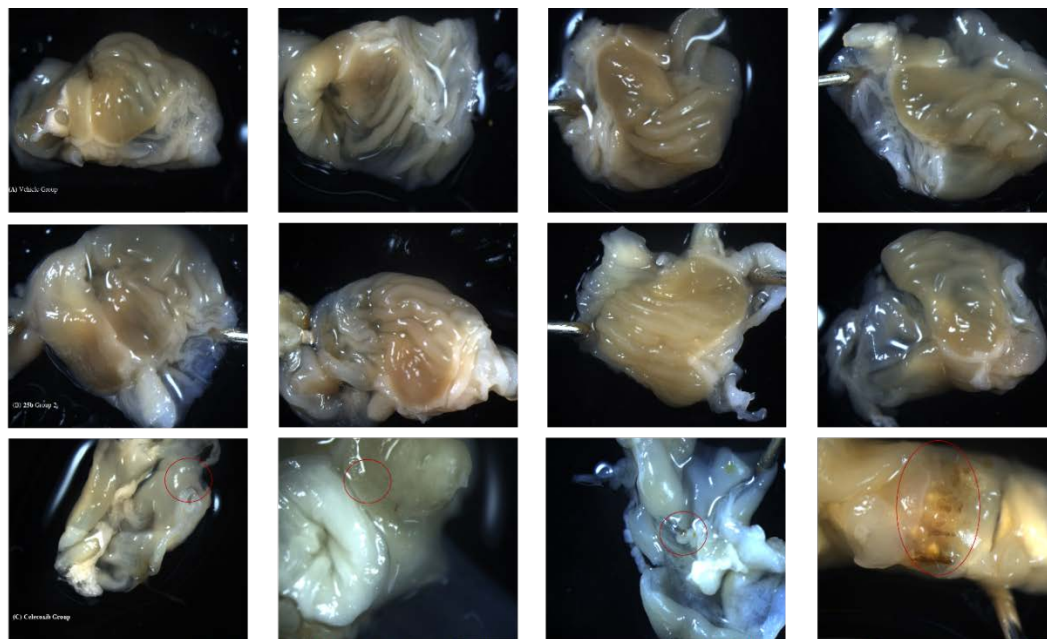


Fig. 2-5. Representative images of stomach tissues collected from mice at 24 h after oral administration of (A) vehicle (oil) or (B) **25b** (1 g/kg in oil) or (C) celecoxib (50 mg/kg in oil). For all mice in the vehicle and **25b** groups, we did not find any bleeding spot on the inner side of stomach samples. Meanwhile, for each mouse in the celecoxib group, we were able to clearly see at least one bleeding spot; the bleeding points are labeled in red circles.

2.8 Conclusion

As well known, inflammation is related to many types of diseases, and mPGES-1 was recognized as the most promising target for developing the highly desirable next generation of anti-inflammatory drugs without the adverse side effects of currently used COX inhibitors. The promise of mPGES-1 as the target was based on understanding of the physiological process and biosynthesis of the pro-inflammatory compound PGE₂, and was supported strongly by the mPGES-1 gene knock-out studies. It is well known that mouse/rat models of inflammation-related diseases have been well-established, enabling to test a potentially promising anti-inflammatory drug candidate in the established mouse/rat models of inflammation-related diseases. Unfortunately, despite of extensive efforts to design and discover various human mPGES-1 inhibitors and the fact that numerous potent inhibitors of human mPGES-1 have already been reported in the literature,

the promise of mPGES-1 as a target for the next generation of anti-inflammatory drugs has never been demonstrated in any wild-type mouse/rat model using an inhibitor of mPGES-1 because none of the previously discovered human mPGES-1 inhibitors can potently inhibit mouse/rat mPGES-1. Without a dual inhibitor (against both human and mouse mPGES-1 enzymes) available, one has to explore alternative animal models by using either other animal species that are less popular for use as animal models of inflammation-related diseases or mPGES-1 gene knock-out/knock-in mice expressing human mPGES-1 instead of mouse mPGES-1. For example, Merck developed the first strain of mPGES-1 gene knock-out/knock-in mice expressing human mPGES-1 instead of mouse mPGES-1. But interpretation of the animal data with the knock-in mice is complicated due to the difference between the original mouse gene and knock-in gene in the localization and amount. So, there is still no clinically useful mPGES-1 inhibitor developed so far. Reported here is the first demonstration that a potent human mPGES-1 inhibitor has potent *in vivo* activity in wild-type mice-based air-pouch model of inflammation. So, we are able to demonstrate in wild-type mice that mPGES-1 is truly a promising target for the next generation of anti-inflammatory drugs.

In this study, we successfully designed, synthesized and conducted biological evaluation of a series of substituted benzylidenebarbituric acid derivatives as inhibitors against both human and mouse mPGES-1 enzymes. A number of the compounds were prepared were capable of inhibiting both enzymes with submicromolar potency without concomitant inhibition against COX isozymes. In addition, selected compound **25b** was further evaluated using wild-type based mouse models of inflammation, the carrageenan air-pouch experiment and the results showed that **25b** administered orally with both doses (20 mg/kg and 10 mg/kg) significantly reduced the PGE₂ levels in both air-pouch fluid and kidney extract samples. The computational chemistry including the generation of simulated 3D structure of mouse mPGES-1 and the docking study were performed by Shuo Zhou and Dr. Yaxia Yuan. The *in vitro* assays were conducted by Dr. Ziyuan Zhou. Animal procedures were performed according to Dr. Charles Loftin's guidance and assisted by Xirong Zheng, Drs. Ting Zhang and Jianzhong Chen.

In general, a traditional drug discovery and development effort is usually focused on

identification of ligands of a human protein target without accounting for the species difference in target protein during the early drug design and discovery stage before finding out that the ligands identified *in vitro* are actually inactive in the *in vivo* animal models. Our study demonstrates a more effective strategy of drug design and discovery to rationally design a dual inhibitor of human and animal target proteins. The general strategy of our structure-based rational design of a dual inhibitor of the human and mouse mPGES-1 enzymes may also be used for other drug targets with significant species differences in the binding pocket.

Chapter 3 (Z)-5-(2-oxoindolin-3-ylidene)thiazolidine-2,4-dione derivatives as potent inhibitors against both human and mouse mPGES-1 enzymes: rational design, synthesis, *in vitro* assays and *in vivo* evaluation

Part of the results described in this chapter has been submitted for consideration of publication (“(Z)-5-(2-oxoindolin-3-ylidene)thiazolidine-2,4-dione derivatives as potent inhibitors against both human and mouse mPGES-1 enzymes: rational design, synthesis, *in vitro* assays and *in vivo* evaluation”, to be published).

3.1 Dual human/mouse mPGES-1 inhibitors enabling preclinical testing in wild-type mice

Currently available treatments for inflammation-related symptoms rely heavily on traditional non-steroidal anti-inflammatory drugs (tNSAIDs) and coxibs, by either non-selectively inhibiting COX isozymes,^[9] or specifically inhibiting COX-2,^[10b] respectively. Both categories of drugs exert anti-inflammatory efficacy by indirectly modulating the production of PGE₂. However, long-term application of tNSAIDs cause ulceration and bleeding in the gastrointestinal (GI) tract due to disturbance of the COX-1-derived protective function.^[79] Coxib application, on the other hand, interferes with the intrinsic balance between vasodilative prostacyclin and vasoconstrictive thromboxane A₂ and thus renders cardiovascular risk.^[14, 80] As several coxibs were withdrawn from the US market,^[9] the direct modulation of PGE₂ production, specifically the inhibition of inducible mPGES-1, has emerged as an attractive therapeutic approach in the development of a new generation of anti-inflammatory drugs. As continued efforts in the development of dual human/mouse mPGES-1 inhibitors, we further designed, synthesized, and biologically evaluated a series of (Z)-5-(2-oxoindolin-3-ylidene)thiazolidine-2,4-dione (isatin-thiazolidine-2,4-dione backbone) derivatives as potent inhibitors against both human and mouse mPGES-1 enzymes. Some of the compounds, such as **44d** (IC₅₀ = 121 nM and 947 nM for human and mouse mPGES-1 enzymes, respectively) and **52e** (IC₅₀ = 25 nM and 685 nM, respectively), were capable of inhibiting both enzymes with submicromolar potency without concomitant inhibition of COX isozymes (≤ 50 % inhibition at a concentration of 100 μM). Following *in vitro* assays, **52e** was selected as a candidate for *in vivo* evaluation in mice. A pilot mouse carrageenan air-pouch experiment was performed

with double doses of **52e** in its meglumine salt form (**52e-MEG**), which indicated that **52e** was effective in reducing PGE₂ levels in both air-pouch fluid and kidney extract as compared to negative vehicle control.

3.2 Design of the (*Z*)-5-(2-oxoindolin-3-ylidene)thiazolidine-2,4-dione (isatin-thiazolidine-2,4-dione backbone) derivatives

The design of novel inhibitors also started from the molecular docking of compound **19** (Fig. 3-1A) with the human mPGES-1 crystal structure (PDB ID: 4BPM).^[35] The (*Z*)-5-benzylidene-2-iminothiazolidine-4-one derivative **19** was identified as an active human mPGES-1 inhibitor through structure-based virtual screening in our previous work.^[76] Although with moderate inhibitory potency (IC₅₀ = 3.5 μM), it is suggested to bind in a conserved region of the active site in both human and mouse mPGES-1 enzymes, as predicted by the binding mode (Fig. 3-1B). This conserved region is close to amino acid residues S127, side chains of Y28, I32, G35, L39, Y130, T131, L135 and A138 constitute the major hydrophobic pocket in human mPGES-1. In the mouse enzyme, only a few amino acid residues differ from human mPGES-1, where I32, T131 and A138 are replaced by V32, V131 and F138, respectively. Instead of replacing the thiazolidine-2,4-dione with barbituric acid as we did in our previous reports,^[77a, 77b] we kept thiazolidine-2,4-dione *N*-acetic acid in order to maintain the polar interaction with the enzyme while removing the phenyl from the original structure as it might hamper the hydrogen-bond formation. Isatin (2,3-indolinedione) was introduced as the central core not only because of its existence as a substructure in many bioactive molecules, but also its versatility for multifunctionalization.^[81] Similarly, a flexible hydrophobic “tail” was attached to the central isatin, as we did in the previous series of inhibitors.^[77a, 77b] Compounds with isatin-thiazolidine-2,4-dione backbone were thus designed, in which **44d** was selected as an example structure for the docking study. As shown in Fig. 3-1C, compound **44d** binds in a similar region as **19**, and this region is largely conserved in mouse mPGES-1, indicating that the designed inhibitors might also inhibit the mouse enzyme. In addition, while **19** binds with human mPGES-1 with moderate affinity, compound **44d** is predicted to bind more favorably with the enzyme, as a hydrogen bond is observed between the carboxylic carbonyl group of **44d** with the NH group of R52.

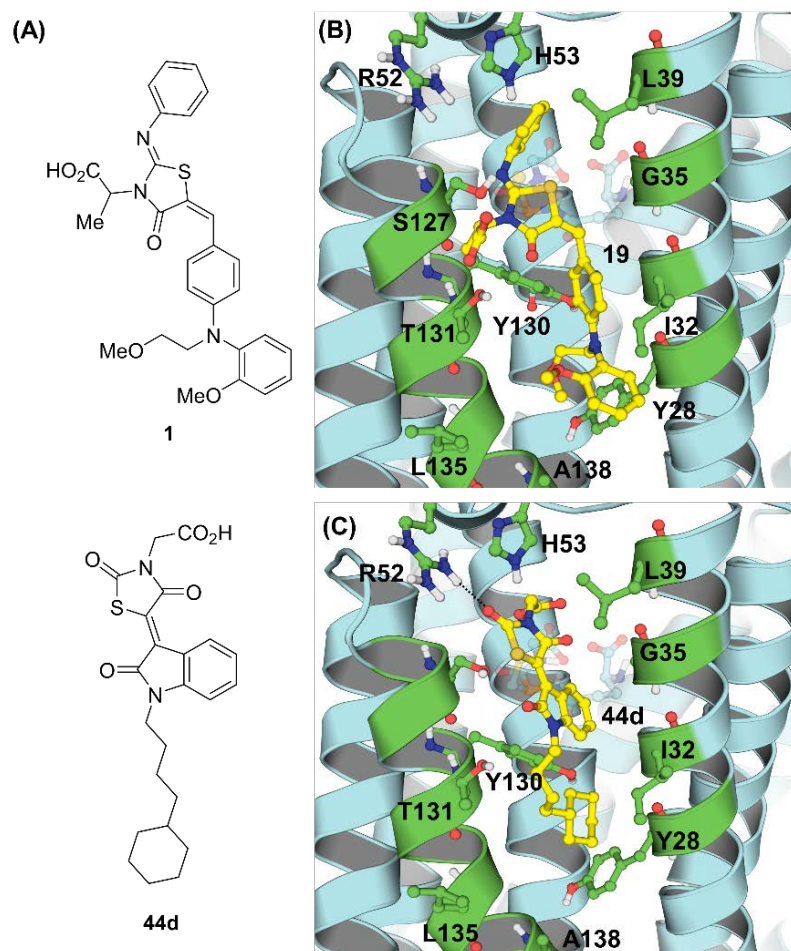


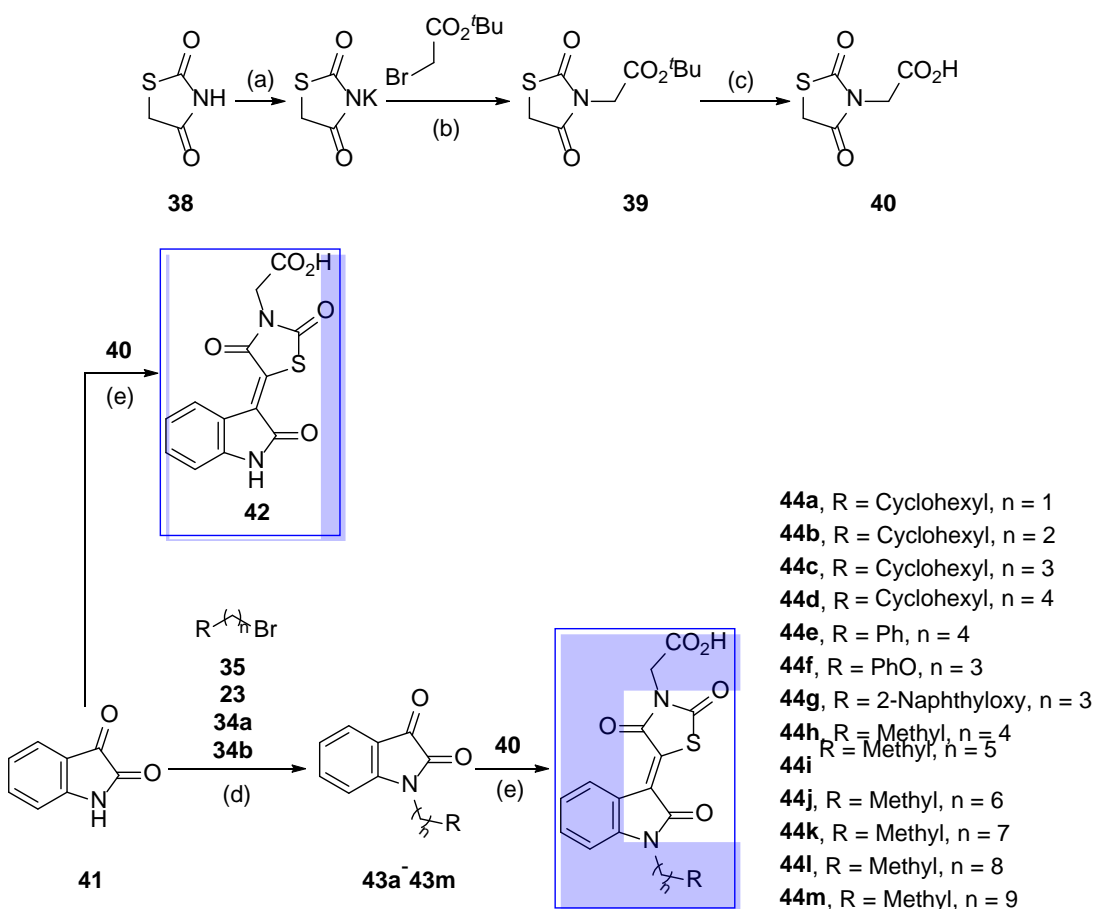
Fig. 3-1. Molecular structures of the lead **19**, designed inhibitor **44d** and their binding with human mPGES-1. (A) Ligand structures; (B) binding with the lead **19**; (C) binding with **44d**.

3.3 Chemistry and SAR study

3.3.1 SAR on 1-substituted isatin derivatives

In the SAR study, we mainly investigated the substitution at isatin-1(*N*)-position and its impact on inhibitory potency. The synthetic protocol of these compounds with a range of side chains is outlined in Scheme 3-1. Commercially available thiazolidine-2,4-dione (**38**) and isatin (**41**) were used as starting materials to construct the building blocks of 2-(2,4-dioxothiazolidin-3-yl)acetic acid (2,4-thiazolidinedione *N*-acetic acid **40**) and 1-substituted isatins (**43a–43m**). After treating **38** with excess potassium hydroxide in hot ethanol, the potassium salt of **38** was precipitated and filtered off.^[82] This salt was reacted with *tert*-

butyl bromoacetate for *N*-substitution. The cleavage of the *tert*-butyl ester (**39**) in trifluoroacetic acid/dichloromethane (1:1, *v/v*) at room temperature led to the formation of the important thiazolidine-2,4-dione based building block (**40**).^[83] The 1-substituted isatins were prepared by the reaction of isatin with alkyl bromides, alcohol tosylates (**23** and **35**)^[84] and alkyl chlorides (**34a** and **34b**)^[85] in the presence of excess potassium carbonate as acid capturer. The obtained 1-substituted isatins (**43a–43m**) and isatin (**41**) were then condensed with **40** catalyzed by ammonium acetate in glacial acetic acid at 108 °C, yielding the final products (**44a–44m** and **42**) with isatin-thiazolidine-2,4-dione backbone.



Scheme 3-1. Synthesis of 1-substituted isatin derivatives. Reagents and conditions: (a) KOH, EtOH, 55 °C, 74%; (b) acetone, reflux, 82%; (c) TFA/DCM (1:1, *v/v*), rt, 97%; (d) 50% KOH, aq., DCM, 0 °C→rt, 83–90%; (e) acetone, reflux, 89–92%; (f) K₂CO₃, DMF, rt, 70–87%; (g) NH₄OAc, glacial AcOH, 108 °C, 38–85%.

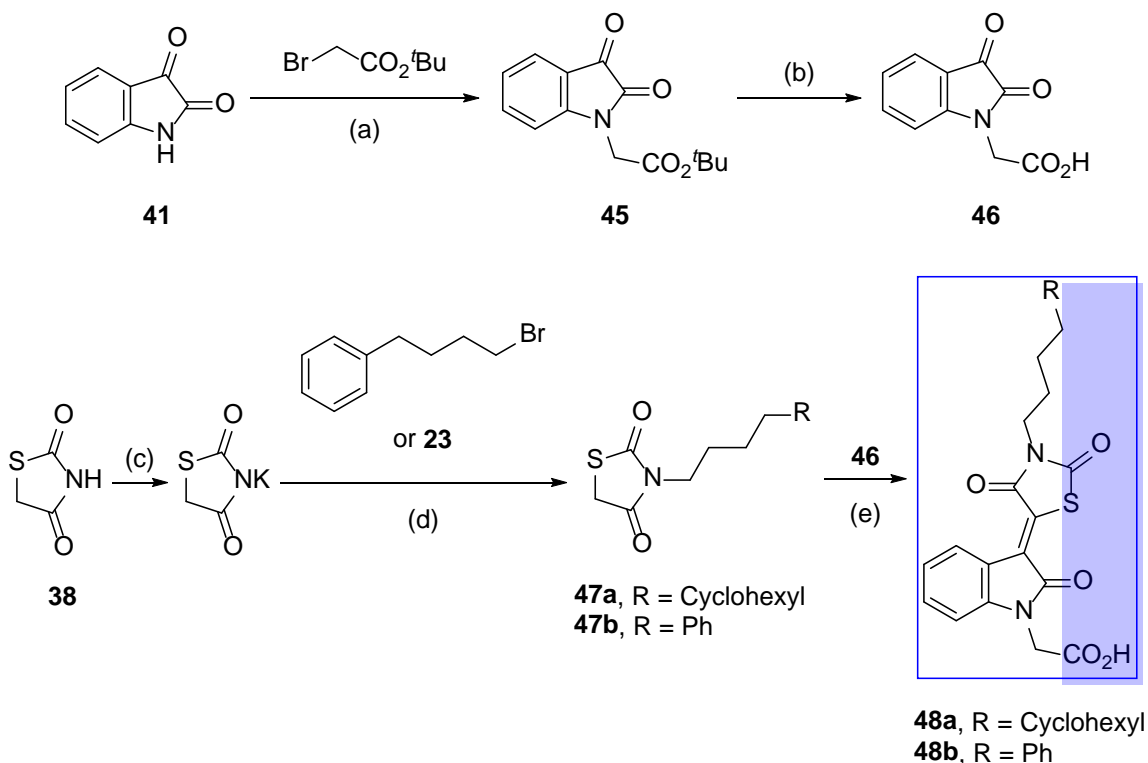
Table 3-1. SAR on 1-Substituted isatin derivatives.

Compound	Inhibition of mPGES-1	
	IC ₅₀ (Human, nM) ^a	IC ₅₀ (Mouse, nM)
42	n.d. ^b (5) ^c	n.d. (10)
44a	1269±104	2728±422
44b	494±32	n.d. (39)
44c	253±30	1518±317
44d	121±25	947±183
44e	963±87	n.d. (61)
44f	805±100	n.d. (41)
44g	1681±168	1023±131
44h	1661±168	n.d. (35)
44i	1073±116	n.d. (57)
44j	324±44	n.d. (67)
44k	314±44	2676±302
44l	199±32	1398±217
44m	217±30	935±135
48a	2560±442	n.d. (64)
48b	962±159	n.d. (44)

^aData are expressed as means ± SD of single determinations obtained in triplicate. ^bn.d. = not determined. ^cThe values in the parentheses refer to the % inhibition of the compound at a concentration of 10 μM against the mPGES-1 enzyme (IC₅₀ values were determined only for the compounds that showed ≥70% inhibition at 10 μM).

The inhibitory potencies against human and mouse mPGES-1 enzymes are shown in Table 3-1. The presence of a hydrophobic substituent at isatin-1-position is of great importance for the compound to gain inhibitory efficacy. Without a substituent, compound **40** was not active against either enzyme. In compound group **44a–44d**, one methylene group (CH₂) was “inserted” into the alkyl chain, with the same cyclohexyl as terminal group. The increased length of the side chain was in accordance with the progressively enhanced inhibitory potency against human and mouse mPGES-1. With bulky cyclohexylbutyl substituted at isatin-1-position, compound **44d** was capable of inhibiting both human and

mouse mPGES-1 enzymes with submicromolar potency ($IC_{50} = 121$ nM and 947 nM for human and mouse mPGES-1 enzymes, respectively). With phenyl, phenoxy and 2-naphthoxy replacing the terminal cyclohexyl or cyclohexylmethyl groups, compounds **44e**, **44f** and **44g** resulted in an 8-fold, 7-fold, and 14-fold decrease in inhibitory potency as compared with **44d**, respectively. Substitution with linear side chains were also investigated in compound group **44h–44m**. In general, the rank order of inhibitory potency was in accordance with the length of the side chain. But compounds with an extremely long aliphatic side chain, such as **44l** and **44m** with nonyl and decyl substitution, were comparable in potency against human mPGES-1 ($IC_{50} = 199$ nM and 217 nM, respectively).



Scheme 3-2. Synthesis of 1-substituted isatin derivatives with reversed polarity. Reagents and conditions: (a) K_2CO_3 , DMF, rt, 77%; (b) TFA/DCM (1;1, v/v), rt, 99%; (c) KOH, EtOH, 55 °C, 72%; (d) acetone, reflux, 82–89%; (e) NH_4OAc , glacial AcOH, 108 °C, 68–74%.

We also tried to switch the positions of hydrophilic “head” and hydrophobic “tail”. In this case, isatin-based building block 2-(2,3-dioxindolin-1-yl)acetic acid (isatin-*N*-acetic acid **46**)^[86] and *N*-substituted thiazolidine-2,4-diones (**47a–47b**)^[87] were prepared respectively.

These two building blocks were then condensed in the presence of ammonium acetate in glacial acetic acid at 108°C to accomplish the preparation of the final products (**48a–48b**) with reversed positions of hydrophobic and hydrophilic moieties. The synthetic protocol of **48a–48b** is depicted in Scheme 3-2. Compared to the “standard” compound **44d**, compound **48a** was 20 times less potent against human mPGES-1. Although **48b** was comparably potent as compared to **44e** in inhibiting human mPGES-1, both **48a** and **48b** were not quite as active for the mouse enzyme. We still focused on the structure as **44d**.

3.3.2 SAR on 1,5-disubstituted isatin derivatives

In the aforementioned SAR study, we successfully identified two compounds (**44d** and **44m**) inhibiting both human and mouse mPGES-1 enzymes with submicromolar potency. As we carefully analyzed the binding mode of **44d** with the human mPGES-1 crystal structure (Fig. 3-1C), we discovered a substantial unoccupied area at the active site, specifically the small hydrophobic pocket above the cofactor glutathione (GSH) of the enzyme and around the central isatin ring of the inhibitor. Therefore, another substituted group at isatin-5-position was introduced to occupy this small hydrophobic pocket. With the same thiazolidine-2,4-dione *N*-acetic acid (**40**) as polar “head” and cyclohexylmethyl as 1-substituent, we varied the substituent at isatin-5-position. The synthetic protocol of these compounds is outlined in Scheme 3-3. Commercially available 5-iodoisatin (**49**) was used as starting material to prepare the building block of 1,5-disubstituted isatins (**52a–52e**). The 1-substitution was first carried out by the reaction of **49** with (bromomethyl)cyclohexane in the presence of excess potassium carbonate as acid capturer.^[88] The resulting 1-substituted-5-iodoisatin (**50**) was then coupled with various aryl boronic acids *via* Suzuki coupling (**51a–51c**),^[89] or with terminal alkynes *via* Sonogashira coupling (**51d–51e**),^[90] respectively. The final products, 1,5-disubstituted isatin derivatives (**52a–52e**) were prepared by the ammonium acetate-catalyzed condensation of isatin-based building blocks (**51a–51e**) with thiazolidine-2,4-dione-based building block **40**. The inhibitory potency data were summarized in Table 3-2. Compared with the corresponding 1-substituted isatin derivative **44a**, the introduction of all phenyl, 4-biphenyl and 2-naphthyl groups at the 5-position enhanced the inhibitory potency against human mPGES-1 by about 6-, 8-, and 2-fold. Moreover, compounds with phenylethynyl

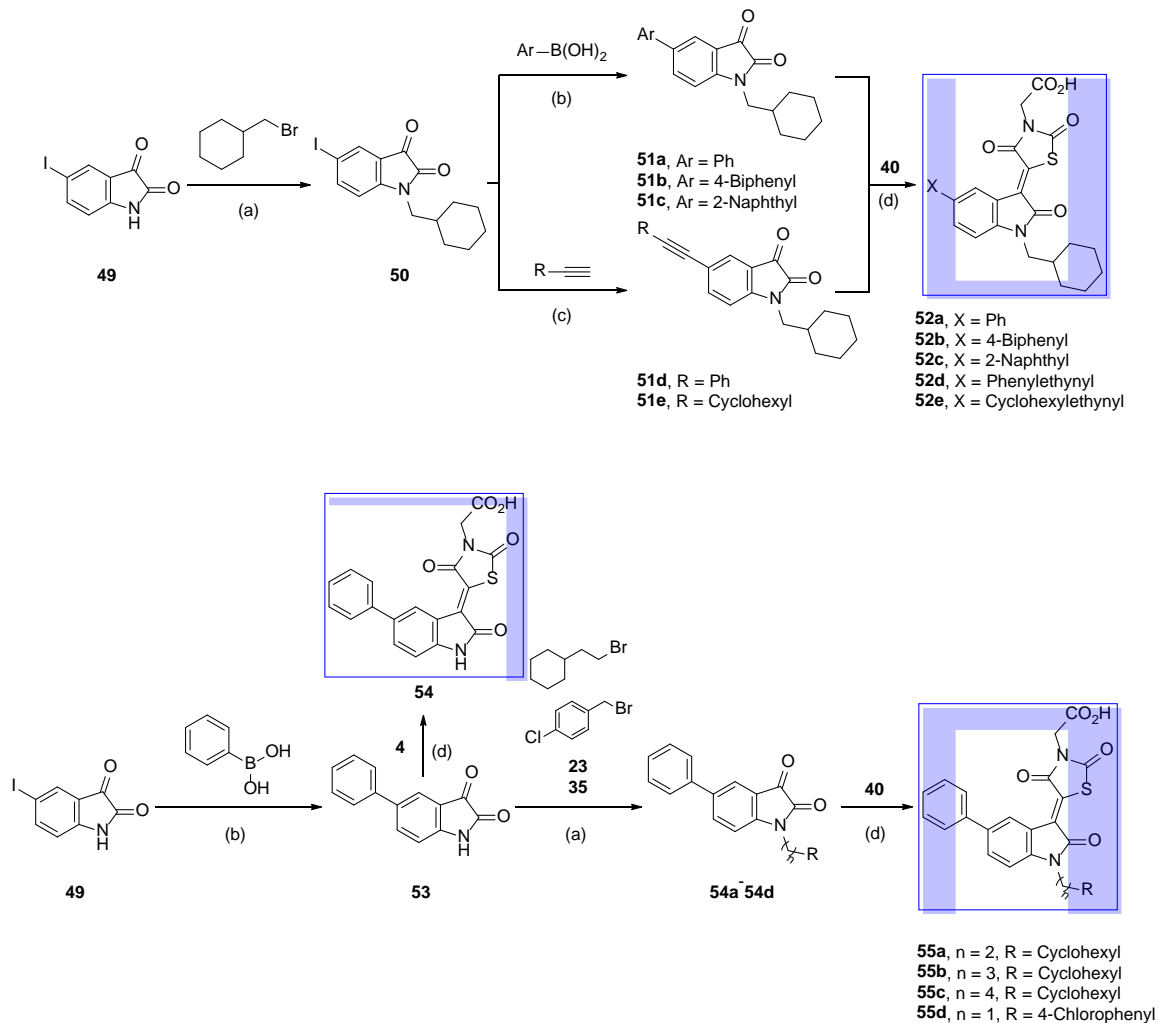
(**52d**) and cyclohexylethynyl (**52e**) substituted at isatin-5-position were identified as low nanomolar human mPGES-1 inhibitors ($IC_{50} = 91$ nM and 25 nM, respectively). In the follow-up SAR study, we fixed phenyl as the 5-substituent and varied the substitution at isatin-1-position. The synthetic protocol was slightly modified, with Suzuki coupling of 5-iodoisatin (**49**) and phenylboronic acid (5-substitution) as the first step, followed by the substitution at isatin-1-position, and the subsequent condensation with **40**. Without substitution at the 1-position, the inhibitory potency was greatly impaired. Compared to **44a**, compound **54** was 36-fold less potent against human mPGES-1. In compound group **52a**, and **55a–55c**, one methylene (CH_2) group was “inserted” into the former structure in the side chain, the inhibitory potency was enhanced along with the increased length of the side chain. With 4-cyclohexylbutyl substituted at isatin-1-position, compound **55c** was identified as human mPGES-1 inhibitor with low nanomolar potency ($IC_{50} = 13$ nM). While with 4-chlorophenyl substitution at the same position, compound **55d**, was potent against human mPGES-1 ($IC_{50} = 54$ nM), it was not effective in inhibiting the mouse enzyme ($IC_{50} = 13236$ nM).

Table 3-2. SAR on 1,5-Diubstituted isatin derivatives.

Compound	Inhibition of mPGES-1	
	IC_{50} (Human, nM) ^a	IC_{50} (Mouse, nM)
52a	221±47	394±58
52b	154±20	1020±162
52c	531±90	244±31
52d	91±23	1960±348
52e	25±5	685±406
24	8023±1050	n.d. ^b (63) ^c
55a	32±6	777±364
55b	16±4	1220±430
55c	13±3	1130±244
55d	54±14	13236±5081

^aData are expressed as means ± SD of single determinations obtained in triplicate. ^bn.d. = not determined. ^cThe value in the parenthesis refers to the % inhibition of the compound at

a concentration of 10 μM against the mPGES-1 enzyme (IC_{50} values were determined only for the compounds that showed $\geq 70\%$ inhibition at 10 μM).



Scheme 3-3. Synthesis of 1,5-disubstituted isatin derivatives. Reagents and conditions: (a) K_2CO_3 , DMF, 80 $^\circ\text{C}$, 73–90%; (b) $\text{Pd}(\text{dppf})_2\text{Cl}_2 \cdot \text{CH}_2\text{Cl}_2$, NaHCO_3 , DME/ H_2O (4:1, v/v), reflux, N_2 atmosphere, 62–76%; (c) $\text{Pd}(\text{dppf})_2\text{Cl}_2 \cdot \text{CH}_2\text{Cl}_2$, CuI, DIPEA, DMF, rt, N_2 atmosphere, 84–90%; (d) NH_4OAc , glacial AcOH, 108 $^\circ\text{C}$, 47–73%.

3.4 Structural analysis

X-ray diffraction analysis of single crystals of compound **42** revealed the double bond between isatin and thiazolidine-2,4-dione moieties adopts the *Z* configuration. The crystal structure of **42** is depicted in Fig. 3-2 and the crystallographic data is given in the

experimental section (Chapter 4).

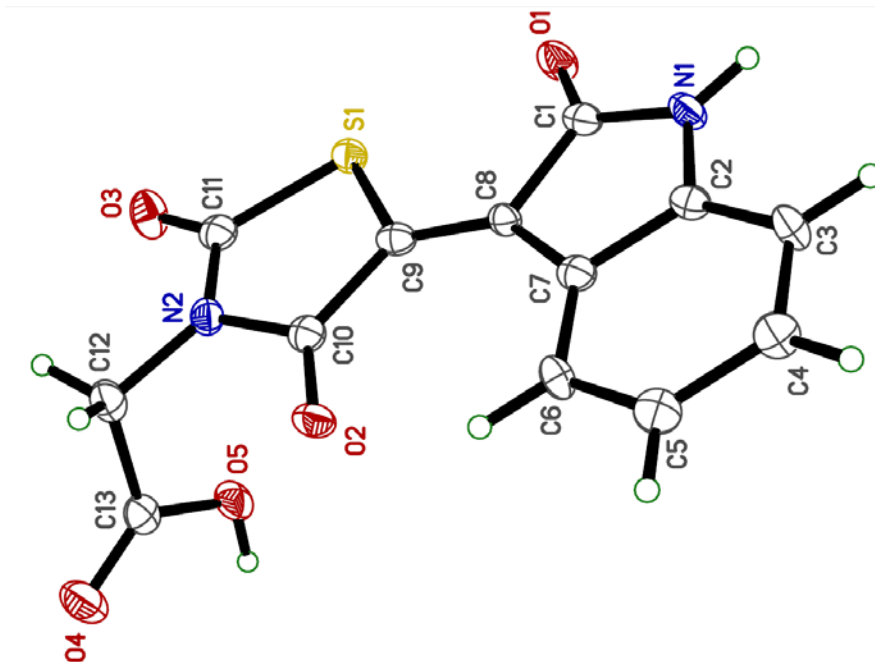


Fig. 3-2. Crystal structure of **42**. Crystals of **42** were non-merohedric twins and crystallized as a DMSO solvate. For the sake of clarity, the DMSO, which was disordered over two orientations, is not shown.

3.5 *In vitro* assays

The synthesized compounds were initially screened at a concentration of 10 μM to calculate the percentages of inhibition against human and mouse mPGES-1 enzymes. Compounds that showed significant inhibition ($\geq 70\%$) were further tested for their IC_{50} values. Depicted in Table 3-1 and Table 3-2 are the *in vitro* inhibitory data for human and mouse mPGES-1 enzymes. As predicted, a number of these compounds did effectively, but not equally inhibit both enzymes. We also investigated whether these mPGES-1 inhibitors have significant inhibitory efficacy against either COX-1 or COX-2. For this purpose, some of the more potent compounds ($\text{IC}_{50} \leq 100 \text{ nM}$ for human mPGES-1) were assayed for their potential inhibitory activities against mixed COXs (denoted as COX-1/2) with equal amounts of COX-1 and COX-2 in terms of enzyme activities. As shown in Table 3-3, at a concentration as high as 100 μM , only **55d** resulted in an inhibition greater than 50 % and all the other compounds investigated (**52d–52e** and **55a–55c**) did not cause significant

inhibition ($\leq 30\%$). The protocol for the protein preparation and purification, and the procedure for *in vitro* activity assays were the same, as described in our previous reports.^[33b, 76-77]

Table 3-3. Inhibition against COX-1/2 of selected compounds.

Compound	% Inhibition at 100 μM^a
52d	1 \pm 3
52e	5 \pm 1
55a	20 \pm 2
55b	17 \pm 0
55c	23 \pm 3
55d	78 \pm 1

^aThe % inhibition of the compound at a concentration of 100 μM against the COX-1/2 (mixed COX-1 and COX-2). The enzyme mixture contained equal amounts of COX-1 and COX-2 in terms of their enzyme activities. In this way, when a compound can significantly inhibit either COX-1 or COX-2, it will show significant inhibitory effects against the mixed COX-1 and COX-2. The error bars were given by the program of GraphPad Prism 7.

3.6 Enzyme-inhibitor binding modes

Knowing the possible binding mode of the inhibitor with the target protein is of great importance in structure optimization. To further elucidate the SAR of these synthesized compounds, as well as to enlighten the design of new inhibitors, we selected compounds **52e** and **55c** as candidates for molecular docking studies, as these compounds were among the most potent inhibitors against both human and mouse mPGES-1 enzymes. The AutoDock Vina^[91] program was employed as molecular docking tool to investigate the binding modes of these compounds with both human and mouse mPGES-1 enzymes. As depicted in Fig. 3-3B and Fig. 3-3C, the cyclohexylmethyl group at the isatin-1-position of **52e** occupies the hydrophobic groove accommodating the long hydrocarbon “tail” of the substrate PGH₂, and the cyclohexylethynyl substituent at isatin-5-position inserts into the membrane structure. Part of thiazolidine-2,4-dione *N*-acetic acid moiety fits into the small

pocket above GSH, and this polar “head” also interacts with S127 and R52 by building hydrogen bonds between the amide carbonyl (of **52e**) with the hydroxyl group (OH of S127), and between the carboxyl carbonyl (of **52e**) with the amine group (NH of R52). However, with 4-cyclohexyl-1-butyl and phenyl groups occupying 1- and 5-positions of isatin respectively, compound **55c** shows a different binding mode with human mPGES-1. As shown in Fig. 3-3F and 3-3G, the smaller 5-substituent (phenyl) fits into the smaller pocket above GSH, and the bulkier 5-substituent (4-cyclohexyl-1-butyl) occupies the larger hydrophobic groove that holds the PGH₂ aliphatic “tail”. The carboxyl carbonyl group of thiazolidine-2,4-dione *N*-acetic acid forms a hydrogen bond with the amino group of R52. In human mPGES-1, the major hydrophobic pocket is surrounded by I32, G35, L39, Y130, T131, L135 and A138. As shown in Fig. 3-3E and Fig 3-3I, this hydrophobic pocket is largely conserved in the mouse enzyme, with only a few amino acid residues altered from human mPGES-1, i.e., V32, V131 and F138 replace I32, T131 and A138, respectively. Both **52e** and **55c** bind in a similar region in mouse mPGES-1 as in the human enzyme, with substituents at isatin-1-position fitting into this major hydrophobic pocket. The most significant differences appear in the upper part of the mouse enzyme, where mutants K52 and R53 take over R52 and H53. The amide carbonyl group of both **52e** and carboxyl carbonyl group of **55c** can also form a hydrogen bond with S127-OH and K52-NH, respectively, ensuring the inhibitory potencies of these compounds against mouse mPGES-1. However, the much greater dimension of R53 (in mouse mPGES-1) than H53 (in human mPGES-1) makes in a steric clash with the ligand structure, resulting in lower affinity of these inhibitors with mouse mPGES-1.

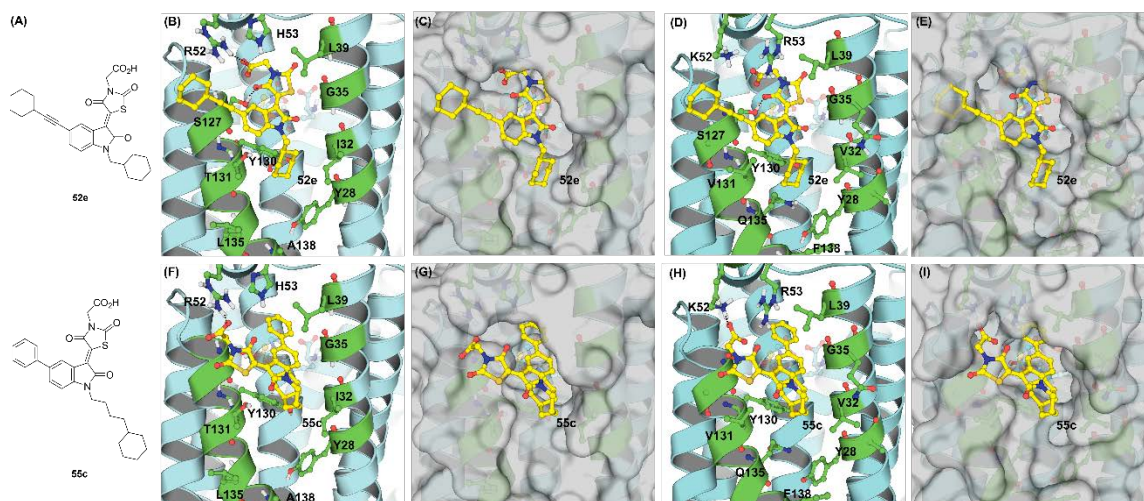
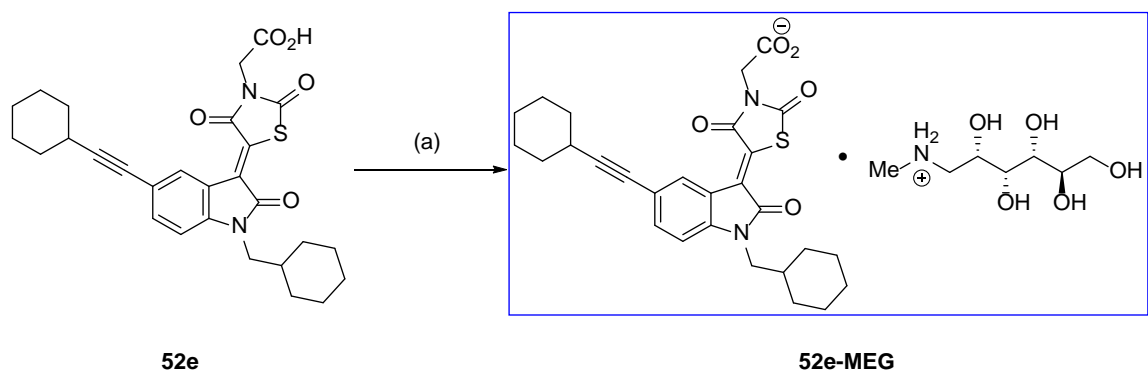


Fig. 3-3. Molecular structures of **52e** and **55c** and their binding with human and mouse mPGES-1 enzymes. (A) Ligand structures; (B) binding of **52e** with human mPGES-1; (C) surface representation of human mPGES-1 using the same orientation as in (B); (D) binding of **52e** with mouse mPGES-1; (E) surface representation of mouse mPGES-1 using the same orientation as in (D); (F) binding of **55c** with human mPGES-1; (G) surface representation of human mPGES-1 using the same orientation as in (F); (H) binding of **55c** with mouse mPGES-1; (I) surface representation of mouse mPGES-1 using the same orientation as in (H).

3.7 *In vivo* anti-inflammatory efficacy

Compound **52e** was selected as candidate for *in vivo* evaluation because of its submicromolar potency against both human and mouse mPGES-1 enzymes. However, although possessing a carboxylic acid group, this compound was barely soluble in distilled water, and so was its sodium salt. We screened a number of conjugate amines and found out the meglumine (*N*-methyl-*D*-glucamine) salt^[92] of **52e** (denoted as **52e-MEG**, synthetic protocol shown in Scheme 3-4) showed excellent aqueous solubility in distilled water (≥ 25 mg/mL). Meglumine has been used as pH modifier and/or counterion in a number of FDA-approved drugs.



Scheme 3-4. Preparation of meglumine salt of **52e**. Reagent and conditions: (a) *N*-methylglucamine, EtOH, reflux, 81%.

Mouse carrageenan air-pouch model of inflammation is widely employed for determining the *in vivo* effectiveness of inhibitors in reducing prostaglandin biosynthesis. Thus, to investigate the anti-inflammatory potential of **52e-MEG**, we performed a pilot mouse carrageenan air-pouch experiment.^[93] The effectiveness of **52e-MEG** was in comparison with the same dose of celecoxib for their capability in reducing PGE₂ levels. Air-pouches were generated by duplicate injection of sterile air under the skin on the back of mice. A single injection of inflammation reagent λ-carrageenan directly into the pouch was followed to induce local inflammation and stimulate PGE₂ biosynthesis. Inflammatory cells were recruited and fluid exudate containing substantial amounts of PGE₂ was produced in response to carrageenan. Then the mice were orally administered with double doses of **52e-MEG**, celecoxib and vehicle for 24 hours before they were sacrificed for the collection of air-pouch fluid and kidney samples. As PGE₂ is more abundant in kidney, we also investigated the effects of **52e-MEG** and celecoxib on the PGE₂ levels in kidney. The air-pouch fluid and kidney samples were assayed for PGE₂ levels and the results were summarized in Fig. 3-4. As shown in Fig. 3-4A, compound **52e-MEG** administered orally with double doses of 100 mg/kg in 24 h significantly decreased the PGE₂ levels in mice ($p = 0.0001$). In addition, no significant difference was observed in the *in vivo* potency between 100 mg/kg **52e-MEG** and the same dose of celecoxib ($p = 0.4974$). The corresponding data in kidney extract was similar as compared to air-pouch fluid, as outlined in Fig. 3-4B.

3.8 Conclusions

By modifying the chemical scaffold of the lead **19**, we have designed, synthesized and conducted biological evaluation of a series of (*Z*)-5-(2-oxoindolin-3-ylidene)thiazolidine-2,4-dione derivatives (**42**, **44a–44m**, **48a–48b**, **52a–52e**, **54**, and **55a–55d**). The structures of the potent inhibitors were rationally optimized in light of molecular docking by focusing on the unoccupied area in the conserved region of the active site in both human and mouse mPGES-1 enzymes. As expected, a number of these compounds, especially those with 1,5-disubstituted isatin substructures (**52a–52e** and **55a–55d**), were capable of inhibiting both human and mouse mPGES-1 enzymes. Some of the more potent compounds were also tested for their selectivity of mPGES-1 over COX isozymes. It was observed at a concentration of 100 μ M, compounds **52d–52e** and **55a–55c** did not cause significant inhibition against COX isozymes. Furthermore, compound **52e** was selected as candidate for *in vivo* pharmacological evaluation. We improved the solubility by preparing the **52e**-meglumine salt (**52e-MEG**) and performed the rat PK study with **52e-MEG** administered both intravenously and orally. A pilot mouse carrageenan air-pouch experiment was carried out with double doses of **52e-MEG** administered orally. The results shown in Fig. 3-5 demonstrated this compound was effective in reducing PGE₂ levels in both air-pouch fluid and kidney extract as compared to vehicle control. Based on the above-mentioned studies, compound **52e** is worthy of further research as a candidate for animal models of inflammation and as a new lead in the design of novel mPGES-1 inhibitors. In the research described in this chapter, Shuo Zhou and Dr. Yaxia Yuan performed the docking study. Dr. Ziyuan Zhou determined the IC₅₀ values by conducting *in vitro* assays. Dr. Charles Loftin directed the air-pouch experiment process, which was assisted by Xirong Zheng and Dr. Jianzhong Chen.

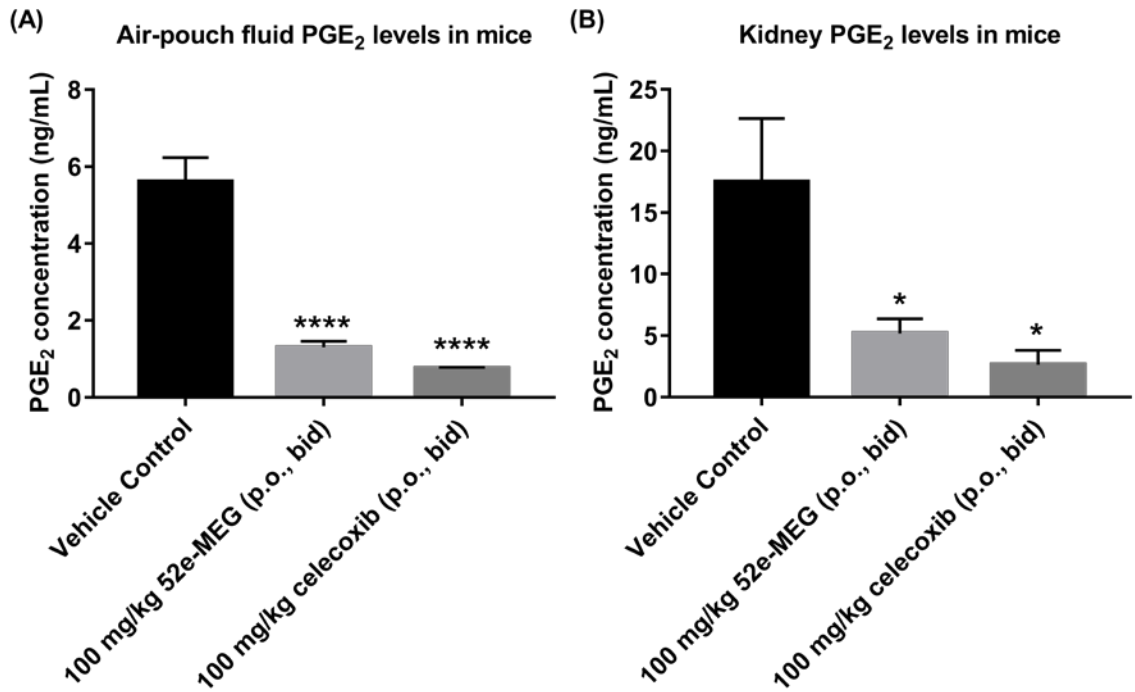


Fig. 3-4. Data from *in vivo* assays using the mouse carrageenan air-pouch model of inflammation (n = 3 for control and **52e-MEG** groups and n = 4 for celecoxib group) with **52e-MEG** or celecoxib dosed orally. (A) the effectiveness of **52e-MEG** in reducing PGE₂ level in air-pouch fluid; (B) the effectiveness of **52e-MEG** in reducing PGE₂ level in kidney (assayed for PGE₂ by ELISA and expressed as Mean ± SEM). Statistical results from the one-way ANOVA analysis of the data in panel B with post hoc tests: $p = 0.0001$ for Vehicle Control vs 100 mg/kg **52e-MEG** (p.o., bid); $p < 0.0001$ for Vehicle Control vs 100 mg/kg celecoxib (p.o., bid); and $p = 0.4974$ for 100 mg/kg 20e-MEG (p.o., bid) vs 100 mg/kg celecoxib (p.o., bid). Statistical results from the one-way ANOVA analysis of the data in panel B with post hoc tests: $p = 0.0386$ for Vehicle Control vs. 100 mg/kg **52e-MEG** (p.o., bid); $p = 0.0122$ for Vehicle Control vs 100 mg/kg celecoxib (p.o., bid); and $p = 0.7978$ for 100 mg/kg **52e-MEG** (p.o., bid) vs 100 mg/kg celecoxib (p.o., bid).

Chapter 4 Experimental Section

4.1 Computational studies

4.1.1 Trimer structure of human mPGES-1

The trimer structure of human mPGES-1 was generated by the symmetry operation *via* **PyMol**,^[94] based on the X-ray crystal structure of the monomer unit for human mPGES-1 (PDB ID: 4BPM).^[34-35]

4.1.2 Trimer structure of mouse mPGES-1

As there is no available X-ray crystal structure of mouse mPGES-1, homology modeling was performed to model the structure of mouse mPGES-1. Sequence alignment was performed on the amino acid sequence of human mPGES-1 (accession number of O14684) and mouse mPGES-1 (accession number of Q9JM51) by using the Basic Local Alignment Search Tool (BLAST) of Uniprot server (<http://www.uniprot.org/align>).^[95] The aligned sequence indicates that human mPGES-1 is highly homologous to mouse mPGES-1, with the sequence identity being 79% and the sequence similarity being 84%. As 40% sequence identity between a template protein and a target protein is considered to be sufficient for constructing a satisfactory homology model,^[96] we built the trimer structure of mouse mPGES-1 based on the aforementioned trimer structure of human mPGES-1 by using the Modeller module^[96a] of **Discovery Studio 2.5.5**.^[97] The GSH cofactor in human mPGES-1 structure was directly transferred to the mouse mPGES-1 model. The final structure was selected from 50 candidate models according to the DOPE score.^[98]

4.1.3 Molecular docking

In order to explore the binding mode of the presented compounds with human and mouse mPGES-1, molecular docking was performed by using the program of AutoDock 4.2^[78]. During the process of molecular docking, Lamarckian genetic algorithm was applied to treat the intermolecular interactions between ligand and protein. The number of the runs was set to 200, and the number of individuals for each run was set to 300. The maximum number of energy evaluations was set to 25,000,000, and the maximum number of

generations to 300,000. The size of grid box was $80 \times 80 \times 80$ points along each axis and the grid spacing was 0.2 Å. All of the candidates generated from the docking operations were evaluated and ranked in terms of binding free energies by using the standard energy score function implemented in the AutoDock 4.2 program. The largest one of the docked binding structure clusters was selected as the finally chosen initial mPGES-1-ligand complex structure, based on the lowest binding free energy (*i.e.* the best energy score from the AutoDock 4.2 scoring function) along with good geometric matching quality with the surrounding residues in the binding site of mPGES-1. Molecular docking was also performed by using the program of AutoDock Vina.^[91]

4.2 Chemistry

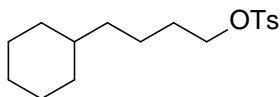
4.2.1 General

All the starting chemicals were purchased from Sigma-Aldrich (St. Louis, MO), Oakwood Chemical (Estill, SC), Alfa Aesar (Haverhill, MA), Frontier Scientific (Logan, UT) or Fisher Scientific (Hampton, NH) and used without further purification. Compounds were purified by SiO₂ flash chromatography (Flash silica gel 32-63 u, Dynamic Adsorbents Inc., Norcross, GA). ¹H and ¹³C NMR spectra were recorded on a Varian Unity Inova 400 MHz spectrometer (Palo Alto, CA) at ambient temperature using 99.8% CDCl₃ and 99.9% DMSO-d₆ (Cambridge Isotope Laboratories, Tewksbury, MA). ¹H and ¹³C chemical shifts were referenced to internal solvent resonances and reported in parts per million (ppm), with coupling constants *J* given in Hz. HR-ESI-MS spectra were recorded on AB SCIEX Triple TOF 5600 system (AB Sciex, Framingham, MA).

4.2.2 Preparation of tosylates **23** and **35**

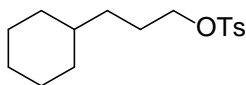
Preparation of 23. To the solution of 4-cyclohexyl-1-butanol (**22**, 1.05 g, 6.72 mmol, 1.00 equiv.) in dichloromethane (40 mL) was added aqueous KOH solution (50 %, 20 mL). The mixture was brought to 0~5 °C using ice-bath and *p*-toluenesulfonyl chloride (1.54 g, 8.06 mmol, 1.20 equiv.) was added portionwise over a period of 30 min. The resulting reaction mixture was stirred at room temperature for 5 h and partitioned between CH₂Cl₂ (30 mL) and water (30 mL). The organic layer was isolated and the aqueous layer was extracted

with CH₂Cl₂ (30 mL × 3). The combined organic phase was washed sequentially with water (30 mL) saturated NaHCO₃ solution (30 mL) and brine (30 mL), dried over anhydrous Na₂SO₄, and evaporated under reduced pressure. The residue was dried under high vacuum using oil pump overnight to afford the tosylate **23** as white wax in high purity (Yield: 1.98 g, 95 %). The tosylation (synthesis of **35**) of 3-cyclohexyl-1-propanol followed the same protocol as described.



4-cyclohexylbutyl 4-methylbenzenesulfonate (23). Yield: 95 %.

White wax-like solid. ¹H NMR (400 MHz, CDCl₃) δ 7.79 (d, *J* = 8.2 Hz, 2H), 7.34 (d, *J* = 6.3 Hz, 2H), 4.02 (t, 2H), 2.45 (d, *J* = 2.0 Hz, 3H), 1.71 – 1.58 (m, 7H), 1.58 – 0.82 (m, 14H), 0.82 – 0.36 (m, 3H). ¹³C NMR (101 MHz, CDCl₃) δ 144.75, 133.36, 129.93, 128.03, 70.87, 37.57, 36.82, 33.39, 29.23, 26.79, 26.48, 22.76, 21.78. HRMS (ESI+) *m/z* calcd for C₁₆H₂₅O₃S [M+H]⁺: 297.1519, found: 297.1522.



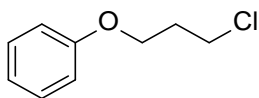
3-Cyclohexylpropyl 4-methylbenzenesulfonate (35). Compound 35

was prepared from 3-cyclohexyl-1-propanol and *p*-toluenesulfonyl chloride followed the same method as described in the preparation of **23**. Yield: 67 %. Colorless oil. ¹H NMR (400 MHz, CDCl₃) δ 7.79 (d, *J* = 8.3 Hz, 2H), 7.35 (d, *J* = 8.0 Hz, 2H), 4.00 (t, *J* = 6.6 Hz, 2H), 2.44 (s, 3H), 1.71 – 1.55 (m, 7H), 1.25 – 1.04 (m, 6H), 0.88 – 0.71 (m, 2H). ¹³C NMR (101 MHz, CDCl₃) δ 144.67, 133.12, 129.80, 127.85, 71.07, 36.96, 33.08, 32.83, 26.52, 26.21, 26.17, 21.61. HRMS (ESI+) *m/z* calcd for C₁₇H₂₇O₃S [M+NH₄]⁺: 328.1941, found: 328.1945.

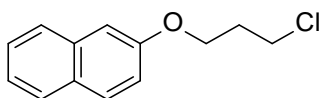
4.2.3 Preparation of the chlorides 32a–32c

Preparation 32a. The suspension of phenol (1.89 g, 20.1 mmol, 1.00 equiv.), 1-bromo-3-chloropropane (1.50 equiv., 30.1 mmol, 4.74 g), K₂CO₃ (2.00 equiv., 40.2 mmol, 5.55 g) in acetone was stirred at reflux. The reaction mixture was cooled to room temperature after

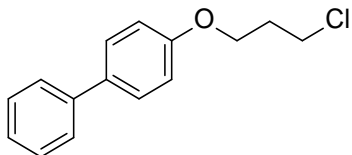
TLC indicating the total consumption of phenol (~6 h). The solid was removed by filtration and the filtrate was concentrated under reduced pressure.^[85] The residue was dried under vacuum overnight to give **32a** as a colorless oil (4.57 g, 26.8 mmol, 89% yield). Compound **32b** and **32c** was prepared using the same method with 2-naphthol as starting material.



(3-Chloropropoxy)benzene (32a). Yield: 89%. Colorless oil. ¹H NMR (400 MHz, CDCl₃) δ 7.40 – 7.28 (m, 2H), 7.05 – 6.85 (m, 3H), 4.14 (t, *J* = 5.8 Hz, 2H), 3.78 (t, *J* = 6.4 Hz, 2H), 2.26 (p, *J* = 6.1 Hz, 2H). ¹³C NMR (101 MHz, CDCl₃) δ 158.78, 129.59, 120.99, 114.58, 64.22, 41.68, 32.40.



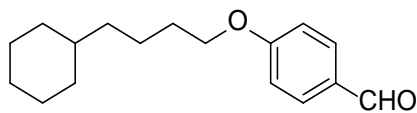
2-(3-Chloropropoxy)naphthalene (32b). Compound **32b** was prepared from 2-naphthol and 1-bromo-3-chloropropane with the same method as described in the preparation of **32a**. Yield: 92%. White solid. ¹H NMR (400 MHz, CDCl₃) δ 7.76 (dd, *J* = 16.1, 7.3 Hz, 3H), 7.50 – 7.40 (m, 1H), 7.40 – 7.30 (m, 1H), 7.21 – 7.11 (m, 2H), 4.25 (t, *J* = 5.9 Hz, 2H), 3.80 (t, *J* = 6.3 Hz, 2H), 2.31 (p, *J* = 6.1 Hz, 2H). ¹³C NMR (101 MHz, CDCl₃) δ 156.76, 134.64, 129.58, 129.15, 127.78, 126.88, 126.54, 123.83, 118.92, 106.83, 64.42, 41.75, 32.39. HRMS (ESI+) *m/z* calcd for C₁₃H₁₄ClO [M+H]⁺: 221.0728, found: 221.0724.



4-(3-Chloropropoxy)biphenyl (32c). Compound **32c** was prepared from 4-phenylphenol and 1-bromo-3-chloropropane with the same method as described in the preparation of **32a**. Yield: 92%. ¹H NMR (400 MHz, CDCl₃) δ 7.65 – 7.53 (m, 4H), 7.53 – 7.29 (m, 3H), 7.00 (d, *J* = 8.7 Hz, 2H), 4.18 (t, *J* = 5.8 Hz, 2H), 3.78 (t, *J* = 6.3 Hz, 2H), 2.28 (p, *J* = 6.1 Hz, 2H). ¹³C NMR (101 MHz, CDCl₃) δ 158.40, 140.89, 134.15, 128.86, 128.32, 126.87, 126.83, 114.93, 64.50, 41.67, 32.44.

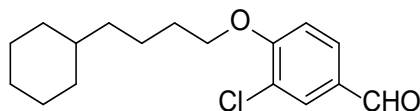
4.2.4 Preparation of the aldehyde intermediates 24a–24q, 30, 33a–33c and 36a–36e

Preparation of 24b. The suspension of 3-chloro-4-hydroxybenzaldehyde (0.32 g, 2.04 mmol, 1.00 equiv.), 4-cyclohexyl-1-butanol tosylate (**23**) (0.63 g, 2.04 mmol, 1.00 equiv.) and potassium carbonate (0.56 g, 4.09 mmol, 2.00 equiv.) in DMF (10 mL) was heated at 80 °C for 12 h (or overnight). The reaction mixture was then diluted with water (20 mL) and extracted with ethyl acetate (30 mL × 3). The combined organic phase was washed sequentially with saturated NaHCO₃ solution (30 mL), water (30 mL) and brine (30 mL), dried over anhydrous Na₂SO₄, evaporated under reduced pressure and dried under vacuum at room temperature. The crude product was used in subsequent step without further purification. However, the analytical sample can be obtained as light yellow oil by flash chromatography on silica gel using a mixture of hexanes and EtOAc (4:1) as eluent. The preparation of other aldehyde intermediates (**24a**, **24c–24q**, **30**, **33a–33c** and **36a–36e**) followed the similar protocol as described, with different starting materials.



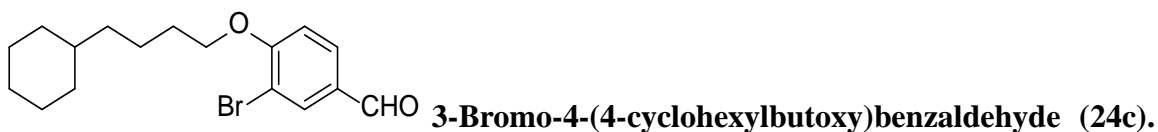
4-(4-Cyclohexylbutoxy)benzaldehyde (24a).

Obtained from the reaction of 4-hydroxybenzaldehyde and **23**. Yield: 76 %. Colorless oil. ¹H NMR (400 MHz, CDCl₃) δ 9.86 (s, 1H), 7.80 (d, *J* = 8.7 Hz, 2H), 6.97 (d, *J* = 8.6 Hz, 2H), 4.02 (t, *J* = 6.5 Hz, 2H), 1.81 – 1.60 (m, 7H), 1.50 – 1.41 (m, 2H), 1.26 – 1.07 (m, 6H), 0.92 – 0.81 (m, 2H). ¹³C NMR (101 MHz, CDCl₃) δ 191.14, 164.67, 132.36, 130.15, 115.15, 68.84, 37.99, 37.54, 33.77, 29.76, 27.11, 26.81, 23.65.



3-Chloro-4-(4-cyclohexylbutoxy)benzaldehyde (24b).

Obtained from the reaction of 3-chloro-4-hydroxybenzaldehyde and **23**. Yield: 88 %. Light yellow oil. ¹H NMR (400 MHz, CDCl₃) δ 9.82 (s, 1H), 7.87 (d, *J* = 2.0 Hz, 1H), 7.72 (dd, *J* = 8.5, 2.0 Hz, 1H), 6.99 (d, *J* = 8.5 Hz, 1H), 4.09 (t, *J* = 6.5 Hz, 2H), 1.87 – 1.79 (m, 2H), 1.73 – 1.59 (m, 5H), 1.54 – 1.45 (m, 2H), 1.28 – 1.07 (m, 6H), 0.92 – 0.80 (m, 2H). ¹³C NMR (101 MHz, CDCl₃) δ 189.75, 159.58, 131.26, 130.52, 130.08, 124.02, 112.55, 69.61, 37.60, 37.13, 33.43, 29.24, 26.79, 26.48, 23.22.



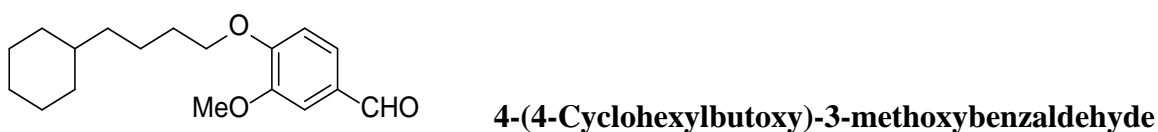
Obtained from the reaction of 3-bromo-4-hydroxybenzaldehyde and **23**. Yield: 86%. Yellow oil. ^1H NMR (400 MHz, CDCl_3) δ 9.82 (s, 1H), 8.06 (d, $J = 1.9$ Hz, 1H), 7.78 (dd, $J = 8.5, 1.8$ Hz, 1H), 6.96 (d, $J = 8.5$ Hz, 1H), 4.10 (t, $J = 6.4$ Hz, 2H), 1.89 – 1.79 (m, 2H), 1.74 – 1.60 (m, 5H), 1.56 – 1.46 (m, 2H), 1.28 – 1.04 (m, 6H), 0.95 – 0.80 (m, 2H). ^{13}C NMR (101 MHz, CDCl_3) δ 189.69, 160.41, 134.67, 131.18, 130.54, 113.08, 112.40, 69.70, 37.61, 37.15, 33.45, 29.24, 26.81, 26.51, 23.26.



Obtained from the reaction of 4-hydroxy-3-methylbenzaldehyde and **23**. Yield: 82 %. Orange oil. ^1H NMR (400 MHz, CDCl_3) δ 9.84 (s, 1H), 7.68 (d, $J = 7.3$ Hz, 2H), 6.89 (d, $J = 7.7$ Hz, 1H), 4.04 (t, $J = 5.5$ Hz, 2H), 2.26 (s, 3H), 1.86 – 1.77 (m, 2H), 1.74 – 1.62 (m, 5H), 1.54 – 1.44 (m, 2H), 1.28 – 1.11 (m, 6H), 0.93 – 0.80 (m, 2H). ^{13}C NMR (101 MHz, CDCl_3) δ 191.31, 162.64, 131.57, 130.79, 129.31, 127.83, 110.48, 68.46, 37.70, 37.26, 33.49, 29.50, 26.84, 26.54, 23.43, 16.38.



Obtained from the reaction of 3,4-dihydroxybenzaldehyde and **23**. Yield: 74 %. White solid. ^1H NMR (400 MHz, CDCl_3) δ 9.82 (s, 1H), 7.47 – 7.36 (m, 2H), 6.94 (d, $J = 8.2$ Hz, 1H), 4.12 (t, $J = 6.6$ Hz, 2H), 1.87 – 1.77 (m, 2H), 1.73 – 1.61 (m, 5H), 1.51 – 1.41 (m, 2H), 1.26 – 1.11 (m, 6H), 0.93 – 0.83 (m, 2H). ^{13}C NMR (101 MHz, CDCl_3) δ 191.14, 151.45, 146.32, 130.55, 124.62, 114.17, 111.02, 69.44, 37.68, 37.21, 33.46, 29.40, 26.78, 26.49, 23.32.



Obtained from the reaction of vanillin and **23**. Yield: 78 %. Colorless oil. ^1H NMR

(400 MHz, CDCl₃) δ 9.82 (s, 1H), 7.44 – 7.35 (m, 2H), 6.94 (d, J = 8.1 Hz, 1H), 4.07 (t, J = 6.8 Hz, 2H), 3.90 (s, 3H), 1.88 – 1.79 (m, 2H), 1.71 – 1.58 (m, 5H), 1.50 – 1.40 (m, 2H), 1.25 – 1.05 (m, 6H), 0.91 – 0.80 (m, 2H). ¹³C NMR (101 MHz, CDCl₃) δ 190.92, 154.29, 149.93, 129.94, 126.83, 111.48, 109.38, 69.28, 56.09, 37.59, 37.18, 33.42, 29.27, 26.77, 26.47, 23.24.



Obtained from the reaction of 3-ethoxy-4-hydroxybenzaldehyde and **23**. Yield: 76 %. Colorless oil. ¹H NMR (400 MHz, CDCl₃) δ 9.83 (s, 1H), 7.45 – 7.34 (m, 2H), 6.95 (d, J = 6.1 Hz, 1H), 4.19 – 4.02 (m, 4H), 1.89 – 1.80 (m, 2H), 1.76 – 1.60 (m, 5H), 1.52 – 1.42 (m, 5H), 1.28 – 1.10 (m, 6H), 0.93 – 0.84 (m, 2H). ¹³C NMR (101 MHz, CDCl₃) δ 191.06, 154.68, 149.29, 129.98, 126.73, 111.85, 111.04, 69.30, 64.69, 37.64, 37.21, 33.46, 33.29, 29.30, 26.83, 26.52, 23.26, 14.80.

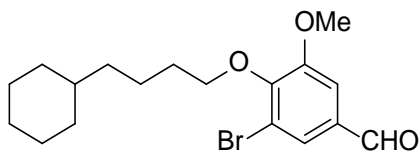


Obtained from the reaction of 4-hydroxy-3-nitrobenzaldehyde and **23**. Yield: 93 %. Yellow oil. ¹H NMR (400 MHz, CDCl₃) δ 9.91 (s, 1H), 8.32 (s, 1H), 8.05 (d, J = 7.3 Hz, 1H), 7.20 (d, J = 8.7 Hz, 1H), 4.19 (t, J = 6.4 Hz, 2H), 1.88 – 1.79 (m, 2H), 1.71 – 1.55 (m, 6H), 1.27 – 1.09 (m, 7H), 0.91 – 0.79 (m, 2H). ¹³C NMR (101 MHz, CDCl₃) δ 188.93, 156.91, 140.03, 134.67, 128.79, 127.51, 114.60, 70.49, 37.58, 37.07, 33.42, 29.11, 26.78, 26.48, 23.11.



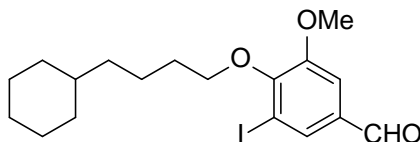
Obtained from the reaction of 3-chloro-4-hydroxy-5-methoxybenzaldehyde and **23**. Yield: 83 %. Light yellow oil. ¹H NMR (400 MHz, CDCl₃) δ 9.81 (s, 1H), 7.46 (d, J = 1.8 Hz, 1H), 7.31 (d, J = 1.8 Hz, 1H), 4.09 (t, J = 6.6 Hz, 2H), 3.90 (s, 3H), 1.79 – 1.60 (m, 7H), 1.52 – 1.42 (m, 2H), 1.25 – 1.10 (m, 6H), 0.91 – 0.79 (m, 2H). ¹³C NMR (101 MHz, CDCl₃) δ 190.04, 154.47, 150.37, 132.23, 129.07, 125.89,

109.46, 74.05, 56.29, 37.69, 37.27, 33.47, 30.56, 26.81, 26.50, 23.16.



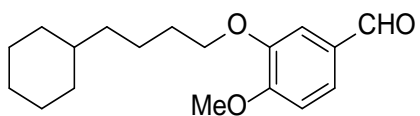
3-Bromo-4-(4-cyclohexylbutoxy)-5-

methoxybenzaldehyde (24j). Obtained from the reaction of 3-bromo-4-hydroxy-5-methoxybenzaldehyde and **23**. Yield: 82 %. Yellow oil. ^1H NMR (400 MHz, CDCl_3) δ 9.82 (d, $J = 0.9$ Hz, 1H), 7.64 (dd, $J = 1.8, 0.8$ Hz, 1H), 7.36 (d, $J = 1.8$ Hz, 1H), 4.09 (t, $J = 6.6$ Hz, 2H), 3.91 (s, 3H), 1.82 – 1.60 (m, 7H), 1.54 – 1.43 (m, 2H), 1.27 – 1.08 (m, 6H), 0.92 – 0.81 (m, 2H). ^{13}C NMR (101 MHz, CDCl_3) δ 190.00, 154.30, 151.47, 132.86, 129.02, 118.27, 110.12, 74.02, 56.32, 37.75, 37.33, 33.53, 30.62, 26.85, 26.55, 23.27.



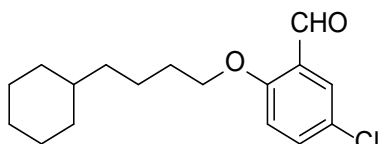
4-(4-Cyclohexylbutoxy)-3-iodo-5-

methoxybenzaldehyde (24k). Obtained from the reaction of 4-hydroxy-3-iodo-5-methoxybenzaldehyde and **23**. Yield: 76 %. Brown oil. ^1H NMR (400 MHz, CDCl_3) δ 9.80 (s, 1H), 7.84 (d, $J = 1.8$ Hz, 1H), 7.38 (d, $J = 1.8$ Hz, 1H), 4.09 (t, $J = 6.6$ Hz, 2H), 3.89 (s, 3H), 1.85 – 1.60 (m, 7H), 1.56 – 1.44 (m, 2H), 1.28 – 1.10 (m, 6H), 1.01 – 0.78 (m, 2H). ^{13}C NMR (101 MHz, CDCl_3) δ 189.83, 153.87, 153.02, 135.02, 133.74, 111.12, 92.62, 73.89, 56.19, 37.74, 37.33, 33.53, 30.70, 26.85, 26.55, 23.41.



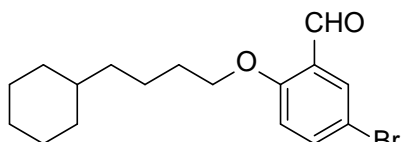
3-(4-Cyclohexylbutoxy)-4-methoxybenzaldehyde (24l).

Obtained from the reaction of isovanillin and **23**. Yield: 79 %. Colorless oil. ^1H NMR (400 MHz, CDCl_3) δ 9.83 (s, 1H), 7.46 – 7.36 (m, 2H), 6.96 (d, $J = 8.2$ Hz, 1H), 4.05 (t, $J = 6.9$ Hz, 2H), 3.93 (s, 3H), 1.87 – 1.78 (m, 2H), 1.73 – 1.59 (m, 5H), 1.45 (dt, $J = 9.4, 8.0$ Hz, 2H), 1.27 – 1.06 (m, 6H), 0.92 – 0.80 (m, 2H). ^{13}C NMR (101 MHz, CDCl_3) δ 191.05, 154.95, 149.27, 130.19, 126.67, 110.69, 110.40, 69.21, 56.26, 37.64, 37.22, 33.46, 29.36, 26.82, 26.52, 23.30.



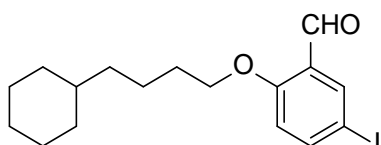
5-Chloro-2-(4-cyclohexylbutoxy)benzaldehyde (24m).

Obtained from the reaction of 5-chlorosalicylaldehyde and **23**. Yield: 75 %. Yellow oil. ^1H NMR (400 MHz, CDCl_3) δ 10.41 (s, 1H), 7.74 (d, $J = 2.8$ Hz, 1H), 7.44 (dd, $J = 8.9, 2.8$ Hz, 1H), 6.91 (d, $J = 8.9$ Hz, 1H), 4.04 (t, $J = 6.4$ Hz, 2H), 1.87 – 1.75 (m, 2H), 1.72 – 1.58 (m, 5H), 1.51 – 1.41 (m, 2H), 1.26 – 1.07 (m, 6H), 0.92 – 0.81 (m, 2H). ^{13}C NMR (101 MHz, CDCl_3) δ 188.59, 160.08, 135.44, 127.79, 126.19, 125.81, 114.26, 69.13, 37.64, 37.19, 33.45, 29.39, 26.78, 26.47, 23.35.



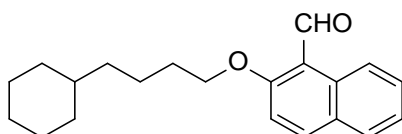
5-Bromo-2-(4-cyclohexylbutoxy)benzaldehyde (24n).

Obtained from the reaction of 5-bromosalicylaldehyde and **23**. Yield: 85 %. Yellow oil. ^1H NMR (400 MHz, CDCl_3) δ 10.39 (s, 1H), 7.88 (d, $J = 2.6$ Hz, 1H), 7.63 – 7.52 (m, 1H), 6.86 (d, $J = 8.9$ Hz, 1H), 4.03 (t, $J = 6.4$ Hz, 2H), 1.85 – 1.77 (m, 2H), 1.72 – 1.59 (m, 6H), 1.51 – 1.41 (m, 2H), 1.26 – 1.10 (m, 7H). ^{13}C NMR (101 MHz, CDCl_3) δ 188.51, 160.50, 138.33, 130.81, 126.15, 114.63, 113.26, 69.04, 37.61, 37.19, 33.43, 29.35, 26.76, 26.47, 23.34.



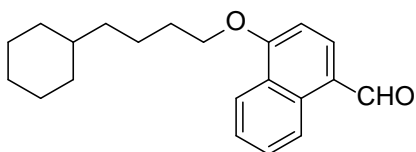
2-(4-Cyclohexylbutoxy)-5-iodobenzaldehyde (24o).

Obtained from the reaction of 5-iodosalicylaldehyde and **23**. Yield: 81 %. Yellow oil. ^1H NMR (400 MHz, CDCl_3) δ 10.36 (s, 1H), 8.08 (s, 1H), 7.81 – 7.72 (m, 1H), 6.76 (d, $J = 8.8$ Hz, 1H), 4.04 (t, $J = 6.4$ Hz, 2H), 1.85 – 1.77 (m, 2H), 1.73 – 1.61 (m, 6H), 1.52 – 1.42 (m, 2H), 1.28 – 1.09 (m, 7H). ^{13}C NMR (101 MHz, CDCl_3) δ 188.50, 161.23, 144.19, 136.90, 126.65, 115.10, 82.83, 68.95, 37.64, 37.21, 33.46, 29.35, 26.79, 26.49, 23.36.



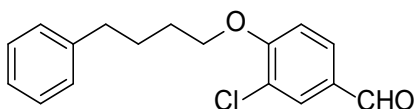
2-(4-Cyclohexylbutoxy)-1-naphthaldehyde (24p).

Obtained from the reaction of 2-hydroxy-1-naphthaldehyde and **23**. Yield: 76 %. White wax-like solid. ^1H NMR (400 MHz, CDCl_3) δ 10.92 (s, 1H), 9.29 (d, $J = 8.7$ Hz, 1H), 8.08 – 7.97 (m, 1H), 7.75 (d, $J = 8.1$ Hz, 1H), 7.65 – 7.56 (m, 1H), 7.45 – 7.36 (m, 1H), 7.24 (s, 1H), 4.19 (t, $J = 6.5$ Hz, 2H), 1.90 – 1.80 (m, 2H), 1.72 – 1.63 (m, 6H), 1.28 – 1.17 (m, 7H), 0.91 – 0.84 (m, 2H). ^{13}C NMR (101 MHz, CDCl_3) δ 192.23, 163.85, 161.30, 137.60, 131.69, 129.90, 128.49, 128.29, 125.02, 124.76, 116.78, 113.66, 69.70, 37.67, 33.47, 33.43, 29.70, 26.80, 26.50, 23.43.



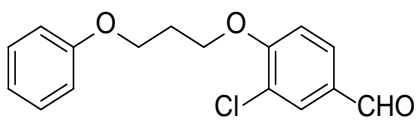
4-(4-Phenylbutoxy)-1-naphthaldehyde (24q). Obtained

from the reaction of 4-hydroxy-1-naphthaldehyde and **23**. Yield: 86 %. White wax-like solid. ^1H NMR (400 MHz, CDCl_3) δ 10.19 (s, 1H), 9.31 (d, $J = 8.6$ Hz, 1H), 8.35 (d, $J = 8.3$ Hz, 1H), 7.90 (d, $J = 8.1$ Hz, 1H), 7.74 – 7.65 (m, 1H), 7.57 (t, $J = 7.6$ Hz, 1H), 6.90 (d, $J = 8.1$ Hz, 1H), 4.23 (t, $J = 6.4$ Hz, 2H), 1.99 – 1.90 (m, 2H), 1.77 – 1.55 (m, 7H), 1.34 – 1.13 (m, 6H), 0.96 – 0.85 (m, 2H). ^{13}C NMR (101 MHz, CDCl_3) δ 192.62, 160.79, 140.17, 132.35, 129.85, 126.67, 126.01, 125.24, 125.11, 122.84, 103.91, 69.19, 37.97, 37.55, 33.78, 29.72, 27.10, 26.80, 23.83.



3-Chloro-4-(4-phenylbutoxy)benzaldehyde (30).

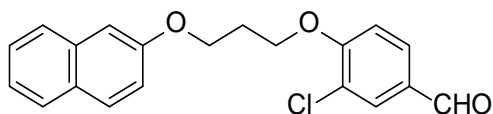
Obtained from the reaction of 3-chloro-4-hydroxybenzaldehyde and 1-bromo-4-phenylbutane. Yield: 96 %. Yellow solid. ^1H NMR (400 MHz, CDCl_3) δ 9.84 (s, 1H), 7.90 (d, $J = 1.4$ Hz, 1H), 7.74 (dd, $J = 8.5, 1.4$ Hz, 1H), 7.32 – 7.18 (m, 4H), 6.99 (d, $J = 8.5$ Hz, 1H), 4.12 (t, $J = 5.8$ Hz, 2H), 2.73 (t, $J = 7.1$ Hz, 2H), 1.99 – 1.83 (m, 4H). ^{13}C NMR (101 MHz, CDCl_3) δ 189.82, 159.45, 141.98, 131.29, 130.53, 130.09, 128.49, 128.45, 125.97, 123.96, 112.50, 69.32, 35.49, 28.45, 27.63.



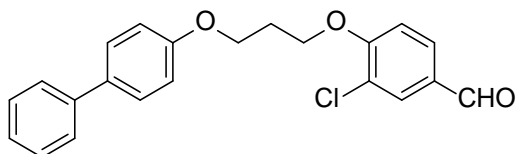
3-Chloro-4-(3-phenoxypropoxy)benzaldehyde (33a).

Obtained from the reaction of 3-chloro-4-hydroxybenzaldehyde and **32a**. Yield: 71 %.

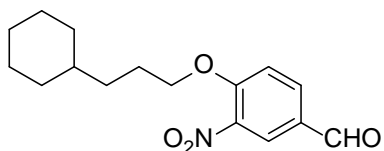
Yellow solid. ^1H NMR (400 MHz, CDCl_3) δ 9.84 (s, 1H), 7.90 (d, $J = 1.2$ Hz, 1H), 7.75 (dd, $J = 8.5, 1.2$ Hz, 1H), 7.29 (t, $J = 7.7$ Hz, 2H), 7.06 (d, $J = 8.5$ Hz, 1H), 6.94 (dd, $J = 14.9, 8.0$ Hz, 3H), 4.33 (t, $J = 6.0$ Hz, 2H), 4.22 (t, $J = 5.9$ Hz, 2H), 2.36 (p, $J = 5.9$ Hz, 2H). ^{13}C NMR (101 MHz, CDCl_3) δ 189.88, 159.31, 158.75, 131.36, 130.62, 130.33, 129.64, 124.06, 121.02, 114.56, 112.65, 66.02, 63.83, 29.17.



3-Chloro-4-(3-(naphthalen-2-yloxy)propoxy)benzaldehyde (33b). Obtained from the reaction of 3-chloro-4-hydroxybenzaldehyde and **32b**. Yield: 70 %. Yellow solid. ^1H NMR (400 MHz, CDCl_3) δ 9.84 (s, 1H), 7.91 (d, $J = 1.9$ Hz, 1H), 7.81 – 7.68 (m, 4H), 7.44 (t, $J = 7.4$ Hz, 1H), 7.34 (t, $J = 7.5$ Hz, 1H), 7.21 – 7.11 (m, 2H), 7.07 (d, $J = 8.5$ Hz, 1H), 4.36 (dt, $J = 8.6, 6.0$ Hz, 4H), 2.43 (p, $J = 5.9$ Hz, 2H). ^{13}C NMR (101 MHz, CDCl_3) δ 189.83, 159.33, 156.75, 134.65, 131.41, 130.59, 130.41, 129.60, 129.16, 127.77, 126.88, 126.57, 124.14, 123.86, 118.87, 112.71, 106.90, 66.11, 64.08, 29.20.

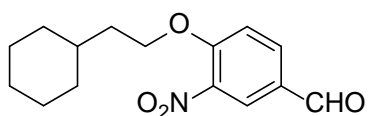


4-(3-([1,1'-Biphenyl]-4-yloxy)propoxy)-3-chlorobenzaldehyde (33c). Obtained from the reaction of 3-chloro-4-hydroxybenzaldehyde and **32c**. Yield: 75 %. Yellow solid. ^1H NMR (400 MHz, CDCl_3) δ 9.85 (s, 1H), 7.94 – 7.89 (m, 1H), 7.76 (dd, $J = 8.5, 0.7$ Hz, 1H), 7.53 (t, $J = 8.1$ Hz, 4H), 7.42 (t, $J = 7.5$ Hz, 2H), 7.31 (dd, $J = 11.3, 4.5$ Hz, 1H), 7.07 (d, $J = 8.5$ Hz, 1H), 7.00 (d, $J = 7.9$ Hz, 2H), 4.33 (t, 2H), 4.27 (t, $J = 5.8$ Hz, 2H), 2.39 (p, $J = 5.8$ Hz, 2H). ^{13}C NMR (101 MHz, CDCl_3) δ 189.87, 159.32, 158.35, 140.84, 134.16, 131.40, 130.62, 130.39, 128.87, 128.34, 126.86, 124.11, 114.89, 112.68, 110.15, 66.00, 64.08, 29.20.



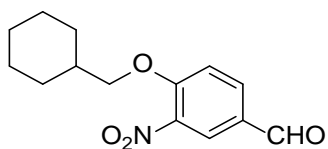
3-Nitro-4-(3-cyclohexylpropoxy)benzaldehyde (36a). Obtained from the reaction of 4-hydroxy-3-nitrobenzaldehyde and **35**. Yield: 93 %. Yellow

wax-like solid. ^1H NMR (400 MHz, CDCl_3) δ 9.92 (s, 1H), 8.33 (d, $J = 2.1$ Hz, 1H), 8.05 (dd, $J = 8.7, 2.1$ Hz, 1H), 7.20 (d, $J = 8.7$ Hz, 1H), 4.18 (t, $J = 6.5$ Hz, 2H), 1.91 – 1.83 (m, 2H), 1.75 – 1.63 (m, 5H), 1.36 – 1.16 (m, 6H), 0.96 – 0.85 (m, 2H). ^{13}C NMR (101 MHz, CDCl_3) δ 188.94, 156.93, 140.06, 134.66, 128.81, 127.59, 114.61, 70.89, 37.38, 33.49, 33.36, 26.71, 26.42, 26.27.



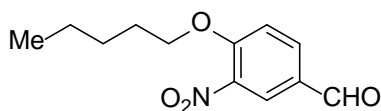
4-(2-cyclohexylethoxy)-3-nitrobenzaldehyde (36b).

Obtained from the reaction of 4-hydroxy-3-nitrobenzaldehyde and 1-bromo-2-cyclohexylethane. Yield: 91 %. Yellow solid. ^1H NMR (400 MHz, CDCl_3) δ 9.91 (s, 1H), 8.31 (d, $J = 2.1$ Hz, 1H), 8.04 (dd, $J = 8.7, 2.1$ Hz, 1H), 7.21 (d, $J = 8.7$ Hz, 1H), 4.23 (t, $J = 6.6$ Hz, 2H), 1.78 – 1.62 (m, 7H), 1.59 – 1.46 (m, 1H), 1.31 – 1.09 (m, 3H), 1.03 – 0.90 (m, 2H). ^{13}C NMR (101 MHz, CDCl_3) δ 188.92, 156.87, 140.06, 134.68, 128.77, 127.43, 114.59, 68.59, 36.04, 34.38, 33.20, 26.50, 26.20.



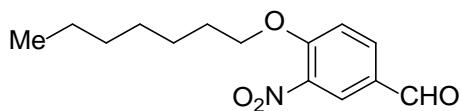
4-(Cyclohexylmethoxy)-3-nitrobenzaldehyde (36c).

Obtained from the reaction of 4-hydroxy-3-nitrobenzaldehyde and (bromomethyl)cyclohexane. Yield: 97 %. White solid. ^1H NMR (400 MHz, CDCl_3) δ 9.92 (s, 1H), 8.33 (d, $J = 2.1$ Hz, 1H), 8.05 (dd, $J = 8.7, 2.1$ Hz, 1H), 7.19 (d, $J = 8.7$ Hz, 1H), 3.99 (d, $J = 5.9$ Hz, 2H), 1.93 – 1.67 (m, 6H), 1.38 – 1.05 (m, 5H). ^{13}C NMR (101 MHz, CDCl_3) δ 188.93, 157.08, 134.66, 128.79, 127.58, 114.61, 75.65, 37.52, 29.64, 26.40, 25.79.



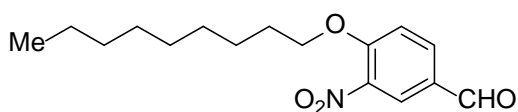
3-Nitro-4-(pentyloxy)benzaldehyde (36d)

Obtained from the reaction of 4-hydroxy-3-nitrobenzaldehyde and 1-bromopentane. Yield: 96 %. Yellow solid. ^1H NMR (400 MHz, CDCl_3) δ 9.92 (s, 1H), 8.32 (d, $J = 2.0$ Hz, 1H), 8.05 (dd, $J = 8.7, 2.1$ Hz, 1H), 7.20 (d, $J = 8.7$ Hz, 1H), 4.20 (t, $J = 6.5$ Hz, 2H), 1.92 – 1.80 (m, 2H), 1.53 – 1.32 (m, 4H), 0.93 (t, $J = 7.2$ Hz, 3H). ^{13}C NMR (101 MHz, CDCl_3) δ 188.94, 156.91, 140.07, 134.68, 128.81, 127.52, 114.59, 70.50, 28.55, 28.00, 22.40, 14.06.



4-(Heptyloxy)-3-nitrobenzaldehyde (36e). Obtained

from the reaction of 4-hydroxy-3-nitrobenzaldehyde and 1-bromoheptane. Yield: 92 %. Yellow solid. ^1H NMR (400 MHz, CDCl_3) δ 9.92 (s, 1H), 8.32 (d, $J = 1.9$ Hz, 1H), 8.09 – 8.01 (m, 1H), 7.20 (d, $J = 8.7$ Hz, 1H), 4.20 (t, $J = 6.4$ Hz, 2H), 1.93 – 1.78 (m, 2H), 1.52 – 1.43 (m, 2H), 1.39 – 1.24 (m, 6H), 0.88 (t, $J = 6.6$ Hz, 3H). ^{13}C NMR (101 MHz, CDCl_3) δ 188.94, 156.92, 140.07, 134.67, 128.81, 127.53, 114.60, 70.52, 31.78, 28.98, 28.86, 25.83, 22.69, 14.19.

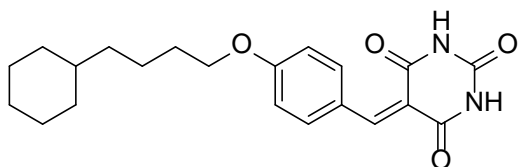


3-Nitro-4-(nonyloxy)benzaldehyde (36f).

Obtained from the reaction of 4-hydroxy-3-nitrobenzaldehyde and 1-bromoheptane. Yield: 87 %. Yellow solid. ^1H NMR (400 MHz, CDCl_3) δ 9.91 (s, 1H), 8.31 (d, $J = 2.0$ Hz, 1H), 8.04 (dd, $J = 8.7, 2.1$ Hz, 1H), 7.20 (d, $J = 8.7$ Hz, 1H), 4.19 (t, $J = 6.4$ Hz, 2H), 1.92 – 1.79 (m, 2H), 1.52 – 1.42 (m, 2H), 1.36 – 1.21 (m, 10H), 0.86 (t, $J = 6.8$ Hz, 3H). ^{13}C NMR (101 MHz, CDCl_3) δ 188.93, 156.89, 140.04, 134.69, 128.78, 127.48, 114.59, 70.50, 31.94, 29.53, 29.31, 29.30, 28.83, 25.84, 22.76, 14.21.

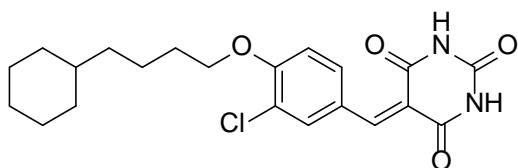
4.2.5 Preparation of the benzylidenenbarbituric acid derivatives 25a–25q, 27a–27c, 29a–29c, 31, 34a–34c and 37a–37f

Preparation of 25b. The suspension of **24b** (0.30 g, 1.02 mmol, 1.00 equiv.) and barbituric acid (0.13 g, 1.02 mmol, 1.00 equiv.) in absolute ethanol and distilled water (4:1, v/v) was heated at reflux for 5 h and the reaction mixture was cooled to room temperature. The precipitate was filtered off, washed with hot water and ethanol, and dried under vacuum to afford the product as yellow powders in high purity (0.37 g, 90 %). The analytical sample was obtained by recrystallization from a mixture of ethanol and DMF. The synthesis for other benzylidenebarbituric acid derivatives followed the same protocol as described, but with different starting materials.



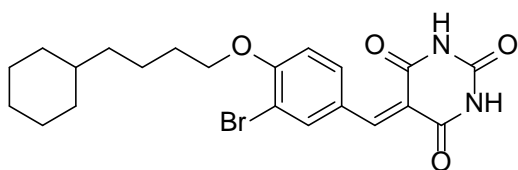
5-(4-(4-

Cyclohexylbutoxy)benzylidene)pyrimidine-2,4,6(1H,3H,5H)-trione (25a). Obtained from the condensation of **24a** with barbituric acid. Yield: 86 %. Yellow solid. ¹H NMR (400 MHz, DMSO) δ 11.29 (s, 1H), 11.16 (s, 1H), 8.36 (d, *J* = 8.1 Hz, 2H), 8.24 (s, 1H), 7.04 (d, *J* = 8.0 Hz, 2H), 4.09 (t, *J* = 6.4 Hz, 2H), 1.75 – 1.55 (m, 7H), 1.47 – 1.36 (m, 2H), 1.25 – 1.06 (m, 6H), 0.92 – 0.75 (m, 2H). ¹³C NMR (101 MHz, DMSO) δ 163.90, 162.96, 162.16, 154.95, 150.17, 137.54, 124.98, 115.37, 114.32, 68.02, 36.98, 36.53, 32.82, 28.77, 26.20, 25.83, 22.68. HRMS (ESI⁺) *m/z* calcd for C₂₁H₂₇N₂O₄ (MH)⁺: 371.1965, found: 371.1971.



5-(3-Chloro-4-(4-

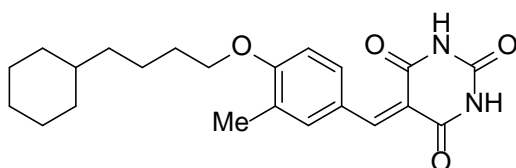
cyclohexylbutoxy)benzylidene)pyrimidine-2,4,6(1H,3H,5H)-trione (25b). Obtained from the condensation of **24b** with barbituric acid. Yield: 90 %. Yellow solid. ¹H NMR (400 MHz, DMSO) δ 11.34 (s, 1H), 11.23 (s, 1H), 8.66 (d, *J* = 2.1 Hz, 1H), 8.20 (s, 1H), 8.15 (dd, *J* = 9.1, 2.2 Hz, 1H), 7.25 (d, *J* = 8.9 Hz, 1H), 4.18 (t, *J* = 6.4 Hz, 2H), 1.82 – 1.49 (m, 7H), 1.49 – 1.36 (m, 2H), 1.30 – 1.02 (m, 6H), 0.97 – 0.73 (m, 2H). ¹³C NMR (101 MHz, DMSO) δ 163.58, 162.12, 157.54, 153.26, 150.13, 136.54, 135.20, 125.66, 120.96, 116.92, 112.94, 69.09, 36.94, 36.41, 32.80, 28.57, 26.20, 25.83, 22.59. HRMS (ESI⁺) *m/z* calcd for C₂₁H₂₆BrN₂O₄ (MH)⁺: 405.1576, found: 405.1574.



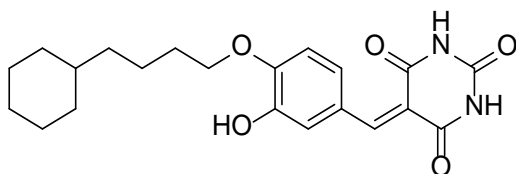
5-(3-Bromo-4-(4-

cyclohexylbutoxy)benzylidene)pyrimidine-2,4,6(1H,3H,5H)-trione (25c). Obtained from the condensation of **24c** with barbituric acid. Yield: 92 %. Yellow solid. ¹H NMR (400 MHz, DMSO) δ 11.34 (s, 1H), 11.22 (s, 1H), 8.81 (d, *J* = 2.1 Hz, 1H), 8.19 (dd, *J* = 8.2,

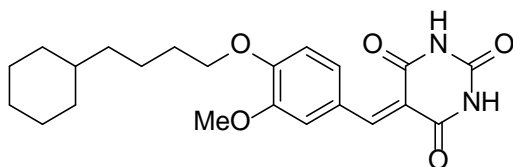
2.7 Hz, 2H), 7.21 (d, $J = 8.9$ Hz, 1H), 4.17 (t, $J = 6.3$ Hz, 2H), 1.78 – 1.58 (m, 7H), 1.50 – 1.41 (m, 2H), 1.26 – 1.05 (m, 6H), 0.90 – 0.79 (m, 2H). ^{13}C NMR (101 MHz, DMSO) δ 163.57, 162.12, 158.38, 153.15, 150.13, 138.34, 137.09, 126.19, 116.87, 112.73, 110.60, 69.14, 36.95, 36.40, 32.80, 28.57, 26.20, 25.83, 22.61. HRMS (ESI+) m/z calcd for $\text{C}_{21}\text{H}_{26}\text{BrN}_2\text{O}_4$ (MH) $^+$: 449.1070, found: 449.1059.



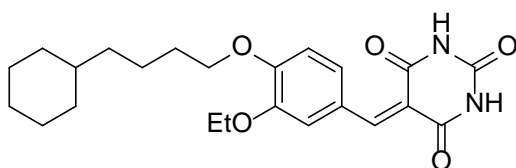
5-(4-(4-Cyclohexylbutoxy)-3-methylbenzylidene)pyrimidine-2,4,6(1H,3H,5H)-trione (25d) Obtained from the condensation of **24d** with barbituric acid. Yield: 82 %. Orange solid. ^1H NMR (400 MHz, DMSO) δ 11.27 (s, 1H), 11.14 (s, 1H), 8.30 (dd, $J = 8.8, 2.1$ Hz, 1H), 8.21 (s, 2H), 7.05 (d, $J = 8.8$ Hz, 1H), 4.10 (t, $J = 6.3$ Hz, 2H), 2.17 (s, 3H), 1.77 – 1.57 (m, 7H), 1.49 – 1.39 (m, 2H), 1.25 – 1.04 (m, 6H), 0.90 – 0.79 (m, 2H). ^{13}C NMR (101 MHz, DMSO) δ 163.96, 162.15, 161.34, 155.30, 150.19, 137.51, 135.98, 125.63, 124.56, 114.97, 110.88, 68.00, 36.95, 36.50, 32.81, 28.77, 26.20, 25.84, 22.72, 15.88. HRMS (ESI+) m/z calcd for $\text{C}_{22}\text{H}_{29}\text{N}_2\text{O}_4$ (MH) $^+$: 385.2122, found: 385.2125.



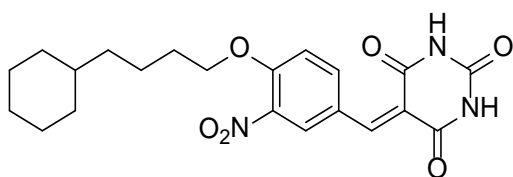
5-(4-(4-Cyclohexylbutoxy)-3-hydroxybenzylidene)pyrimidine-2,4,6(1H,3H,5H)-trione (25e) Obtained from the condensation of **24e** with barbituric acid. Yield: 86 %. Yellow solid. ^1H NMR (400 MHz, DMSO) δ 11.26 (s, 1H), 11.14 (s, 1H), 9.32 (s, 1H), 8.14 (d, $J = 4.9$ Hz, 2H), 7.71 (d, $J = 8.5$ Hz, 1H), 7.04 (d, $J = 8.0$ Hz, 1H), 4.08 (t, $J = 5.6$ Hz, 2H), 1.78 – 1.57 (m, 7H), 1.49 – 1.38 (m, 2H), 1.28 – 1.05 (m, 6H), 0.93 – 0.79 (m, 2H). ^{13}C NMR (101 MHz, DMSO) δ 164.00, 162.11, 155.55, 152.39, 150.19, 145.86, 130.37, 125.18, 120.49, 114.86, 112.05, 68.32, 37.04, 36.59, 32.84, 28.84, 26.21, 25.85, 22.70. HRMS (ESI+) m/z calcd for $\text{C}_{21}\text{H}_{27}\text{N}_2\text{O}_5$ (MH) $^+$: 387.1914, found: 387.1920.



5-(4-(4-Cyclohexylbutoxy)-3-methoxybenzylidene)pyrimidine-2,4,6(1H,3H,5H)-trione (25f) Obtained from the condensation of **24f** with barbituric acid. Yield: 95 %. Yellow solid. ^1H NMR (400 MHz, DMSO) δ 11.30 (s, 1H), 11.17 (s, 1H), 8.41 (s, 1H), 8.24 (s, 1H), 7.87 (d, $J = 8.5$ Hz, 1H), 7.08 (d, $J = 8.5$ Hz, 1H), 4.07 (t, $J = 5.9$ Hz, 2H), 3.81 (s, 3H), 1.77 – 1.54 (m, 7H), 1.46 – 1.03 (m, 8H), 0.92 – 0.77 (m, 2H). ^{13}C NMR (101 MHz, DMSO) δ 163.99, 162.36, 155.50, 153.19, 150.17, 147.87, 131.80, 125.11, 117.04, 115.06, 111.79, 68.43, 55.45, 36.99, 36.53, 32.83, 28.77, 26.22, 25.85, 22.73. HRMS (ESI+) m/z calcd for $\text{C}_{22}\text{H}_{29}\text{N}_2\text{O}_5$ (MH) $^+$: 401.2071, found: 401.2074.

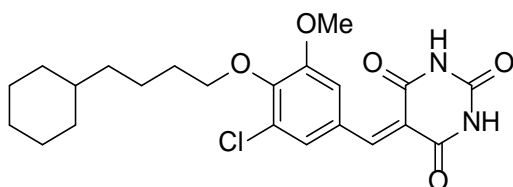


5-(4-(4-Cyclohexylbutoxy)-3-ethoxybenzylidene)pyrimidine-2,4,6(1H,3H,5H)-trione (25g) Obtained from the condensation of **24g** with barbituric acid. Yield: 92 %. Yellow solid. ^1H NMR (400 MHz, DMSO) δ 11.28 (d, $J = 1.3$ Hz, 1H), 11.16 (d, $J = 1.4$ Hz, 1H), 8.42 (d, $J = 2.1$ Hz, 1H), 8.23 (s, 1H), 7.82 (dd, $J = 8.7, 2.0$ Hz, 1H), 7.08 (d, $J = 8.7$ Hz, 1H), 4.12 – 4.02 (m, 4H), 1.75 – 1.56 (m, 7H), 1.46 – 1.32 (m, 5H), 1.25 – 1.03 (m, 6H), 0.96 – 0.72 (m, 2H). ^{13}C NMR (101 MHz, DMSO) δ 163.96, 162.35, 155.53, 153.46, 150.14, 147.07, 131.88, 125.12, 118.29, 114.99, 112.05, 68.39, 63.82, 36.95, 36.46, 32.79, 28.70, 26.21, 25.84, 22.64, 14.58. HRMS (ESI+) m/z calcd for $\text{C}_{23}\text{H}_{31}\text{N}_2\text{O}_5$ (MH) $^+$: 415.2227, found: 415.2231.

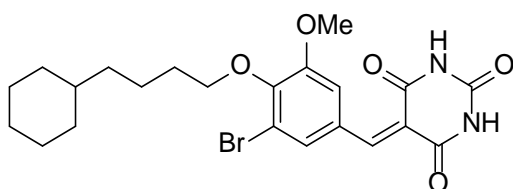


5-(4-(4-Cyclohexylbutoxy)-3-nitrobenzylidene)pyrimidine-2,4,6(1H,3H,5H)-trione (25h) Obtained from the condensation of **24h** with barbituric acid. Yield: 94 %. Yellow solid. ^1H NMR (400 MHz, DMSO) δ 11.40 (s, 1H), 11.29 (s, 1H), 8.99 (d, $J = 2.1$ Hz, 1H), 8.37 (dd, $J = 9.2, 2.2$ Hz,

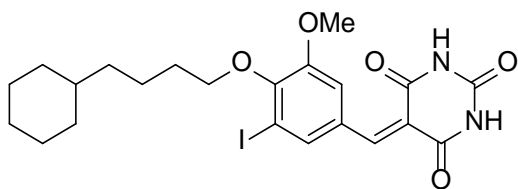
1H), 8.25 (s, 1H), 7.45 (d, $J = 9.0$ Hz, 1H), 4.26 (t, $J = 6.3$ Hz, 2H), 1.75 – 1.56 (m, 7H), 1.47 – 1.37 (m, 2H), 1.25 – 1.06 (m, 6H), 0.84 (dd, $J = 20.8, 10.4$ Hz, 2H). ^{13}C NMR (101 MHz, DMSO) δ 163.73, 162.48, 154.62, 152.44, 150.57, 141.09, 139.09, 130.47, 124.99, 118.90, 114.90, 70.22, 37.36, 36.77, 33.21, 28.87, 26.64, 26.26, 22.89. HRMS (ESI+) m/z calcd for $\text{C}_{21}\text{H}_{29}\text{N}_4\text{O}_6$ ($\text{M}+\text{NH}_4$) $^+$: 433.2082, found: 433.2084.



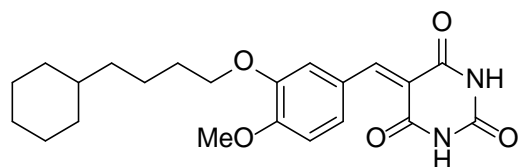
5-(3-Chloro-4-(4-cyclohexylbutoxy)-5-methoxybenzylidene)pyrimidine-2,4,6(1H,3H,5H)-trione (25i) Obtained from the condensation of **24i** with barbituric acid. Yield: 75 %. Yellow solid. ^1H NMR (400 MHz, DMSO) δ 11.40 (s, 1H), 11.27 (s, 1H), 8.20 (s, 1H), 8.06 (s, 1H), 7.99 (s, 1H), 4.07 (t, $J = 6.3$ Hz, 2H), 3.85 (s, 3H), 1.77 – 1.52 (m, 7H), 1.52 – 1.32 (m, 2H), 1.32 – 1.01 (m, 6H), 0.98 – 0.52 (m, 2H). ^{13}C NMR (101 MHz, DMSO) δ 163.36, 161.89, 152.98, 152.40, 150.11, 147.27, 128.51, 127.50, 126.32, 118.70, 117.56, 73.20, 56.27, 37.00, 36.54, 32.84, 29.94, 26.21, 25.85, 22.58. HRMS (ESI+) m/z calcd for $\text{C}_{21}\text{H}_{28}\text{ClN}_2\text{O}_4$ (MH) $^+$: 435.1681, found: 435.1681.



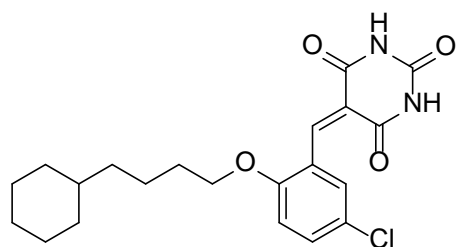
5-(3-Bromo-4-(4-cyclohexylbutoxy)-5-methoxybenzylidene)pyrimidine-2,4,6(1H,3H,5H)-trione (25j) Obtained from the condensation of **24j** with barbituric acid. Yield: 76 %. Yellow solid. ^1H NMR (400 MHz, DMSO) δ 11.40 (s, 1H), 11.27 (s, 1H), 8.23 – 8.16 (m, 2H), 8.02 (d, $J = 1.8$ Hz, 1H), 4.06 (t, $J = 6.4$ Hz, 2H), 3.85 (s, 3H), 1.73 – 1.57 (m, 7H), 1.50 – 1.40 (m, 2H), 1.27 – 1.05 (m, 6H), 0.92 – 0.78 (m, 2H). ^{13}C NMR (101 MHz, DMSO) δ 163.36, 161.90, 152.85, 152.15, 150.11, 148.27, 130.37, 129.20, 118.67, 118.13, 116.04, 73.11, 56.25, 36.99, 36.57, 32.85, 29.96, 26.21, 25.85, 22.65. HRMS (ESI+) m/z calcd for $\text{C}_{22}\text{H}_{31}\text{BrN}_3\text{O}_5$ ($\text{M}+\text{NH}_4$) $^+$: 496.1442, found: 496.1438.



5-(4-(4-Cyclohexylbutoxy)-3-iodo-5-methoxybenzylidene)pyrimidine-2,4,6(1H,3H,5H)-trione (25k) Obtained from the condensation of **24k** with barbituric acid. Yield: 72 %. Yellow solid. ^1H NMR (400 MHz, DMSO) δ 11.38 (s, 1H), 11.25 (s, 1H), 8.33 (d, $J = 1.7$ Hz, 1H), 8.18 (s, 1H), 8.05 (d, $J = 1.8$ Hz, 1H), 4.04 (t, $J = 6.4$ Hz, 2H), 3.83 (s, 3H), 1.78 – 1.48 (m, 7H), 1.48 – 1.38 (m, 2H), 1.36 – 0.97 (m, 6H), 0.97 – 0.73 (m, 2H). ^{13}C NMR (101 MHz, DMSO) δ 163.38, 161.91, 152.87, 150.93, 150.86, 150.11, 136.51, 130.03, 118.85, 118.31, 92.17, 72.92, 56.07, 36.99, 36.61, 32.86, 30.07, 26.22, 25.86, 22.82. HRMS (ESI+) m/z calcd for $\text{C}_{21}\text{H}_{28}\text{IN}_2\text{O}_4$ (MH) $^+$: 527.1037, found: 527.1034.

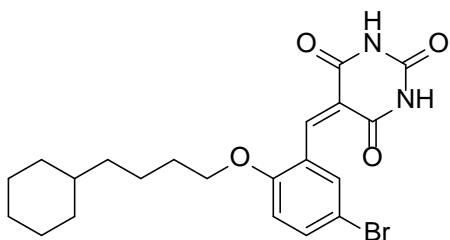


5-(3-(4-Cyclohexylbutoxy)-4-methoxybenzylidene)pyrimidine-2,4,6(1H,3H,5H)-trione (25l) Obtained from the condensation of **24l** with barbituric acid. Yield: 83 %. Yellow solid. ^1H NMR (400 MHz, DMSO) δ 11.29 (s, 1H), 11.16 (s, 1H), 8.40 (d, $J = 1.9$ Hz, 1H), 8.24 (s, 1H), 7.86 (dd, $J = 8.6, 1.8$ Hz, 1H), 7.09 (d, $J = 8.6$ Hz, 1H), 3.99 (t, $J = 6.5$ Hz, 2H), 3.88 (s, 3H), 1.80 – 1.47 (m, 7H), 1.47 – 1.32 (m, 2H), 1.32 – 1.00 (m, 6H), 0.97 – 0.73 (m, 2H). ^{13}C NMR (101 MHz, DMSO) δ 163.96, 162.34, 155.53, 153.86, 150.14, 147.15, 131.66, 125.26, 117.84, 115.14, 111.19, 68.15, 55.86, 36.98, 36.56, 32.83, 28.85, 26.21, 25.85, 22.79. HRMS (ESI+) m/z calcd for $\text{C}_{22}\text{H}_{29}\text{N}_2\text{O}_5$ (MH) $^+$: 401.2071, found: 401.2076.

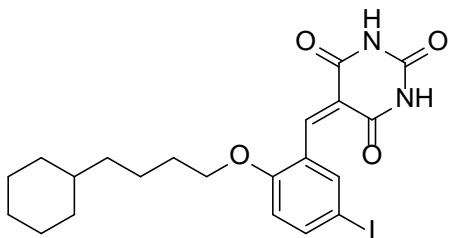


5-(5-Chloro-2-(4-cyclohexylbutoxy)benzylidene)pyrimidine-2,4,6(1H,3H,5H)-trione (25m) Obtained

from the condensation of **24m** with barbituric acid. Yield: 73 %. Yellow solid. ¹H NMR (400 MHz, DMSO) δ 11.39 (s, 1H), 11.21 (s, 1H), 8.38 (s, 1H), 8.00 (d, *J* = 2.6 Hz, 1H), 7.50 (dd, *J* = 8.9, 2.7 Hz, 1H), 7.12 (d, *J* = 9.0 Hz, 1H), 4.07 (t, *J* = 6.3 Hz, 2H), 1.79 – 1.47 (m, 7H), 1.47 – 1.32 (m, 2H), 1.32 – 0.97 (m, 6H), 0.96 – 0.72 (m, 2H). ¹³C NMR (101 MHz, DMSO) δ 162.98, 161.41, 156.96, 150.17, 147.86, 132.78, 131.31, 123.31, 123.14, 119.98, 113.72, 68.75, 36.95, 36.48, 32.77, 28.67, 26.20, 25.83, 22.67. HRMS (ESI+) *m/z* calcd for C₂₁H₂₆ClN₂O₄ (MH)⁺: 405.1576, found: 405.1578.

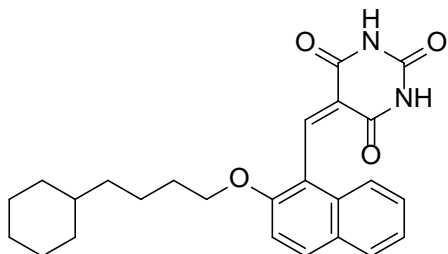


5-(5-Bromo-2-(4-cyclohexylbutoxy)benzylidene)pyrimidine-2,4,6(1H,3H,5H)-trione (25n) Obtained from the condensation of **24n** with barbituric acid. Yield: 75 %. Yellow solid. ¹H NMR (400 MHz, DMSO) δ 11.38 (s, 1H), 11.21 (s, 1H), 8.36 (s, 1H), 8.11 (d, *J* = 2.1 Hz, 1H), 7.62 (dd, *J* = 8.9, 2.6 Hz, 1H), 7.07 (d, *J* = 9.0 Hz, 1H), 4.07 (t, *J* = 6.3 Hz, 2H), 1.73 – 1.56 (m, 7H), 1.46 – 1.35 (m, 2H), 1.24 – 1.06 (m, 6H), 0.89 – 0.77 (m, 2H). ¹³C NMR (101 MHz, DMSO) δ 162.99, 161.43, 157.35, 150.19, 147.74, 135.59, 134.10, 123.85, 120.01, 114.21, 110.77, 68.69, 36.96, 36.47, 32.78, 28.65, 26.21, 25.83, 22.67. HRMS (ESI+) *m/z* calcd for C₂₁H₂₆BrN₂O₄ (MH)⁺: 449.1070, found: 449.1070.

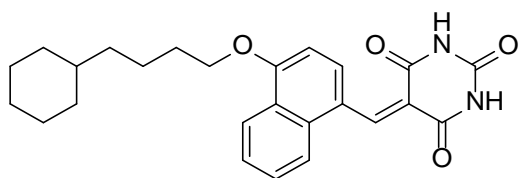


5-(2-(4-Cyclohexylbutoxy)-5-iodobenzylidene)pyrimidine-2,4,6(1H,3H,5H)-trione (25o) Obtained from the condensation of **24o** with barbituric acid. Yield: 71 %. Orange solid. ¹H NMR (400 MHz, DMSO) δ 11.37 (s, 1H), 11.20 (s, 1H), 8.34 (s, 1H), 8.25 (dd, *J* = 2.3, 0.6 Hz, 1H), 7.75 (dd, *J* = 8.8, 2.2 Hz, 1H), 6.93 (d, *J* = 8.9 Hz, 1H), 4.05 (t, *J* = 6.3 Hz, 2H), 1.78 – 1.47 (m, 7H), 1.47 – 1.30 (m, 2H), 1.30 – 1.01 (m, 6H), 0.96 – 0.48 (m, 2H). ¹³C NMR (101 MHz,

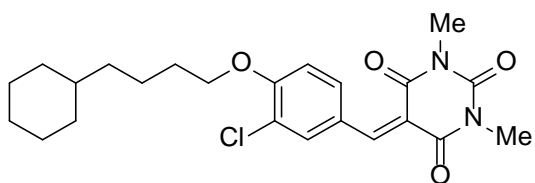
DMSO) δ 162.99, 161.44, 157.94, 150.18, 147.84, 141.40, 139.86, 124.28, 119.74, 114.59, 81.95, 68.53, 36.95, 36.47, 32.77, 28.64, 26.20, 25.82, 22.66. HRMS (ESI+) m/z calcd for $C_{21}H_{26}IN_2O_4$ (MH)⁺: 497.0932, found: 497.0931.



5-((2-(4-Cyclohexylbutoxy)naphthalen-1-yl)methylene)pyrimidine-2,4,6(1H,3H,5H)-trione (25p) Obtained from the condensation of **24p** with barbituric acid. Yield: 73 %. Yellow solid. ¹H NMR (400 MHz, DMSO) δ 11.43 (s, 1H), 11.13 (s, 1H), 8.55 (s, 1H), 8.01 (d, J = 9.1 Hz, 1H), 7.89 (d, J = 8.0 Hz, 1H), 7.65 (d, J = 8.4 Hz, 1H), 7.51 – 7.34 (m, 3H), 4.13 (t, J = 6.2 Hz, 2H), 1.76 – 1.50 (m, 7H), 1.50 – 1.16 (m, 5H), 1.16 – 0.93 (m, 3H), 0.93 – 0.67 (m, 2H). ¹³C NMR (101 MHz, DMSO) δ 162.68, 160.77, 154.57, 150.29, 148.68, 132.03, 131.04, 128.32, 127.92, 127.11, 124.15, 123.75, 122.55, 117.27, 114.08, 68.67, 36.99, 36.61, 32.77, 29.07, 26.21, 25.83, 22.83. HRMS (ESI+) m/z calcd for $C_{25}H_{29}N_2O_4$ (MH)⁺: 421.2122, found: 421.2124.



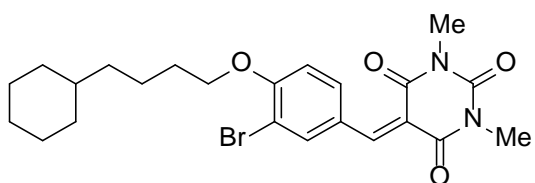
5-((4-(4-Cyclohexylbutoxy)naphthalen-1-yl)methylene)pyrimidine-2,4,6(1H,3H,5H)-trione (25q) Obtained from the condensation of **24q** with barbituric acid. Yield: 76 %. Orange solid. ¹H NMR (400 MHz, DMSO) δ 11.37 (s, 1H), 11.13 (s, 1H), 8.86 (s, 1H), 8.28 (dd, J = 19.6, 8.3 Hz, 2H), 7.94 (d, J = 8.4 Hz, 1H), 7.72 – 7.55 (m, 2H), 7.08 (d, J = 8.5 Hz, 1H), 4.26 (t, J = 6.3 Hz, 2H), 1.93 – 1.78 (m, 2H), 1.78 – 1.45 (m, 7H), 1.34 – 1.02 (m, 6H), 0.97 – 0.73 (m, 2H). ¹³C NMR (101 MHz, DMSO) δ 163.64, 161.49, 157.99, 151.79, 150.32, 133.34, 132.97, 128.18, 125.73, 124.42, 123.71, 122.34, 121.55, 118.13, 104.51, 68.38, 36.96, 36.54, 32.83, 28.77, 26.20, 25.83, 22.89. HRMS (ESI+) m/z calcd for $C_{25}H_{29}N_2O_4$ (MH)⁺: 421.2122, found: 421.2123.



5-(3-Chloro-4-(4-

cyclohexylbutoxy)benzylidene)-1,3-dimethylpyrimidine-2,4,6(1*H*,3*H*,5*H*)-trione

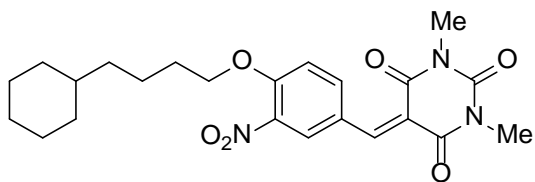
(27a). Obtained from the condensation of **24b** with 1,3-dimethylbarbituric acid. Yield: 94 %. Yellow solid. ¹H NMR (400 MHz, DMSO) δ 8.63 (d, *J* = 2.2 Hz, 1H), 8.27 (s, 1H), 8.13 (dd, *J* = 9.0, 2.2 Hz, 1H), 7.26 (d, *J* = 8.8 Hz, 1H), 4.19 (t, *J* = 6.4 Hz, 2H), 3.22 (d, *J* = 7.8 Hz, 6H), 1.82 – 1.49 (m, 7H), 1.49 – 1.38 (m, 2H), 1.31 – 1.04 (m, 6H), 0.97 – 0.75 (m, 2H). ¹³C NMR (101 MHz, DMSO) δ 162.31, 160.75, 157.56, 154.08, 151.02, 136.48, 134.99, 125.68, 120.97, 116.70, 112.93, 69.09, 36.94, 36.41, 32.80, 28.64, 28.56, 28.07, 26.20, 25.82, 22.58. HRMS (ESI+) *m/z* calcd for C₂₃H₃₀ClN₂O₄ (MH)⁺: 433.1889, found: 433.1890.



5-(3-bromo-4-(4-

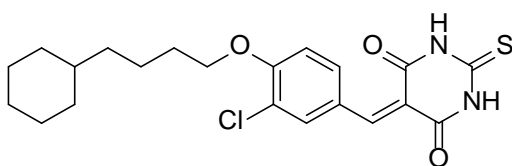
cyclohexylbutoxy)benzylidene)-1,3-dimethylpyrimidine-2,4,6(1*H*,3*H*,5*H*)-trione

(27b). Obtained from the condensation of **24c** with 1,3-dimethylbarbituric acid. Yield: 91 %. Yellow solid. ¹H NMR (400 MHz, DMSO) δ 8.78 (d, *J* = 2.1 Hz, 1H), 8.26 (s, 1H), 8.16 (dd, *J* = 9.1, 2.1 Hz, 1H), 7.22 (d, *J* = 8.8 Hz, 1H), 4.18 (t, *J* = 6.3 Hz, 2H), 3.22 (d, *J* = 7.4 Hz, 6H), 1.78 – 1.58 (m, 7H), 1.51 – 1.41 (m, 2H), 1.27 – 1.07 (m, 6H), 0.91 – 0.79 (m, 2H). ¹³C NMR (101 MHz, DMSO) δ 162.31, 160.75, 158.42, 154.01, 151.02, 138.16, 137.09, 126.21, 116.61, 112.72, 110.62, 69.15, 36.96, 36.42, 32.81, 28.65, 28.58, 28.08, 26.21, 25.84, 22.62. HRMS (ESI+) *m/z* calcd for C₂₃H₃₀BrN₂O₄ (MH)⁺: 477.1383, found: 477.1380.



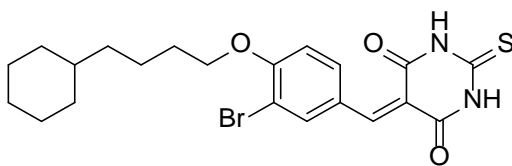
5-(4-(4-cyclohexylbutoxy)-3-

nitrobenzylidene)-1,3-dimethylpyrimidine-2,4,6(1H,3H,5H)-trione (27c). Obtained from the condensation of **24h** with 1,3-dimethylbarbituric acid. Yield: 95 %. Yellow solid. ^1H NMR (400 MHz, DMSO) δ 8.94 (d, $J = 2.0$ Hz, 1H), 8.39 – 8.29 (m, 2H), 7.45 (d, $J = 9.0$ Hz, 1H), 4.26 (t, $J = 6.3$ Hz, 2H), 3.21 (d, $J = 13.5$ Hz, 6H), 1.77 – 1.57 (m, 7H), 1.47 – 1.36 (m, 2H), 1.26 – 1.04 (m, 6H), 0.92 – 0.78 (m, 2H). ^{13}C NMR (101 MHz, DMSO) δ 162.02, 160.64, 154.21, 152.91, 150.97, 140.50, 138.66, 129.87, 124.57, 118.13, 114.45, 69.80, 36.92, 36.34, 32.77, 28.63, 28.43, 28.08, 26.20, 25.82, 22.45. HRMS (ESI+) m/z calcd for $\text{C}_{23}\text{H}_{30}\text{N}_3\text{O}_6$ (MH) $^+$: 444.2129, found: 444.2130.



5-(3-Chloro-4-(4-cyclohexylbutoxy)benzylidene)-2-thioxodihydropyrimidine-4,6(1H,5H)-dione (29a)

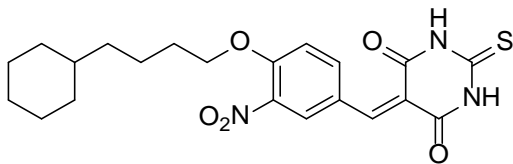
Obtained from the condensation of **24b** with 2-thiobarbituric acid. Yield: 90 %. Yellow solid. ^1H NMR (400 MHz, DMSO) δ 12.42 (s, 1H), 12.33 (s, 1H), 8.72 (d, $J = 2.0$ Hz, 1H), 8.24 – 8.16 (m, 2H), 7.27 (d, $J = 8.9$ Hz, 1H), 4.20 (t, $J = 6.4$ Hz, 2H), 1.82 – 1.49 (m, 7H), 1.49 – 1.36 (m, 2H), 1.30 – 1.03 (m, 6H), 0.96 – 0.73 (m, 2H). ^{13}C NMR (101 MHz, DMSO) δ 178.33, 161.89, 159.92, 157.99, 154.23, 137.05, 135.46, 125.74, 121.09, 116.96, 113.04, 69.19, 36.93, 36.41, 32.80, 28.55, 26.20, 25.82, 22.57. HRMS (ESI+) m/z calcd for $\text{C}_{21}\text{H}_{26}\text{ClN}_2\text{O}_3\text{S}$ (MH) $^+$: 421.1347, found: 421.1348.



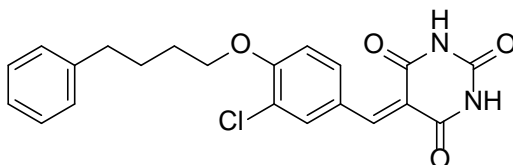
5-(3-Bromo-4-(4-cyclohexylbutoxy)benzylidene)-2-thioxodihydropyrimidine-4,6(1H,5H)-dione (29b)

Obtained from the condensation of **24c** with 2-thiobarbituric acid. Yield: 83 %. Yellow solid. ^1H NMR (400 MHz, DMSO) δ 12.42 (s, 1H), 12.33 (s, 1H), 8.87 (d, $J = 2.1$ Hz, 1H), 8.27 – 8.18 (m, 2H), 7.22 (d, $J = 8.8$ Hz, 1H), 4.18 (t, $J = 6.3$ Hz, 2H), 1.77 – 1.56 (m, 7H), 1.50 – 1.40 (m, 2H), 1.26 – 1.06 (m, 6H), 0.90 – 0.78 (m, 2H). ^{13}C NMR (101 MHz, DMSO) δ 178.32, 161.88, 159.93, 158.85, 154.15, 138.63, 137.64, 126.28, 116.88, 112.81, 110.74, 69.24, 36.95, 36.42, 32.81, 28.57, 26.21, 25.84, 22.61. HRMS (ESI+) m/z calcd for

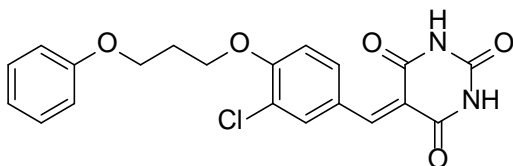
C₂₁H₂₆BrN₂O₃S (MH)⁺: 465.0842, found: 465.0842.



5-(4-(4-Cyclohexylbutoxy)-3-nitrobenzylidene)-2-thioxodihydropyrimidine-4,6(1H,5H)-dione (29c). Obtained from the condensation of **24h** with 2-thiobarbituric acid. Yield: 86 %. Yellow solid. ¹H NMR (400 MHz, DMSO) δ 12.47 (s, 1H), 12.38 (s, 1H), 9.06 (d, *J* = 2.0 Hz, 1H), 8.41 (dd, *J* = 9.3, 2.3 Hz, 1H), 8.27 (s, 1H), 7.46 (d, *J* = 9.0 Hz, 1H), 4.28 (t, *J* = 6.3 Hz, 2H), 1.75 – 1.57 (m, 7H), 1.47 – 1.38 (m, 2H), 1.26 – 1.07 (m, 6H), 0.90 – 0.79 (m, 2H). ¹³C NMR (101 MHz, DMSO) δ 178.44, 161.59, 159.85, 154.55, 152.93, 141.02, 138.70, 130.30, 124.59, 118.46, 114.56, 69.89, 36.92, 36.33, 32.77, 28.42, 26.20, 25.82, 22.45. HRMS (ESI⁺) *m/z* calcd for C₂₁H₂₆N₃O₅S (MH)⁺: 432.1588, found: 432.1587.

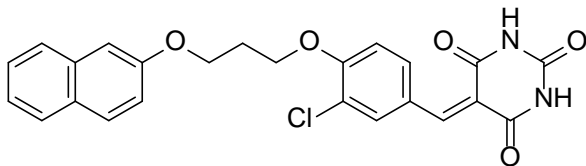


5-(3-chloro-4-(4-phenylbutoxy)benzylidene)pyrimidine-2,4,6(1H,3H,5H)-trione (31). Obtained from the condensation of **30** with barbituric acid. Yield: 89 %. Yellow solid. ¹H NMR (400 MHz, DMSO) δ 11.36 (s, 1H), 11.24 (s, 1H), 8.66 (d, *J* = 2.1 Hz, 1H), 8.22 – 8.11 (m, 2H), 7.32 – 7.12 (m, 6H), 4.21 (t, *J* = 5.6 Hz, 2H), 2.66 (t, *J* = 7.0 Hz, 2H), 1.91 – 1.51 (m, 4H). ¹³C NMR (101 MHz, DMSO) δ 163.62, 162.16, 157.52, 153.27, 150.18, 141.93, 136.57, 135.23, 128.30, 125.74, 125.71, 120.97, 116.96, 112.96, 68.94, 34.63, 27.89, 27.22. HRMS (ESI⁺) *m/z* calcd for C₂₁H₂₀ClN₂O₄ (MH)⁺: 399.1106, found: 399.1103.

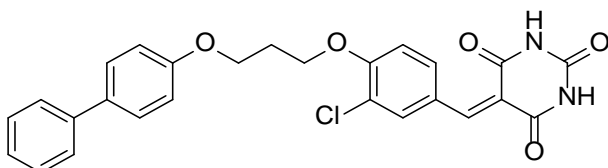


5-(3-Chloro-4-(3-phenoxypropoxy)benzylidene)pyrimidine-2,4,6(1H,3H,5H)-trione (34a) Obtained from the condensation of **33a** with barbituric acid. Yield: 84 %. White-yellow solid. ¹H

NMR (400 MHz, DMSO) δ 11.35 (s, 1H), 11.24 (s, 1H), 8.66 (d, $J = 2.0$ Hz, 1H), 8.23 – 8.12 (m, 2H), 7.35 – 7.24 (m, 3H), 6.93 (dd, $J = 15.3, 7.6$ Hz, 3H), 4.36 (t, $J = 6.1$ Hz, 2H), 4.16 (t, $J = 6.2$ Hz, 2H), 2.24 (p, $J = 6.1$ Hz, 2H). ^{13}C NMR (101 MHz, DMSO) δ 163.58, 162.13, 158.38, 157.27, 153.16, 150.16, 136.48, 135.20, 129.52, 125.90, 120.99, 120.61, 117.13, 114.42, 113.00, 65.93, 63.77, 28.37. HRMS (ESI+) m/z calcd for $\text{C}_{20}\text{H}_{18}\text{ClN}_2\text{O}_5$ (MH) $^+$: 401.0899, found: 401.0893.

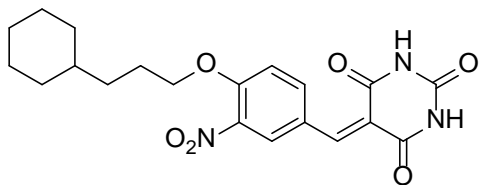


5-(3-Chloro-4-(3-(naphthalen-2-yloxy)propoxy)benzylidene)pyrimidine-2,4,6(1H,3H,5H)-trione (34b). Obtained from the condensation of **33b** with barbituric acid. Yield: 78 %. Yellow solid. ^1H NMR (400 MHz, DMSO) δ 11.35 (s, 1H), 11.23 (s, 1H), 8.66 (d, $J = 2.0$ Hz, 1H), 8.23 – 8.13 (m, 2H), 7.81 (t, $J = 8.6$ Hz, 3H), 7.45 (t, $J = 7.5$ Hz, 1H), 7.38 – 7.29 (m, 3H), 7.18 (dd, $J = 8.9, 2.3$ Hz, 1H), 4.41 (t, $J = 6.1$ Hz, 2H), 4.30 (t, $J = 6.2$ Hz, 2H), 2.32 (p, $J = 6.1$ Hz, 2H). ^{13}C NMR (101 MHz, DMSO) δ 163.54, 162.10, 157.26, 156.30, 153.14, 150.13, 136.44, 135.19, 134.25, 129.30, 128.48, 127.47, 126.66, 126.36, 125.91, 123.56, 120.99, 118.68, 117.12, 113.01, 106.67, 65.97, 64.05, 28.35. HRMS (ESI+) m/z calcd for $\text{C}_{24}\text{H}_{20}\text{ClN}_2\text{O}_5$ (MH) $^+$: 451.1055, found: 451.1051.

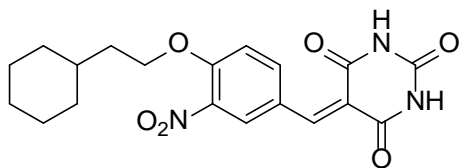


5-(4-(3-([1,1'-Biphenyl]-4-yloxy)propoxy)-3-chlorobenzylidene)pyrimidine-2,4,6(1H,3H,5H)-trione (34c). Obtained from the condensation of **33c** with barbituric acid. Yield: 80 %. Yellow solid. ^1H NMR (400 MHz, DMSO) δ 11.35 (s, 1H), 11.24 (s, 1H), 8.66 (d, $J = 2.1$ Hz, 1H), 8.20 (s, 1H), 8.16 (dd, $J = 8.9, 2.0$ Hz, 1H), 7.66 – 7.52 (m, 4H), 7.42 (t, $J = 7.7$ Hz, 2H), 7.37 – 7.24 (m, 2H), 7.04 (d, $J = 8.8$ Hz, 2H), 4.38 (t, $J = 6.0$ Hz, 2H), 4.22 (t, $J = 6.1$ Hz, 2H), 2.26 (p, $J = 5.9$ Hz, 2H). ^{13}C NMR (101 MHz, DMSO) δ 163.56, 162.11, 158.03, 157.28, 153.18, 150.15, 139.78, 136.47, 135.20, 132.65, 128.83, 127.77, 126.70, 126.15, 125.91, 121.01, 117.10, 114.90, 113.00, 65.92, 64.03, 28.37. HRMS (ESI+) m/z calcd for

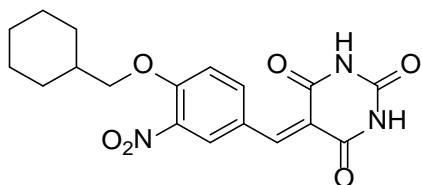
$C_{26}H_{22}ClN_2O_5$ (MH)⁺: 477.1212, found: 477.1209.



5-(4-(3-Cyclohexylpropoxy))-3-nitrobenzylidene)pyrimidine-2,4,6(1H,3H,5H)-trione (37a) Obtained from the condensation of **36a** with barbituric acid. Yield: 95 %. Yellow solid. ¹H NMR (400 MHz, DMSO) δ 11.40 (s, 1H), 11.29 (s, 1H), 8.99 (d, $J = 2.2$ Hz, 1H), 8.37 (dd, $J = 9.1, 2.2$ Hz, 1H), 8.25 (s, 1H), 7.45 (d, $J = 9.0$ Hz, 1H), 4.26 (t, $J = 6.3$ Hz, 2H), 1.79 – 1.59 (m, 7H), 1.35 – 1.10 (m, 6H), 0.93 – 0.81 (m, 2H). ¹³C NMR (101 MHz, DMSO) δ 163.28, 162.03, 154.17, 152.00, 150.12, 140.63, 138.67, 130.02, 124.56, 118.47, 114.47, 70.15, 36.54, 32.90, 32.77, 26.14, 25.75, 25.59. HRMS (ESI+) m/z calcd for $C_{20}H_{24}N_3O_6$ (MH)⁺: 402.1660, found: 402.1656.

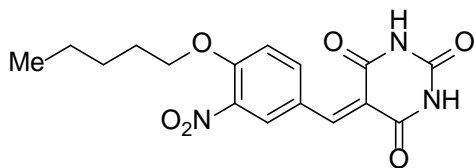


5-(4-(2-Cyclohexylethoxy))-3-nitrobenzylidene)pyrimidine-2,4,6(1H,3H,5H)-trione (37b) Obtained from the condensation of **36b** with barbituric acid. Yield: 87 %. Yellow solid. ¹H NMR (400 MHz, DMSO) δ 11.40 (s, 1H), 11.29 (s, 1H), 8.98 (s, 1H), 8.37 (d, $J = 8.1$ Hz, 1H), 8.25 (s, 1H), 7.47 (d, $J = 9.0$ Hz, 1H), 4.30 (t, $J = 6.5$ Hz, 2H), 1.76 – 1.59 (m, 7H), 1.51 – 1.41 (m, 1H), 1.26 – 1.08 (m, 3H), 1.00 – 0.89 (m, 2H). ¹³C NMR (101 MHz, DMSO) δ 163.28, 162.03, 154.14, 152.02, 150.12, 140.61, 138.70, 129.98, 124.57, 118.45, 114.50, 68.06, 35.45, 33.91, 32.50, 25.99, 25.70. HRMS (ESI+) m/z calcd for $C_{19}H_{22}N_3O_6$ (MH)⁺: 388.1503, found: 388.1495.



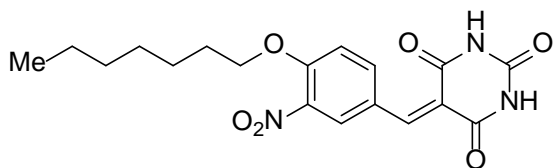
5-(4-(cyclohexylmethoxy))-3-nitrobenzylidene)pyrimidine-2,4,6(1H,3H,5H)-trione (37c) Obtained from the

condensation of **36c** with barbituric acid. Yield: 88 %. Yellow solid. ^1H NMR (400 MHz, DMSO) δ 11.40 (s, 1H), 11.29 (s, 1H), 9.00 (d, $J = 2.1$ Hz, 1H), 8.37 (dd, $J = 9.2, 2.2$ Hz, 1H), 8.25 (s, 1H), 7.45 (d, $J = 9.0$ Hz, 1H), 4.08 (d, $J = 5.9$ Hz, 2H), 1.89 – 1.53 (m, 6H), 1.35 – 0.95 (m, 5H). ^{13}C NMR (101 MHz, DMSO) δ 163.29, 162.04, 154.29, 152.03, 150.13, 140.67, 138.59, 130.09, 124.53, 118.44, 114.43, 74.59, 36.78, 28.80, 25.93, 25.14. HRMS (ESI+) m/z calcd for $\text{C}_{18}\text{H}_{20}\text{N}_3\text{O}_6$ (MH) $^+$: 374.1347, found: 374.1338.



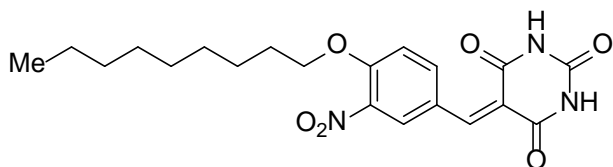
5-(3-Nitro-4-(pentyloxy)benzylidene)pyrimidine-

2,4,6(1H,3H,5H)-trione (37d) Obtained from the condensation of **36d** with barbituric acid. Yield: 92 %. Yellow solid. ^1H NMR (400 MHz, DMSO) δ 11.40 (s, 1H), 11.29 (s, 1H), 8.99 (d, $J = 2.2$ Hz, 1H), 8.37 (dd, $J = 9.2, 2.2$ Hz, 1H), 8.25 (s, 1H), 7.46 (d, $J = 9.0$ Hz, 1H), 4.27 (t, $J = 6.4$ Hz, 2H), 1.81 – 1.66 (m, 2H), 1.44 – 1.29 (m, 4H), 0.89 (t, $J = 7.1$ Hz, 3H). ^{13}C NMR (101 MHz, DMSO) δ 163.29, 162.04, 154.18, 152.02, 150.14, 140.64, 138.68, 130.03, 124.57, 118.48, 114.47, 69.82, 27.88, 27.41, 21.69, 13.87. HRMS (ESI+) m/z calcd for $\text{C}_{16}\text{H}_{18}\text{N}_3\text{O}_6$ (MH) $^+$: 348.1190, found: 348.1191.



5-(4-(heptyloxy)-3-

nitrobenzylidene)pyrimidine-2,4,6(1H,3H,5H)-trione (37e) Obtained from the condensation of **36e** with barbituric acid. Yield: 86 %. Yellow solid. ^1H NMR (400 MHz, DMSO) δ 11.40 (s, 1H), 11.30 (s, 1H), 9.00 (d, $J = 2.1$ Hz, 1H), 8.36 (dd, $J = 9.1, 2.2$ Hz, 1H), 8.24 (s, 1H), 7.44 (d, $J = 9.0$ Hz, 1H), 4.26 (t, $J = 6.3$ Hz, 2H), 1.81 – 1.66 (m, 2H), 1.45 – 1.23 (m, 8H), 0.85 (t, $J = 6.8$ Hz, 3H). ^{13}C NMR (101 MHz, DMSO) δ 163.30, 162.05, 154.22, 152.07, 150.14, 140.70, 138.66, 130.08, 124.56, 118.42, 114.45, 69.83, 31.20, 28.25, 28.20, 25.19, 22.02, 13.92. HRMS (ESI+) m/z calcd for $\text{C}_{18}\text{H}_{22}\text{N}_3\text{O}_6$ (MH) $^+$: 376.1503, found: 376.1494.

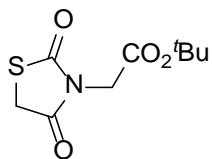


5-(3-nitro-4-

(nonyloxy)benzylidene)pyrimidine-2,4,6(1H,3H,5H)-trione (37f) Obtained from the condensation of **36f** with barbituric acid. Yield: 83 %. Yellow solid. ^1H NMR (400 MHz, DMSO) δ 11.40 (s, 1H), 11.29 (s, 1H), 9.00 (d, $J = 1.4$ Hz, 1H), 8.37 (dd, $J = 8.9, 1.5$ Hz, 1H), 8.25 (s, 1H), 7.45 (d, $J = 9.0$ Hz, 1H), 4.26 (t, $J = 6.3$ Hz, 2H), 1.77 – 1.69 (m, 2H), 1.43 – 1.22 (m, 12H), 0.85 (t, $J = 6.6$ Hz, 3H). ^{13}C NMR (101 MHz, DMSO) δ 163.29, 162.04, 154.20, 152.04, 150.13, 140.68, 138.67, 130.06, 124.56, 118.44, 114.46, 69.82, 31.26, 28.91, 28.59, 28.55, 28.18, 25.19, 22.10, 13.94. HRMS (ESI+) m/z calcd for $\text{C}_{20}\text{H}_{26}\text{N}_3\text{O}_6$ (MH) $^+$: 404.1816, found: 404.1810.

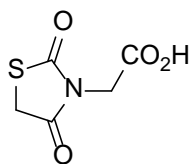
4.2.6 Preparation of 2-(2,4-dioxothiazolidin-3-yl)acetic acid (40)

Preparation of *tert*-butyl 2-(2,4-dioxothiazolidin-3-yl)acetate (39). The protocol was slightly modified as described in the literature.^[82] Potassium hydroxide (61.5 mmol, 3.45 g, 1.20 equiv.) was dissolved in absolute EtOH (20 mL) assisted by sonication. This solution was added dropwise into the solution of thiazolidine-2,4-dione (**2**, 6.00 g, 51.2 mmol, 1.00 equiv.) in hot absolute EtOH (25 mL) at 55–60 °C. The reaction mixture was stirred at this temperature for 3 h before cooled to room temperature. The white precipitate was filtered off and washed with cold EtOH (25 mL \times 3) and dried with infrared heat lamp. The potassium salt of thiazolidine-2,4-dione was thus obtained and used in the subsequent step without further purification (74% yield). The suspension of thiazolidine-2,4-dione potassium salt (2.97 g, 19.1 mmol) and *tert*-butyl bromoacetate (19.1 mmol, 3.73 g) in acetone was stirred at reflux for 5 h and then cooled to room temperature. The solid was removed by vacuum filtration and washed with acetone (25 mL \times 3). The filtrate was concentrated and dried under vacuum overnight. The product was obtained as peach solid (3.63 g, 15.7 mmol, 82% yield).



tert-Butyl 2-(2,4-dioxothiazolidin-3-yl)acetate (39). Yield: 82%. Peach solid. ^1H NMR (400 MHz, CDCl_3) δ 4.23 (s, 2H), 4.01 (s, 2H), 1.45 (s, 9H). ^{13}C NMR (101 MHz, CDCl_3) δ 171.29, 170.87, 165.25, 83.40, 42.98, 33.96, 28.07.

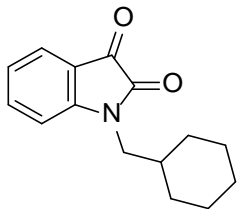
Preparation of 2-(2,4-dioxothiazolidin-3-yl)acetic acid (40). The solution of **39** (3.50 g, 15.1 mmol) in trifluoroacetic acid (15 mL) and dichloromethane (15 mL) was stirred at room temperature for 2 h.^[83] The solvents were removed under reduced pressure and the residue was dried under vacuum overnight to obtain **40** as white solid (2.57 g, 14.7 mmol, 97% yield).



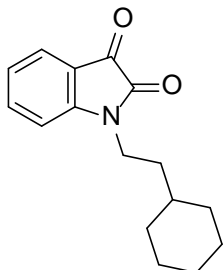
2-(2,4-Dioxothiazolidin-3-yl)acetic acid (40). Yield: 97%. White solid. ^1H NMR (400 MHz, DMSO) δ 13.30 (s, 1H), 4.32 (s, 2H), 4.20 (s, 2H). ^{13}C NMR (101 MHz, DMSO) δ 171.90, 171.48, 168.11, 42.06, 34.04. HRMS (ESI+) m/z calcd for $\text{C}_5\text{H}_4\text{NO}_4\text{S}$ $[\text{M}-\text{H}]^+$: 173.9867, found:173.9926.

4.2.7 Preparation of 1-substituted isatins 43a–43m

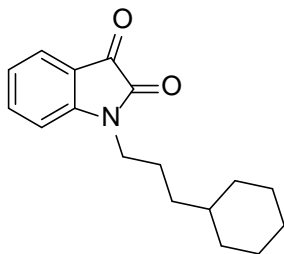
Preparation of 1-(cyclohexylmethyl)indoline-2,3-dione (43a). The protocol was slightly modified as described in the literature.^[99] The suspension of isatin (**41**, 0.45 g, 3.06 mmol, 1.00 equiv.), (bromomethyl)cyclohexane (1.20 equiv., 3.67 mmol, 0.65 g) and K_2CO_3 (2.00 equiv., 61.2 mmol, 0.85 g) was stirred at room temperature in DMF for 24 h. The reaction mixture was poured into ice water with vigorous stirring. The precipitate was filtered off, washed with water (25 mL \times 3) and cold EtOH (10 mL), air-dried and recrystallized from EtOH to obtain **43a** as red crystals (0.64 g, 2.63 mmol, 86% yield). Compounds **43b–43m** were prepared following the same protocol as described here.



1-(Cyclohexylmethyl)indoline-2,3-dione (43a). Yield: 87%. ^1H NMR (400 MHz, CDCl_3) δ 7.62 – 7.49 (m, 2H), 7.13 – 7.01 (m, 1H), 6.87 (d, $J = 7.9$ Hz, 1H), 3.50 (d, $J = 6.1$ Hz, 2H), 1.82 – 1.57 (m, 6H), 1.22 – 0.96 (m, 5H). ^{13}C NMR (101 MHz, CDCl_3) δ 183.63, 158.44, 151.58, 138.38, 125.26, 123.56, 117.47, 110.56, 46.56, 36.20, 30.91, 26.13, 25.65. HRMS (ESI+) m/z calcd for $\text{C}_{15}\text{H}_{18}\text{NO}_2$ $[\text{M}+\text{H}]^+$: 244.1332, found: 244.1329.

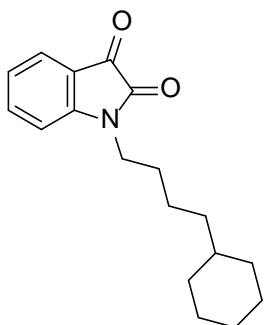


1-(2-Cyclohexylethyl)indoline-2,3-dione (43b). Compound **43b** was prepared from isatin (**41**) and 1-bromo-2-cyclohexylethane as described in the preparation of **43a**. Yield: 81%. Red crystals. ^1H NMR (400 MHz, CDCl_3) δ 7.65 – 7.50 (m, 2H), 7.08 (t, $J = 7.5$ Hz, 1H), 6.87 (d, $J = 8.1$ Hz, 1H), 3.71 (dd, $J = 8.2, 7.2$ Hz, 2H), 1.82 – 1.47 (m, 7H), 1.38 – 1.06 (m, 4H), 1.03 – 0.87 (m, 2H). ^{13}C NMR (101 MHz, CDCl_3) δ 183.77, 158.06, 151.03, 138.41, 125.43, 123.64, 117.67, 110.21, 38.25, 35.46, 34.48, 33.14, 26.46, 26.16. HRMS (ESI+) m/z calcd for $\text{C}_{16}\text{H}_{20}\text{NO}_2$ $[\text{M}+\text{H}]^+$: 258.1489, found: 258.1484.

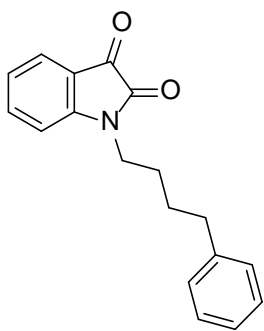


1-(3-Cyclohexylpropyl)indoline-2,3-dione (43c). Compound **11c** was prepared from isatin (**41**) and **35** as described in the preparation of **43a**. Yield: 87%. Scarlet crystals. ^1H NMR (400 MHz, CDCl_3) δ 7.65 – 7.51 (m, 2H), 7.11 (t, $J = 7.1$ Hz, 1H), 6.88 (d, $J = 7.5$ Hz, 1H), 3.69 (t, $J = 6.7$ Hz, 2H), 1.74 – 1.55 (m, 7H), 1.30 – 1.07 (m, 6H), 0.93 – 0.73 (m, 2H). ^{13}C NMR (101 MHz, CDCl_3) δ 183.82, 158.24, 151.23,

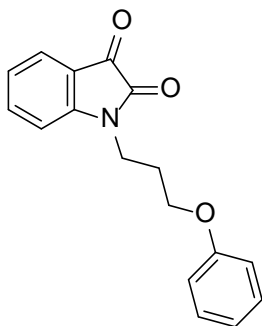
138.42, 125.59, 123.71, 117.74, 110.28, 40.72, 37.51, 34.62, 33.38, 26.69, 26.42, 24.79.
HRMS (ESI+) m/z calcd for $C_{17}H_{22}NO_2$ $[M+H]^+$: 272.1645, found: 272.1641.



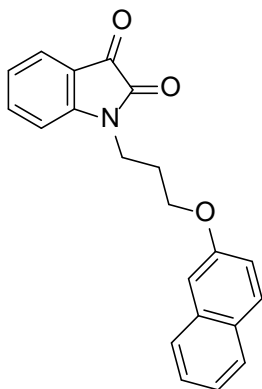
1-(4-Cyclohexylbutyl)indoline-2,3-dione (43d). Compound **43d** was prepared from isatin (**41**) and **23** as described in the preparation of **43a**. Yield: 82%. Scarlet crystals. 1H NMR (400 MHz, $CDCl_3$) δ 7.64 – 7.53 (m, 2H), 7.11 (td, $J = 7.6, 0.8$ Hz, 1H), 6.89 (d, $J = 7.9$ Hz, 1H), 3.75 – 3.67 (m, 2H), 1.74 – 1.51 (m, 8H), 1.42 – 1.31 (m, 2H), 1.30 – 1.08 (m, 6H), 0.95 – 0.77 (m, 2H). ^{13}C NMR (101 MHz, $CDCl_3$) δ 158.26, 151.24, 138.40, 125.59, 123.71, 121.46, 117.77, 110.29, 40.44, 37.70, 37.18, 33.48, 27.72, 26.79, 26.50, 24.35. HRMS (ESI+) m/z calcd for $C_{18}H_{24}NO_2$ $[M+H]^+$: 286.1802, found: 286.1805.



1-(4-Phenylbutyl)indoline-2,3-dione (43e). Compound **43e** was prepared from isatin (**41**) and 1-bromo-4-phenylbutane as described in the preparation of **43a**. Yield: 78%. Scarlet crystals. 1H NMR (400 MHz, $CDCl_3$) δ 7.62 – 7.51 (m, 2H), 7.31 – 7.23 (m, 2H), 7.23 – 7.05 (m, 4H), 6.83 (d, $J = 7.9$ Hz, 1H), 3.73 (t, $J = 6.8$ Hz, 2H), 2.67 (t, $J = 6.9$ Hz, 2H), 1.78 – 1.68 (m, 4H). ^{13}C NMR (101 MHz, $CDCl_3$) δ 183.65, 158.25, 151.03, 141.63, 138.42, 128.50, 128.49, 126.06, 125.52, 123.72, 117.67, 110.24, 40.11, 35.36, 28.53, 26.77. HRMS (ESI+) m/z calcd for $C_{18}H_{18}NO_2$ $[M+H]^+$: 280.1332, found: 280.1334.

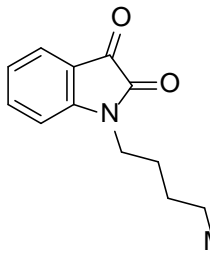


1-(3-Phenoxypropyl)indoline-2,3-dione (43f). Compound **43f** was prepared from isatin (**41**) and **34a** as described in the preparation of **43a**. Yield: 72%. Red crystals. ^1H NMR (400 MHz, CDCl_3) δ 7.63 – 7.47 (m, 2H), 7.35 – 7.24 (m, 2H), 7.10 (t, $J = 7.6$ Hz, 1H), 7.02 – 6.92 (m, 2H), 6.88 (dd, $J = 7.8, 1.0$ Hz, 2H), 4.05 (t, $J = 5.7$ Hz, 2H), 3.96 (t, $J = 7.0$ Hz, 2H), 2.21 (p, 2H). ^{13}C NMR (101 MHz, CDCl_3) δ 183.53, 158.48, 151.15, 138.55, 129.67, 125.55, 123.82, 121.22, 117.68, 114.56, 110.30, 64.81, 37.52, 27.48. HRMS (ESI+) m/z calcd for $\text{C}_{17}\text{H}_{16}\text{NO}_3$ $[\text{M}+\text{H}]^+$: 282.1125, found: 282.1126.

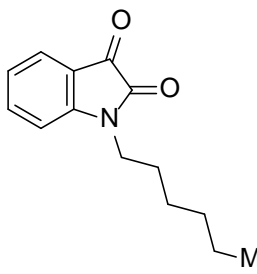


1-(3-(Naphthalen-2-yloxy)propyl)indoline-2,3-dione (43g).

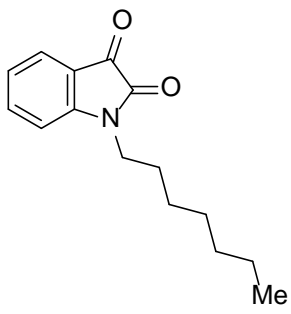
Compound **43g** was prepared from isatin (**41**) and **34b** as described in the preparation of **43a**. Yield: 68%. Scarlet crystals. ^1H NMR (400 MHz, CDCl_3) δ 7.86 – 7.67 (m, 3H), 7.63 (d, $J = 7.4$ Hz, 1H), 7.57 – 7.44 (m, 2H), 7.41 – 7.28 (m, 1H), 7.23 – 7.03 (m, 3H), 7.00 (d, $J = 7.9$ Hz, 1H), 4.19 (t, $J = 5.7$ Hz, 2H), 4.02 (t, $J = 6.9$ Hz, 2H), 2.30 (p, 2H). ^{13}C NMR (101 MHz, CDCl_3) δ 183.53, 158.51, 156.42, 151.16, 138.56, 134.58, 129.68, 129.22, 127.77, 126.90, 126.61, 125.58, 123.95, 123.84, 118.67, 117.69, 110.26, 106.92, 64.96, 37.58, 27.47. HRMS (ESI+) m/z calcd for $\text{C}_{21}\text{H}_{18}\text{NO}_3$ $[\text{M}+\text{H}]^+$: 332.1281, found: 332.1289.



Me 1-Pentylindoline-2,3-dione (43h). Compound **43h** was prepared from isatin (**41**) and 1-bromopentane as described in the preparation of **43a**. Yield: 84%. Red crystals. ^1H NMR (400 MHz, CDCl_3) δ 7.58 – 7.46 (m, 2H), 7.08 – 6.99 (m, 1H), 6.90 – 6.83 (m, 1H), 3.69 – 3.60 (m, 2H), 1.75 – 1.52 (m, 2H), 1.50 – 1.21 (m, 4H), 0.82 (t, $J = 7.0$ Hz, 3H). ^{13}C NMR (101 MHz, CDCl_3) δ 183.61, 158.05, 150.97, 138.40, 125.21, 123.53, 117.43, 110.23, 40.14, 28.89, 26.85, 22.21, 13.84. HRMS (ESI+) m/z calcd for $\text{C}_{13}\text{H}_{16}\text{NO}_2$ $[\text{M}+\text{H}]^+$: 218.1176, found: 218.1171.

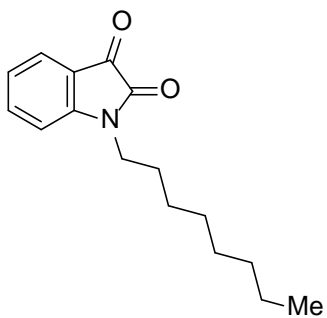


Me 1-Hexylindoline-2,3-dione (43i). Compound **43i** was prepared from isatin (**41**) and 1-bromohexane as described in the preparation of **43a**. Yield: 80%. Red crystals. ^1H NMR (400 MHz, CDCl_3) δ 7.63 – 7.51 (m, 2H), 7.09 (t, $J = 7.5$ Hz, 1H), 6.92 – 6.85 (m, 1H), 3.70 (t, $J = 7.4$ Hz, 2H), 1.90 – 1.49 (m, 2H), 1.49 – 1.09 (m, 6H), 0.87 (t, $J = 6.7$ Hz, 3H). ^{13}C NMR (101 MHz, CDCl_3) δ 183.79, 158.23, 151.20, 138.41, 125.53, 123.69, 117.71, 110.28, 40.39, 31.50, 27.34, 26.68, 22.62, 14.09. HRMS (ESI+) m/z calcd for $\text{C}_{14}\text{H}_{18}\text{NO}_2$ $[\text{M}+\text{H}]^+$: 232.1332, found: 232.1325.

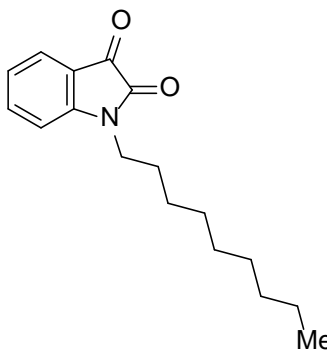


Me 1-Heptylindoline-2,3-dione (43j). Compound **43j** was prepared from isatin (**41**) and 1-bromoheptane as described in the preparation of **43a**. Yield: 80%.

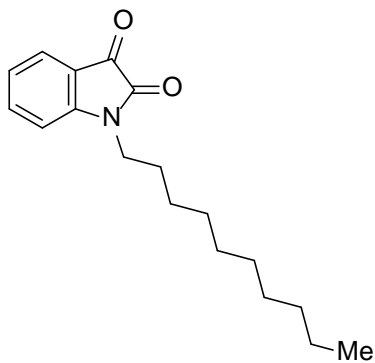
Red solid. ^1H NMR (400 MHz, CDCl_3) δ 7.62 – 7.53 (m, 2H), 7.14 – 7.05 (m, 1H), 6.92 – 6.85 (m, 1H), 3.70 (t, 2H), 1.78 – 1.60 (m, 2H), 1.46 – 0.97 (m, 9H), 0.86 (t, $J = 6.9$ Hz, 3H). ^{13}C NMR (101 MHz, CDCl_3) δ 183.77, 158.22, 151.19, 138.41, 125.51, 123.68, 117.70, 110.28, 40.39, 31.77, 28.99, 27.37, 26.96, 22.65, 14.14. HRMS (ESI+) m/z calcd for $\text{C}_{15}\text{H}_{20}\text{NO}_2$ $[\text{M}+\text{H}]^+$: 246.1489, found: 246.1484.



1-Octylindoline-2,3-dione (43k). Compound **43k** was prepared from isatin (**41**) and 1-bromooctane as described in the preparation of **43a**. Yield: 72%. Red solid. ^1H NMR (400 MHz, CDCl_3) δ 7.59 – 7.48 (m, 2H), 7.05 (td, $J = 7.5, 0.8$ Hz, 1H), 6.90 – 6.83 (m, 1H), 3.70 – 3.61 (m, 2H), 1.71 – 1.58 (m, 2H), 1.35 – 1.14 (m, 10H), 0.81 (t, $J = 6.9$ Hz, 3H). ^{13}C NMR (101 MHz, CDCl_3) δ 183.65, 158.08, 151.04, 138.38, 125.28, 123.56, 117.51, 110.24, 40.23, 31.70, 29.14, 29.10, 27.22, 26.86, 22.57, 14.03. HRMS (ESI+) m/z calcd for $\text{C}_{16}\text{H}_{22}\text{NO}_2$ $[\text{M}+\text{H}]^+$: 260.1645, found: 260.1644.



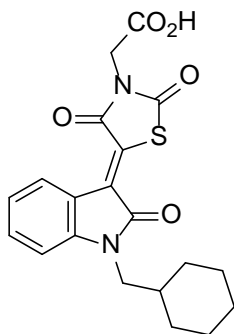
1-Nonylindoline-2,3-dione (43l). Compound **43l** was prepared from isatin (**41**) and 1-bromononane as described in the preparation of **43a**. Yield: 74%. Red solid. ^1H NMR (400 MHz, CDCl_3) δ 7.60 – 7.47 (m, 2H), 7.07 (td, $J = 7.5, 0.5$ Hz, 1H), 6.88 (d, $J = 7.9$ Hz, 1H), 3.67 (t, $J = 7.3$ Hz, 2H), 1.71 – 1.59 (m, 2H), 1.40 – 1.07 (m, 12H), 0.82 (t, $J = 6.0$ Hz, 3H). ^{13}C NMR (101 MHz, CDCl_3) δ 183.69, 158.12, 151.07, 138.41, 125.36, 123.60, 117.55, 110.26, 40.27, 31.81, 29.43, 29.23, 29.20, 27.26, 26.90, 22.64, 14.11. HRMS (ESI+) m/z calcd for $\text{C}_{17}\text{H}_{24}\text{NO}_2$ $[\text{M}+\text{H}]^+$: 274.1802, found: 274.1793.



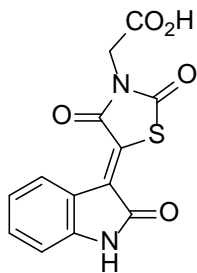
1-Decylindoline-2,3-dione (43m). Compound **43m** was prepared from isatin (**41**) and 1-bromodecane as described in the preparation of **43a**. Yield: 70%. Red solid. ^1H NMR (400 MHz, CDCl_3) δ 7.57 (t, $J = 6.8$ Hz, 2H), 7.09 (t, $J = 7.5$ Hz, 1H), 6.89 (d, $J = 8.3$ Hz, 1H), 3.70 (t, $J = 7.4$ Hz, 2H), 1.77 – 1.59 (m, 2H), 1.44 – 1.14 (m, 14H), 0.85 (t, $J = 6.8$ Hz, 3H). ^{13}C NMR (101 MHz, CDCl_3) δ 178.84, 153.26, 146.23, 133.48, 120.56, 118.74, 112.73, 105.34, 35.43, 27.01, 24.65, 24.63, 24.42, 24.38, 22.41, 22.05, 17.82, 9.28. HRMS (ESI+) m/z calcd for $\text{C}_{18}\text{H}_{26}\text{NO}_2$ $[\text{M}+\text{H}]^+$: 288.1958, found: 288.1955.

4.2.8 Preparation of (Z)-5-(2-oxoindolin-3-ylidene)thiazolidine-2,4-dione derivatives **42** and **44a–44m**

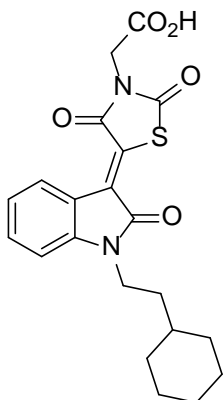
Preparation of (Z)-2-(5-(1-(cyclohexylmethyl)-2-oxoindolin-3-ylidene)-2,4-dioxothiazolidin-3-yl)acetic acid (44a). The suspension of **43a** (0.26 g, 1.07 mmol, 1.00 equiv.), **40** (1.10 equiv., 1.18 mmol, 0.21 g) and NH_4OAc (2.00 equiv., 2.14 mmol, 0.16 g) in glacial AcOH (2 mL) was heated at 108 °C for 12 h or overnight. The reaction mixture was cooled to room temperature. The precipitate was filtered off, washed with cold EtOH , air-dried and recrystallized from EtOH . Compound **44a** was thus formed as maroon crystals (0.36 g, 0.90 mmol, 84% yield). Compounds **42** and **44b–44m** were prepared as described here with different 1-substituted isatins.



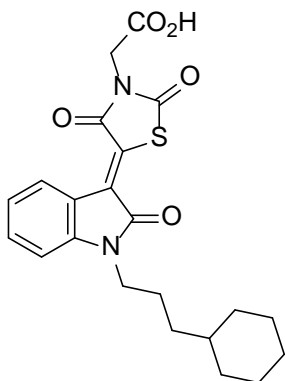
(Z)-2-(5-(1-(Cyclohexylmethyl)-2-oxoindolin-3-ylidene)-2,4-dioxothiazolidin-3-yl)acetic acid (12a). Yield: 84%. Maroon crystals. ^1H NMR (400 MHz, DMSO) δ 13.52 (s, 1H), 8.81 (dd, $J = 7.9, 0.8$ Hz, 1H), 7.50 (td, $J = 7.8, 1.2$ Hz, 1H), 7.25 – 7.11 (m, 2H), 4.44 (s, 2H), 3.63 (d, $J = 7.3$ Hz, 2H), 1.81 – 1.56 (m, 6H), 1.19 – 0.94 (m, 5H). ^{13}C NMR (101 MHz, DMSO) δ 169.31, 167.86, 166.92, 164.83, 144.87, 133.02, 129.34, 127.74, 126.91, 122.60, 119.02, 109.94, 45.90, 41.92, 35.85, 30.20, 25.78, 25.17. HRMS (ESI+) m/z calcd for $\text{C}_{20}\text{H}_{19}\text{N}_2\text{O}_5\text{S}$ $[\text{M}-\text{H}]^-$: 399.1020, found: 399.1027.



(Z)-2-(2,4-Dioxo-5-(2-oxoindolin-3-ylidene)thiazolidin-3-yl)acetic acid (42). Compound **42** was prepared from isatin (**41**) with **40** as described in the preparation of **42a**. Yield: 85%. Maroon crystals. ^1H NMR (400 MHz, DMSO) δ 8.76 (d, $J = 7.9$ Hz, 1H), 7.38 (t, $J = 7.5$ Hz, 1H), 7.04 (t, $J = 7.7$ Hz, 1H), 6.95 (d, $J = 7.8$ Hz, 1H), 4.04 (s, 2H). ^{13}C NMR (101 MHz, DMSO) δ 169.71, 168.27, 167.54, 165.37, 144.04, 132.66, 129.76, 127.87, 127.05, 122.00, 119.83, 110.56, 44.51. HRMS (ESI+) m/z calcd for $\text{C}_{13}\text{H}_7\text{N}_2\text{O}_5\text{S}$ $[\text{M}-\text{H}]^-$: 303.0081, found: 303.0081.

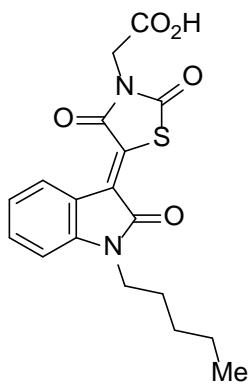


(Z)-2-(5-(1-(2-Cyclohexylethyl)-2-oxoindolin-3-ylidene)-2,4-dioxothiazolidin-3-yl)acetic acid (44b). Compound **44b** was prepared from **43b** with **40** as described in the preparation of **44a**. Yield: 81%. Maroon crystals. ^1H NMR (400 MHz, DMSO) δ 13.54 (s, 1H), 8.84 – 8.77 (m, 1H), 7.51 (td, $J = 7.8, 1.2$ Hz, 1H), 7.21 – 7.11 (m, 2H), 4.43 (s, 2H), 3.80 (t, 2H), 1.81 – 1.46 (m, 7H), 1.32 – 1.05 (m, 4H), 1.04 – 0.84 (m, 2H). ^{13}C NMR (101 MHz, DMSO) δ 169.32, 167.89, 166.51, 164.85, 144.26, 133.10, 127.85, 126.96, 122.67, 119.18, 109.59, 42.00, 40.15, 39.94, 39.73, 39.52, 39.31, 39.10, 38.89, 37.79, 34.69, 34.16, 32.50, 26.01, 25.66. HRMS (ESI+) m/z calcd for $\text{C}_{21}\text{H}_{21}\text{N}_2\text{O}_5\text{S}$ $[\text{M}-\text{H}]^-$: 413.1177, found: 413.1191.

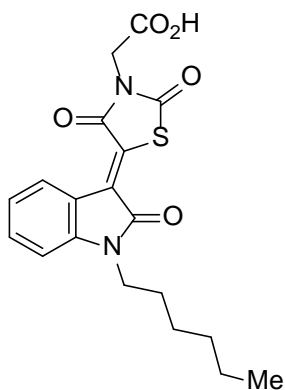


(Z)-2-(5-(1-(3-Cyclohexylpropyl)-2-oxoindolin-3-ylidene)-2,4-dioxothiazolidin-3-yl)acetic acid (44c). Compound **44c** was prepared from **43c** with **40** as described in the preparation of **44a**. Yield: 81%. Maroon crystals. ^1H NMR (400 MHz, DMSO) δ 13.51 (s, 1H), 8.77 (dd, $J = 7.9, 0.6$ Hz, 1H), 7.49 (td, $J = 7.8, 1.1$ Hz, 1H), 7.21 – 7.08 (m, 2H), 4.43 (s, 2H), 3.73 (t, $J = 7.2$ Hz, 2H), 1.81 – 1.42 (m, 7H), 1.31 – 0.98 (m, 6H), 0.89 – 0.73 (m, 2H). ^{13}C NMR (101 MHz, DMSO) δ 169.27, 167.85, 166.57, 164.77, 144.38, 133.04, 129.23, 127.80, 126.97, 122.60, 119.08, 109.58, 41.91, 36.70, 33.81, 32.72, 26.11, 25.78, 24.29. HRMS (ESI+) m/z calcd for $\text{C}_{22}\text{H}_{23}\text{N}_2\text{O}_5\text{S}$ $[\text{M}-\text{H}]^-$: 427.1333, found:

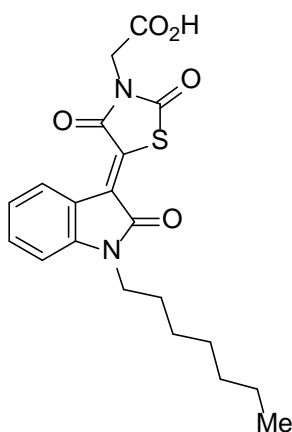
ylidene)-2,4-dioxothiazolidin-3-yl)acetic acid (44g). Compound **44g** was prepared from **43g** with **40** as described in the preparation of **44a**. Yield: 38%. Fire brick red crystals. ^1H NMR (400 MHz, DMSO) δ 13.51 (s, 1H), 8.85 – 8.78 (m, 1H), 7.83 – 7.70 (m, 3H), 7.50 – 7.38 (m, 2H), 7.37 – 7.09 (m, 4H), 7.04 (dd, $J = 8.9, 2.5$ Hz, 1H), 4.43 (s, 2H), 4.15 (t, $J = 5.8$ Hz, 2H), 4.02 (t, $J = 6.7$ Hz, 2H), 2.22 – 2.10 (m, 2H). ^{13}C NMR (101 MHz, DMSO) δ 169.27, 167.91, 166.80, 164.82, 156.17, 144.49, 134.17, 133.01, 129.19, 128.46, 127.48, 127.16, 126.62, 126.35, 123.54, 122.64, 119.25, 118.55, 109.61, 106.72, 65.24, 41.95, 37.41, 26.64. HRMS (ESI+) m/z calcd for $\text{C}_{26}\text{H}_{19}\text{N}_2\text{O}_6\text{S}$ [M-H] $^-$: 487.0969, found: 487.1029.



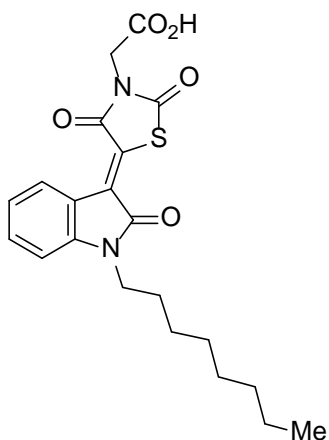
(Z)-2-(2,4-Dioxo-5-(2-oxo-1-pentylindolin-3-ylidene)thiazolidin-3-yl)acetic acid (44h). Compound **44h** was prepared from **43h** with **40** as described in the preparation of **43a**. Yield: 78%. Maroon crystals. ^1H NMR (400 MHz, DMSO) δ 8.76 (d, $J = 7.8$ Hz, 1H), 7.47 (t, $J = 7.4$ Hz, 1H), 7.18 – 7.05 (m, 2H), 4.33 (s, 2H), 3.74 (t, $J = 7.1$ Hz, 2H), 1.72 – 1.48 (m, 2H), 1.35 – 1.15 (m, 4H), 0.84 (t, $J = 6.9$ Hz, 3H). ^{13}C NMR (101 MHz, DMSO) δ 169.32, 167.86, 166.60, 164.88, 144.31, 132.92, 129.57, 127.79, 126.71, 122.58, 119.10, 109.54, 42.57, 39.78, 28.40, 26.63, 21.78, 13.85. HRMS (ESI+) m/z calcd for $\text{C}_{18}\text{H}_{17}\text{N}_2\text{O}_5\text{S}$ [M-H] $^-$: 373.0864, found: 373.0900.



(Z)-2-(5-(1-Hexyl-2-oxoindolin-3-ylidene)-2,4-dioxothiazolidin-3-yl)acetic acid (44i). Compound **44i** was prepared from **43i** with **40** as described in the preparation of **44a**. Yield: 71%. Maroon crystals. ^1H NMR (400 MHz, DMSO) δ 8.78 (d, J = 7.9 Hz, 1H), 7.52 – 7.43 (m, 1H), 7.19 – 7.09 (m, 2H), 4.33 (s, 2H), 3.75 (t, J = 7.1 Hz, 2H), 1.65 – 1.53 (m, 2H), 1.31 – 1.21 (m, 6H), 0.83 (t, J = 6.9 Hz, 3H). ^{13}C NMR (101 MHz, DMSO) δ 169.32, 167.82, 166.60, 164.90, 144.31, 132.93, 129.60, 127.80, 126.71, 122.59, 119.12, 109.55, 42.59, 40.15, 30.82, 26.88, 25.87, 21.98, 13.87. HRMS (ESI+) m/z calcd for $\text{C}_{19}\text{H}_{19}\text{N}_2\text{O}_5\text{S}$ $[\text{M}-\text{H}]^-$: 387.1020, found: 387.1077.

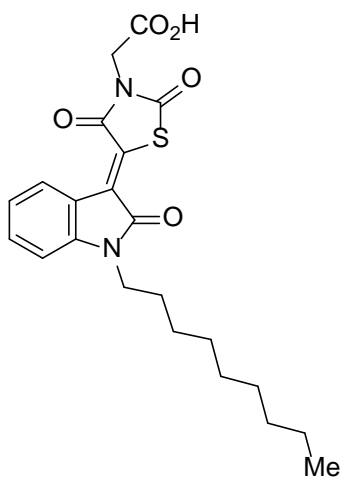


(Z)-2-(5-(1-Heptyl-2-oxoindolin-3-ylidene)-2,4-dioxothiazolidin-3-yl)acetic acid (44j). Compound **44j** was prepared from **43j** with **40** as described in the preparation of **44a**. Yield: 68%. Amber crystals. ^1H NMR (400 MHz, DMSO) δ 8.81 (dd, J = 7.9, 1.1 Hz, 1H), 7.48 (td, J = 7.8, 1.2 Hz, 1H), 7.20 – 7.10 (m, 2H), 4.21 (s, 2H), 3.76 (t, J = 7.1 Hz, 2H), 1.66 – 1.57 (m, 2H), 1.31 – 1.19 (m, 8H), 0.83 (t, J = 6.9 Hz, 3H). ^{13}C NMR (101 MHz, DMSO) δ 169.36, 167.53, 166.66, 165.06, 144.25, 132.80, 126.40, 122.56, 119.18, 109.53, 43.45, 39.78, 31.14, 28.27, 26.92, 26.18, 22.00, 13.92. HRMS (ESI+) m/z calcd for $\text{C}_{20}\text{H}_{21}\text{N}_2\text{O}_5\text{S}$ $[\text{M}-\text{H}]^-$: 401.1177, found: 401.1179.



(Z)-2-(5-(1-Octyl-2-oxoindolin-3-ylidene)-2,4-

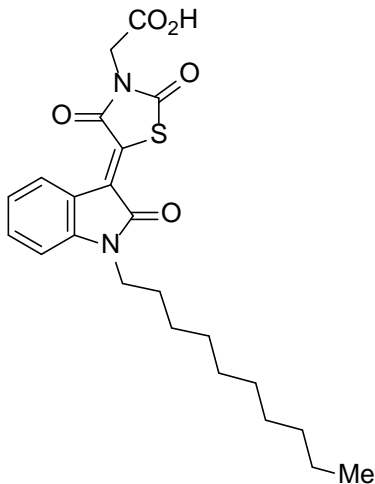
dioxothiazolidin-3-yl)acetic acid (44k). Compound **44k** was prepared from **43k** with **40** as described in the preparation of **44a**. Yield: 60%. Sangria crystals. ^1H NMR (400 MHz, DMSO) δ 8.84 – 8.77 (m, 1H), 7.47 (td, $J = 7.9, 1.1$ Hz, 1H), 7.21 – 7.07 (m, 2H), 4.17 (s, 2H), 3.75 (t, $J = 7.1$ Hz, 2H), 1.67 – 1.53 (m, 2H), 1.31 – 1.16 (m, 10H), 0.83 (t, $J = 6.8$ Hz, 3H). ^{13}C NMR (101 MHz, DMSO) δ 169.36, 167.55, 166.66, 165.09, 144.20, 132.72, 130.24, 127.78, 126.27, 122.53, 119.17, 109.49, 43.72, 40.19, 39.99, 31.18, 28.56, 26.89, 26.21, 22.04, 13.93. HRMS (ESI+) m/z calcd for $\text{C}_{21}\text{H}_{23}\text{N}_2\text{O}_5\text{S}$ [M-H] $^-$: 415.1333, found: 415.1338.



(Z)-2-(5-(1-Nonyl-2-oxoindolin-3-ylidene)-2,4-

dioxothiazolidin-3-yl)acetic acid (44l). Compound **44l** was prepared from **43l** with **40** as described in the preparation of **44a**. Yield: 75%. Sangria crystals. ^1H NMR (400 MHz, DMSO) δ 13.52 (s, 1H), 8.78 (d, $J = 7.9$ Hz, 1H), 7.70 – 7.44 (m, 1H), 7.43 – 7.09 (m, 2H), 4.43 (s, 2H), 3.75 (t, $J = 7.0$ Hz, 2H), 1.60 (s, 2H), 1.35 – 1.16 (m, 12H), 0.83 (t, $J = 6.8$ Hz, 3H). ^{13}C NMR (101 MHz, DMSO) δ 169.29, 167.87, 166.57, 164.78, 144.39, 133.03,

132.35, 129.23, 127.80, 126.96, 122.61, 119.08, 109.61, 41.92, 39.80, 39.79, 31.22, 28.84, 28.59, 26.88, 26.18, 22.08, 13.93. HRMS (ESI+) m/z calcd for C₂₂H₂₅N₂O₅S [M-H]⁻: 429.1490, found: 429.1502.

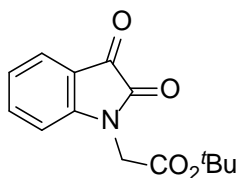


(Z)-2-(5-(1-Decyl-2-oxoindolin-3-ylidene)-2,4-dioxothiazolidin-3-yl)acetic acid (44m). Compound **44m** was prepared from **43m** with **40** as described in the preparation of **44a**. Yield: 72%. Sangria crystals. ¹H NMR (400 MHz, DMSO) δ 13.49 (s, 1H), 8.79 (d, $J = 7.7$ Hz, 1H), 7.49 (t, $J = 7.7$ Hz, 1H), 7.23 – 7.09 (m, 2H), 4.44 (s, 2H), 3.76 (t, $J = 7.1$ Hz, 2H), 1.66 – 1.55 (m, 2H), 1.30 – 1.18 (m, 14H), 0.83 (t, $J = 6.8$ Hz, 3H). ¹³C NMR (101 MHz, DMSO) δ 169.30, 167.88, 166.60, 164.80, 147.95, 144.41, 133.05, 129.26, 127.81, 126.98, 122.63, 119.10, 109.64, 41.92, 40.01, 39.80, 31.27, 28.88, 28.65, 28.58, 26.87, 26.17, 22.09, 13.96. HRMS (ESI+) m/z calcd for C₂₃H₂₇N₂O₅S [M-H]⁻: 443.1646, found: 443.1657.

4.2.9 Preparation of 2-(2,3-dioxoindolin-1-yl)acetic acid (46) from isatin (41)

Preparation of *tert*-butyl 2-(2,3-dioxoindolin-1-yl)acetate (45). The protocol was slightly modified as described in the literature.^[86] The suspension of isatin (**41**, 0.90 g, 6.12 mmol, 1.00 equiv.), *tert*-butyl bromoacetate (1.00 equiv., 6.12 mmol, 1.19 g) and K₂CO₃ (2.00 equiv., 12.2 mmol, 1.69 g) was stirred in DMF (10 mL) at room temperature for 24 h. Water (30 mL) was added and the reaction mixture was extracted with EtOAc (30 mL × 3). The combined organic phase was washed sequentially with saturated NaHCO₃ solution (30 mL), water (30 mL) and brine (30 mL), dried with anhydrous Na₂SO₄, and solvent was removed under reduced pressure. The solid residue was dried under vacuum to give **45** as

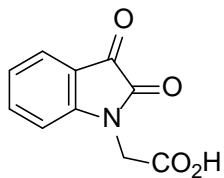
pumpkin powders (1.23 g, 4.71 mmol, 77% yield).



tert-Butyl 2-(2,3-dioxindolin-1-yl)acetate (13). Yield: 77%.

Pumpkin powders. ^1H NMR (400 MHz, CDCl_3) δ 7.68 – 7.54 (m, 2H), 7.15 (t, $J = 7.6$ Hz, 1H), 6.77 (d, $J = 7.9$ Hz, 1H), 4.39 (s, 2H), 1.46 (s, 9H). ^{13}C NMR (101 MHz, CDCl_3) δ 182.75, 165.88, 158.20, 150.70, 138.49, 125.68, 124.22, 117.75, 110.29, 83.58, 42.19, 28.11. HRMS (ESI+) m/z calcd for $\text{C}_{14}\text{H}_{16}\text{NO}_4$ $[\text{M}+\text{H}]^+$: 262.1074, found: 262.1067.

Preparation of 2-(2,3-dioxindolin-1-yl)acetic acid (46). The protocol was slightly modified as described in the literature.^[86] Compound **45** (1.16 g, 4.28 mmol) was stirred in equal volumes of trifluoroacetic acid (10 mL) and DCM (10 mL) at room temperature for 2 h. Solvents were evaporated under reduced pressure and the residue was dried under vacuum overnight to give **46** as a yellow solid (0.87 g, 4.24 mmol, 99% yield).

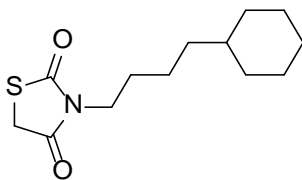


2-(2,3-dioxindolin-1-yl)acetic acid (46). Yield: 99%. Yellow solid. ^1H NMR (400 MHz, DMSO) δ 13.27 (s, 1H), 7.73 – 7.57 (m, 2H), 7.17 (dd, $J = 14.2, 7.5$ Hz, 2H), 4.51 (s, 2H). ^{13}C NMR (101 MHz, DMSO) δ 182.87, 168.84, 158.16, 150.64, 138.49, 124.61, 123.58, 117.26, 111.10, 41.21. HRMS (ESI+) m/z calcd for $\text{C}_{10}\text{H}_8\text{NO}_4$ $[\text{M}+\text{H}]^+$: 206.0448, found: 206.0446.

4.2.10 Preparation of N-substituted thiazolidine-2,4-dione **47a–47b**

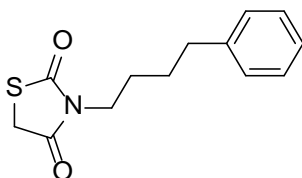
Preparation of 3-(4-cyclohexylbutyl)thiazolidine-2,4-dione (47a). The potassium salt of thiazolidine-2,4-dione (**38**, 0.28 g, 1.80 mmol) and **23** (1.80 mmol, 0.56 g) was stirred in acetone at reflux for 6 h. The reaction mixture was cooled to room temperature and the solid was removed by filtration. The filtrate was concentrated under reduced pressure and dried under vacuum overnight to obtain **47a** as white solid (0.41 g, 1.61 mmol, 89% yield).

Compound **47b** was synthesized with the same protocol as described here.^[87]



3-(4-Cyclohexylbutyl)thiazolidine-2,4-dione (47a). Yield: 89%.

White solid. ¹H NMR (400 MHz, CDCl₃) δ 3.93 (s, 2H), 3.60 (t, 2H), 1.78 – 1.49 (m, 7H), 1.37 – 1.03 (m, 8H), 1.00 – 0.70 (m, 2H). ¹³C NMR (101 MHz, CDCl₃) δ 171.88, 171.59, 42.30, 37.62, 37.04, 33.85, 33.44, 28.00, 26.79, 26.49, 24.12. HRMS (ESI+) *m/z* calcd for C₁₃H₂₂NO₂S [M+H]⁺: 256.1366, found: 256.1350.

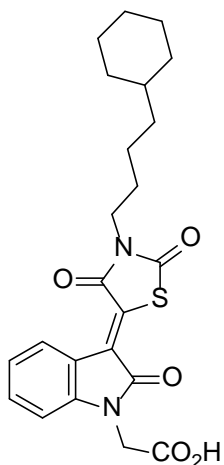


3-(4-Phenylbutyl)thiazolidine-2,4-dione (47b). Compound **47b**

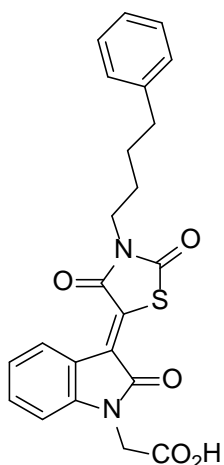
was prepared from the potassium salt of thiazolidine-2,4-dione with 1-bromo-4-phenylbutane as described in the preparation of **47a**. Yield: 82%. White solid. ¹H NMR (400 MHz, CDCl₃) δ 7.40 – 7.01 (m, 5H), 3.93 (s, 2H), 3.65 (t, *J* = 6.7 Hz, 2H), 2.64 (t, *J* = 6.7 Hz, 2H), 1.76 – 1.58 (m, 4H). ¹³C NMR (101 MHz, CDCl₃) δ 171.90, 171.57, 141.89, 128.53, 128.50, 126.02, 41.99, 35.43, 33.87, 28.58, 27.27. HRMS (ESI+) *m/z* calcd for C₁₃H₁₆NO₂S [M+H]⁺: 250.0896, found: 250.0887.

4.2.11 Preparation of (Z)-5-(2-oxoindolin-3-ylidene)thiazolidine-2,4-dione derivatives **48a–48b**

Preparation of (Z)-2-(3-(3-(4-Cyclohexylbutyl)-2,4-dioxothiazolidin-5-ylidene)-2-oxoindolin-1-yl)acetic acid (48a). The suspension of **47a** (0.33 g, 1.29 mmol, 1.00 equiv.), **46** (1.00 equiv., 1.29 mmol, 0.27 g) and NH₄OAc (2.00 equiv., 2.58 mmol, 0.20 g) was stirred in glacial AcOH (2 mL) at 108 °C for 12 h or overnight. The reaction was cooled to room temperature and ice-water (40 mL) was added. The precipitate was filtered off, washed with water (10 mL × 3) and cold EtOH (10 mL), air-dried and recrystallized from EtOH. The product **48a** was thus obtained as orange solid (0.39 g, 0.88 mmol, 68% yield).



(Z)-2-(3-(3-(4-Cyclohexylbutyl)-2,4-dioxothiazolidin-5-ylidene)-2-oxoindolin-1-yl)acetic acid (48a). Yield: 68%. Orange solid. ^1H NMR (400 MHz, DMSO) δ 13.29 (s, 1H), 8.87 (d, $J = 7.9$ Hz, 1H), 7.47 (t, $J = 7.6$ Hz, 1H), 7.17 (d, $J = 4.3$ Hz, 2H), 4.59 (s, 2H), 3.67 (t, $J = 7.0$ Hz, 2H), 1.77 – 1.51 (m, 7H), 1.48 – 1.04 (m, 8H), 0.91 – 0.69 (m, 2H). ^{13}C NMR (101 MHz, DMSO) δ 169.59, 167.05, 165.38, 146.19, 143.99, 132.59, 131.38, 127.73, 125.40, 122.80, 119.14, 109.62, 41.21, 36.92, 36.40, 32.82, 27.29, 26.20, 25.84, 23.48. HRMS (ESI+) m/z calcd for $\text{C}_{23}\text{H}_{25}\text{N}_2\text{O}_5\text{S}$ [M-H] $^-$: 441.1490, found: 441.1588.

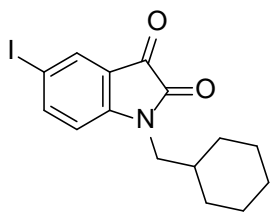


(Z)-2-(3-(2,4-Dioxo-3-(4-phenylbutyl)thiazolidin-5-ylidene)-2-oxoindolin-1-yl)acetic acid (48b). Compound **48b** was synthesized from **47b** and **46** as described in the preparation of **16a**. Yield: 74%. Yellow solid. ^1H NMR (400 MHz, DMSO) δ 13.24 (s, 1H), 8.86 (dd, $J = 8.1, 1.0$ Hz, 1H), 7.47 (td, $J = 7.8, 1.2$ Hz, 1H), 7.37 – 6.95 (m, 7H), 4.59 (s, 2H), 3.71 (t, $J = 6.5$ Hz, 2H), 2.60 (t, $J = 7.1$ Hz, 2H), 1.85 – 1.52 (m, 4H). ^{13}C NMR (101 MHz, DMSO) δ 169.64, 168.87, 167.04, 165.38, 143.93, 141.84,

132.57, 131.41, 128.31, 128.24, 127.73, 125.71, 125.36, 122.81, 119.14, 109.58, 41.39, 41.03, 34.63, 28.22, 26.71. HRMS (ESI+) m/z calcd for $C_{23}H_{19}N_2O_5S$ $[M-H]^-$: 435.1020, found: 435.1118.

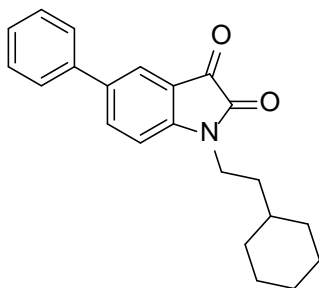
4.2.12 Preparation of 1,5-disubstituted isatins (**50**, **54a–54d**) through *N*-substitution

Preparation of 1-(cyclohexylmethyl)-5-iodoindoline-2,3-dione (50**).** The protocol was slightly modified as described in the literature.^[88] The suspension of 5-iodoisatin (**49**, 5.09 g, 18.6 mmol, 1.00 equiv.), (bromomethyl)cyclohexane (1.20 equiv., 22.4 mmol, 3.96 g) and potassium carbonate (2.00 equiv., 37.3 mmol, 5.15 g) was stirred in DMF (20 mL) at 80 °C overnight. The reaction mixture was cooled to room temperature and poured into ice-water. The precipitate was collected by filtration, washed with water (30 mL \times 3), cold EtOH (10 mL), air-dried and recrystallized from EtOH. The product **50** was obtained as red crystals (0.62 g, 1.68 mmol, 90% yield). The synthesis of compounds **54a–54d** followed the same protocol as described here.



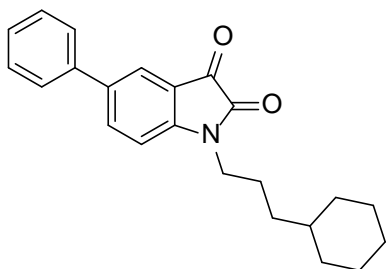
1-(Cyclohexylmethyl)-5-iodoindoline-2,3-dione (50**).** Yield: 90%.

Red crystals. 1H NMR (400 MHz, DMSO) δ 7.94 (dd, $J = 8.3, 1.9$ Hz, 1H), 7.77 (d, $J = 1.8$ Hz, 1H), 7.05 (d, $J = 8.3$ Hz, 1H), 3.46 (d, $J = 6.9$ Hz, 2H), 1.74 – 1.54 (m, 6H), 1.21 – 0.89 (m, 5H). ^{13}C NMR (101 MHz, DMSO) δ 182.09, 157.66, 150.52, 145.47, 131.99, 119.47, 113.44, 85.92, 45.71, 35.74, 30.09, 25.79, 25.24. HRMS (ESI+) m/z calcd for $C_{15}H_{17}INO_2$ $[M+H]^+$: 370.0298, found: 370.0294.



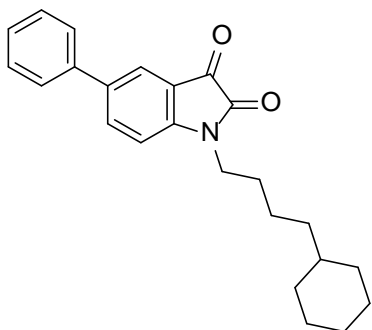
1-(2-Cyclohexylethyl)-5-phenylindoline-2,3-dione (54a**).**

Compound **54a** was synthesized from **53** and 1-bromo-2-cyclohexylethane as described in the preparation of **50**. Yield: 81%. Sangria solid. ^1H NMR (400 MHz, CDCl_3) δ 7.88 – 7.75 (m, 2H), 7.58 – 7.32 (m, 5H), 6.96 (d, $J = 8.1$ Hz, 1H), 3.77 (t, $J = 7.7$ Hz, 2H), 1.80 – 1.55 (m, 7H), 1.38 – 1.14 (m, 4H), 1.05 – 0.93 (m, 2H). ^{13}C NMR (101 MHz, CDCl_3) δ 183.94, 158.27, 150.15, 139.14, 137.28, 136.86, 129.22, 128.01, 126.68, 124.05, 118.22, 110.59, 110.16, 38.48, 35.55, 34.64, 33.24, 26.54, 26.24. HRMS (ESI+) m/z calcd for $\text{C}_{22}\text{H}_{24}\text{NO}_2$ $[\text{M}+\text{H}]^+$: 334.1802, found: 334.1802.



1-(3-Cyclohexylpropyl)-5-phenylindoline-2,3-dione (54b)

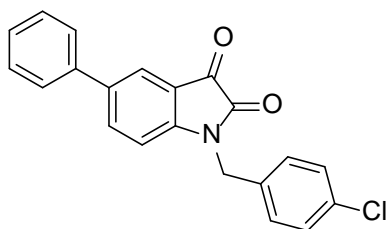
(54b). Compound **54b** was synthesized from **53** and **35** as described in the preparation of **18**. Yield: 76%. Sangria solid. ^1H NMR (400 MHz, CDCl_3) δ 7.82 (d, $J = 14.1$ Hz, 2H), 7.65 – 7.28 (m, 5H), 6.97 (d, $J = 8.1$ Hz, 1H), 3.73 (t, $J = 7.0$ Hz, 2H), 1.77 – 1.60 (m, 7H), 1.31 – 1.11 (m, 6H), 0.96 – 0.85 (m, 2H). ^{13}C NMR (101 MHz, CDCl_3) δ 183.93, 158.37, 150.25, 139.14, 137.29, 136.89, 129.22, 128.02, 126.68, 124.06, 118.16, 110.65, 40.86, 37.52, 34.63, 33.39, 26.68, 26.42, 24.87. HRMS (ESI+) m/z calcd for $\text{C}_{23}\text{H}_{26}\text{NO}_2$ $[\text{M}+\text{H}]^+$: 348.1958, found: 348.1957.



1-(4-Cyclohexylbutyl)-5-phenylindoline-2,3-dione (54c)

Compound **54c** was synthesized from **53** and **23** as described in the preparation of **50**. Yield: 71%. Sangria solid. ^1H NMR (400 MHz, CDCl_3) δ 7.87 – 7.77 (m, 2H), 7.57 – 7.33 (m, 5H), 6.97 (d, $J = 8.1$ Hz, 1H), 3.75 (t, $J = 7.3$ Hz, 2H), 1.76 – 1.61 (m, 7H), 1.46 – 1.34 (m, 2H), 1.25 – 1.07 (m, 6H), 0.91 – 0.79 (m, 2H). ^{13}C NMR (101 MHz, CDCl_3) δ 183.92,

158.38, 150.25, 139.15, 137.30, 136.87, 129.22, 128.02, 126.69, 124.07, 118.18, 110.65, 40.58, 37.69, 37.19, 33.47, 27.79, 26.78, 26.49, 24.37. HRMS (ESI+) m/z calcd for $C_{24}H_{28}NO_2$ $[M+H]^+$: 362.2115, found: 362.2103.



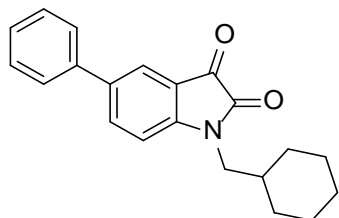
1-(4-Chlorobenzyl)-5-phenylindoline-2,3-dione (54d).

Compound **54d** was synthesized from **53** and 4-chlorobenzyl bromide as described in the preparation of **50**. Yield: 87%. Sangria solid. 1H NMR (400 MHz, $CDCl_3$) δ 7.85 (d, $J = 1.8$ Hz, 1H), 7.72 (dd, $J = 8.2, 1.9$ Hz, 1H), 7.51 – 7.26 (m, 9H), 6.82 (d, $J = 8.2$ Hz, 1H), 4.94 (s, 2H). ^{13}C NMR (101 MHz, $CDCl_3$) δ 183.19, 158.47, 149.51, 138.98, 137.81, 136.93, 134.34, 133.15, 129.46, 129.23, 129.00, 128.12, 126.70, 124.17, 118.28, 111.28, 43.70. HRMS (ESI+) m/z calcd for $C_{21}H_{15}ClNO_2$ $[M+H]^+$: 348.0786, found: 348.0784.

4.2.13 Preparation of 1,5-disubstituted isatins (**51a–51e** and **53**) through Suzuki and Sonogashira coupling

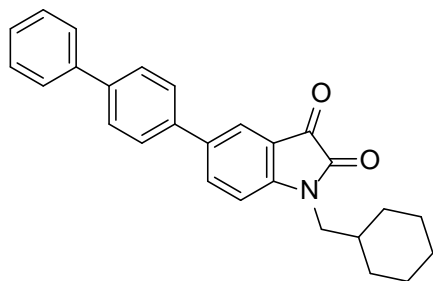
Preparation of 1-(cyclohexylmethyl)-5-phenylindoline-2,3-dione (51a). The protocol was slightly modified as described in the literature.^[89b] The suspension of **50** (0.76 g, 2.06 mmol, 1.00 equiv.), phenylboronic acid (1.50 equiv., 3.09 mmol, 0.38 g), $Pd(dppf)Cl_2 \cdot CH_2Cl_2$ (0.03 equiv., 0.052 mmol, 0.05 g) and $NaHCO_3$ (2.50 equiv., 5.15 mmol, 0.43 g) in DME (8 mL) and distilled water (2 mL) was stirred at reflux under nitrogen atmosphere for 12 h (or overnight). The reaction mixture was cooled to room temperature and partitioned with EtOAc (30 mL) and 1 N HCl solution (30 mL). The organic layer was separated and the aqueous layer was extracted with EtOAc (30 mL \times 3). The combined organic phase was washed with saturated $NaHCO_3$ solution (30 mL), water (30 mL) and brine (30 mL), dried over anhydrous Na_2SO_4 . The drying agent was filtered off and the filtrate was evaporated under reduced pressure. The residue was purified by flash chromatography using a mixture of hexanes and EtOAc (8:1) as eluent. The product **51a** was thus obtained as amber solid (0.50 g, 1.57 mmol, 76% yield). The synthesis of

51b, **51c** and **53** followed the same protocol as described here.



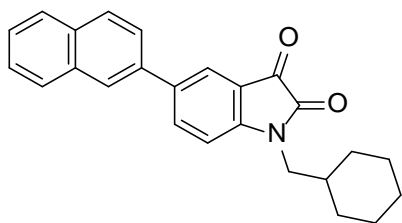
1-(Cyclohexylmethyl)-5-phenylindoline-2,3-dione (51a).

Yield: 76%. ^1H NMR (400 MHz, DMSO) δ 7.96 (dd, $J = 8.3, 2.0$ Hz, 1H), 7.80 (d, $J = 1.9$ Hz, 1H), 7.72 – 7.64 (m, 2H), 7.50 – 7.27 (m, 4H), 3.53 (d, $J = 6.9$ Hz, 2H), 1.88 – 1.55 (m, 6H), 1.28 – 0.86 (m, 5H). ^{13}C NMR (101 MHz, DMSO) δ 183.81, 158.93, 150.87, 139.01, 136.54, 135.63, 129.45, 127.99, 126.73, 122.63, 118.47, 111.92, 46.22, 36.26, 30.59, 26.24, 25.69. HRMS (ESI+) m/z calcd for $\text{C}_{21}\text{H}_{22}\text{NO}_2$ $[\text{M}+\text{H}]^+$: 320.1645, found: 320.1650.



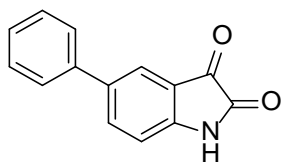
5-([1,1'-Biphenyl]-4-yl)-1-

(cyclohexylmethyl)indoline-2,3-dione (51b). Compound **51b** was synthesized from **50** and 4-biphenylboronic acid as described in the preparation of **51a**. Yield: 67%. Mahogany solid. ^1H NMR (400 MHz, DMSO) δ 8.01 (dd, $J = 8.2, 1.5$ Hz, 1H), 7.87 – 7.69 (m, 7H), 7.48 (t, $J = 7.6$ Hz, 2H), 7.38 (t, $J = 7.3$ Hz, 1H), 7.29 (d, $J = 8.3$ Hz, 1H), 3.53 (d, $J = 6.8$ Hz, 2H), 1.80 – 1.56 (m, 6H), 1.24 – 1.09 (m, 3H), 1.06 – 0.94 (m, 2H). ^{13}C NMR (101 MHz, DMSO) δ 183.37, 158.50, 150.48, 139.47, 139.23, 137.53, 135.96, 134.60, 129.00, 127.58, 127.23, 126.79, 126.55, 122.08, 118.08, 111.52, 45.82, 35.85, 30.18, 25.82, 25.27. HRMS (ESI+) m/z calcd for $\text{C}_{27}\text{H}_{26}\text{NO}_2$ $[\text{M}+\text{H}]^+$: 396.1958, found: 396.1948.



1-(Cyclohexylmethyl)-5-(naphthalen-2-yl)indoline-2,3-

dione (51c). Compound **51c** was synthesized from **50** and 2-naphthylboronic acid as described in the preparation of **51a**. Yield: 65%. Sangria solid. ^1H NMR (400 MHz, DMSO) δ 8.26 (d, $J = 1.3$ Hz, 1H), 8.11 (dd, $J = 8.3, 2.0$ Hz, 1H), 8.04 – 7.90 (m, 4H), 7.86 (dd, $J = 8.6, 1.9$ Hz, 1H), 7.60 – 7.47 (m, 2H), 7.33 (d, $J = 8.3$ Hz, 1H), 3.55 (d, $J = 6.8$ Hz, 2H), 1.81 – 1.56 (m, 6H), 1.27 – 0.95 (m, 5H). ^{13}C NMR (101 MHz, DMSO) δ 183.40, 158.54, 150.49, 136.28, 135.83, 134.95, 133.30, 132.22, 128.56, 128.19, 127.47, 126.48, 126.19, 124.84, 124.58, 122.47, 118.15, 111.54, 45.82, 35.88, 30.18, 25.82, 25.28. HRMS (ESI+) m/z calcd for $\text{C}_{25}\text{H}_{24}\text{NO}_2$ $[\text{M}+\text{H}]^+$: 370.1802, found: 370.1779.

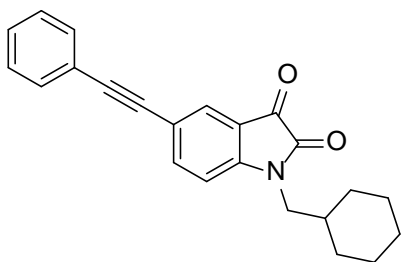


5-Phenylindoline-2,3-dione (54). Compound **54** was synthesized

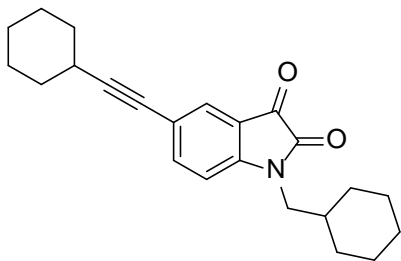
from 5-iodoisatin (**49**) and phenylboronic acid as described in the preparation of **51a**. Yield: 62%. Barn red solid. ^1H NMR (400 MHz, DMSO) δ 11.13 (s, 1H), 7.88 (d, $J = 8.2$ Hz, 1H), 7.74 (s, 1H), 7.63 (d, $J = 7.7$ Hz, 2H), 7.44 (t, $J = 7.5$ Hz, 2H), 7.35 (t, $J = 7.2$ Hz, 1H), 6.99 (d, $J = 8.2$ Hz, 1H). ^{13}C NMR (101 MHz, DMSO) δ 184.36, 159.56, 149.95, 138.73, 136.46, 134.89, 129.01, 127.49, 126.23, 122.46, 118.43, 112.68. HRMS (ESI+) m/z calcd for $\text{C}_{14}\text{H}_{10}\text{NO}_2$ $[\text{M}+\text{H}]^+$: 224.0706, found: 224.0706.

Preparation of 1-(cyclohexylmethyl)-5-(phenylethynyl)indoline-2,3-dione (51d). The suspension of **50** (0.67 g, 1.81 mmol, 1.00 equiv.), phenylacetylene (1.50 equiv., 2.72 mmol, 0.28 g), $\text{Pd}(\text{dppf})\text{Cl}_2 \cdot \text{CH}_2\text{Cl}_2$ (0.03 equiv., 0.0543 mmol, 0.0443 g), CuI (0.02 equiv., 0.0362 mmol, 0.0069 g) and DIPEA (5.00 equiv., 9.06 mmol, 1.17 g) in DMF (5 mL) was stirred at room temperature under nitrogen atmosphere for 24 h before the reaction mixture was partitioned with EtOAc (30 mL) and saturated NH_4Cl solution (30 mL). The organic layer was separated and the aqueous layer was extracted with EtOAc (30 mL \times 3). The combined organic phase was washed with saturated NaHCO_3 solution (30 mL), water (30

mL) and brine (30 mL), dried over anhydrous Na₂SO₄. The drying agent was filtered off and the filtrate was evaporated under reduced pressure. The residue was purified by flash chromatography using a mixture of hexanes and EtOAc (8:1) as eluent. The product **51d** was thus obtained as mahogany solid (0.56 g, 1.63 mmol, 90 % yield). The synthesis of **51e** followed the same protocol as described here.



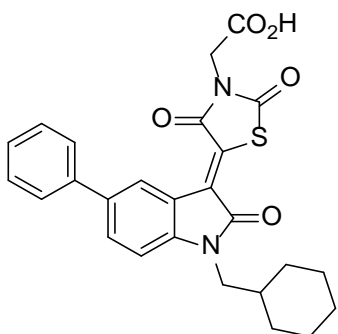
1-(Cyclohexylmethyl)-5-(phenylethynyl)indoline-2,3-dione (51d). Yield: 90%. Mahogany solid. ¹H NMR (400 MHz, CDCl₃) δ 7.78 – 7.65 (m, 2H), 7.55 – 7.44 (m, 2H), 7.39 – 7.31 (m, 3H), 6.89 (d, *J* = 8.2 Hz, 1H), 3.56 (d, *J* = 7.0 Hz, 2H), 1.83 – 1.66 (m, 6H), 1.27 – 1.15 (m, 3H), 1.10 – 1.00 (m, 2H). ¹³C NMR (101 MHz, CDCl₃) δ 183.03, 158.46, 150.86, 141.20, 131.73, 128.79, 128.59, 128.37, 122.74, 119.14, 117.61, 110.70, 90.47, 87.43, 46.89, 36.42, 31.05, 26.22, 25.76. HRMS (ESI+) *m/z* calcd for C₂₃H₂₂NO₂ [M+H]⁺: 344.1645, found: 344.1620.



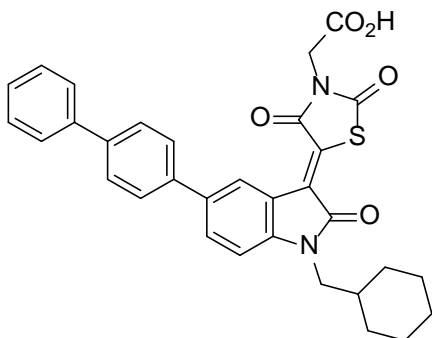
5-(Cyclohexylethynyl)-1-(cyclohexylmethyl)indoline-2,3-dione (51e). Compound **51e** was synthesized from **50** and ethynylcyclohexane as described in the preparation of **51d**. Yield: 84%. Clay color solid. ¹H NMR (400 MHz, CDCl₃) δ 7.62 – 7.53 (m, 2H), 6.81 (d, *J* = 8.2 Hz, 1H), 3.53 (d, *J* = 7.3 Hz, 2H), 2.65 – 2.48 (m, 1H), 1.86 – 1.68 (m, 10H), 1.56 – 1.46 (m, 3H), 1.37 – 0.98 (m, 9H). ¹³C NMR (101 MHz, CDCl₃) δ 183.22, 158.52, 150.24, 141.14, 128.41, 120.06, 117.45, 110.46, 95.71, 78.69, 46.79, 36.37, 32.67, 31.02, 29.72, 26.22, 25.98, 25.75, 24.97. HRMS (ESI+) *m/z* calcd for C₂₃H₂₈NO₂ [M+H]⁺: 350.2115, found: 350.2090.

4.2.14 Preparation of (Z)-5-(2-oxoindolin-3-ylidene)thiazolidine-2,4-dione derivatives 52a–52e, 54 and 55a–55d

Preparation of (Z)-2-(5-(1-(Cyclohexylmethyl)-2-oxo-5-phenylindolin-3-ylidene)-2,4-dioxothiazolidin-3-yl)acetic acid (52a). The suspension of **51a** (0.35 g, 1.10 mmol, 1.00 equiv.) and **40** (1.10 equiv., 1.21 mmol, 0.21g) in the presence of NH₄OAc (2.00 equiv., 2.19 mmol, 0.17g) was stirred in glacial AcOH at 108 °C for 12 h (or overnight). The reaction mixture was cooled to room temperature and the precipitate was collected by filtration. The filter cake was washed with cold EtOH (10 mL), air-dried and recrystallized from a mixture of EtOH and DMF to give the product **52a** as sangria crystals (0.38 g, 0.80 mmol, 73% yield). The synthesis of **52b–52e**, **54** and **55a–55d** followed the same protocol as described here.



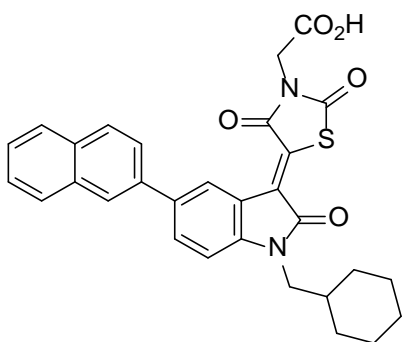
(Z)-2-(5-(1-(Cyclohexylmethyl)-2-oxo-5-phenylindolin-3-ylidene)-2,4-dioxothiazolidin-3-yl)acetic acid (52a). Yield: 73%. Sangria crystals. ¹H NMR (400 MHz, DMSO) δ 9.20 (d, *J* = 1.8 Hz, 1H), 7.77 (dd, *J* = 8.2, 1.9 Hz, 1H), 7.68 – 7.60 (m, 2H), 7.49 (t, *J* = 7.7 Hz, 2H), 7.41 – 7.25 (m, 3H), 4.06 (s, 2H), 3.65 (d, *J* = 7.3 Hz, 2H), 1.88 – 1.52 (m, 6H), 1.27 – 0.90 (m, 5H). ¹³C NMR (101 MHz, DMSO) δ 169.35, 167.13, 167.08, 165.39, 143.97, 139.81, 134.66, 131.23, 130.83, 129.07, 127.21, 126.24, 126.03, 125.97, 124.30, 119.74, 110.17, 109.57, 46.01, 44.55, 35.94, 30.23, 25.81, 25.21. HRMS (ESI+) *m/z* calcd for C₂₆H₂₃N₂O₅S [M-H]⁻: 475.1333, found: 475.1344.



(Z)-2-(5-(5-([1,1'-Biphenyl]-4-yl)-1-

(cyclohexylmethyl)-2-oxoindolin-3-ylidene)-2,4-dioxothiazolidin-3-yl)acetic acid

(52b). Compound **52b** was synthesized from **51b** and **40** as described in the preparation of **52a**. Yield: 64%. Sangria crystal. ^1H NMR (400 MHz, DMSO) δ 13.63 (s, 1H), 9.20 (d, $J = 1.7$ Hz, 1H), 7.85 (dd, $J = 8.2, 1.6$ Hz, 1H), 7.79 (d, $J = 8.3$ Hz, 2H), 7.72 (d, $J = 8.4$ Hz, 4H), 7.49 (t, $J = 7.6$ Hz, 2H), 7.41 – 7.30 (m, 2H), 4.46 (s, 2H), 3.66 (d, $J = 7.2$ Hz, 2H), 1.83 – 1.58 (m, 6H), 1.23 – 1.12 (m, 3H), 1.07 – 0.96 (m, 2H). ^{13}C NMR (101 MHz, DMSO) δ 169.37, 168.02, 167.12, 165.06, 144.36, 139.63, 139.07, 138.78, 134.27, 131.25, 130.01, 129.10, 127.65, 127.44, 127.01, 126.80, 126.64, 125.95, 119.76, 110.48, 46.14, 42.07, 36.02, 30.29, 25.87, 25.29. HRMS (ESI+) m/z calcd for $\text{C}_{32}\text{H}_{27}\text{N}_2\text{O}_5\text{S}$ [M-H] $^-$: 551.1646, found: 551.1680.

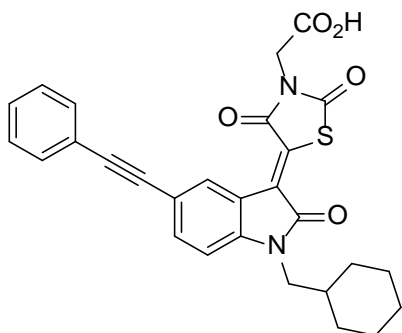


(Z)-2-(5-(1-(Cyclohexylmethyl)-5-(naphthalen-2-yl)-2-

oxoindolin-3-ylidene)-2,4-dioxothiazolidin-3-yl)acetic acid (52c). Compound **52c** was

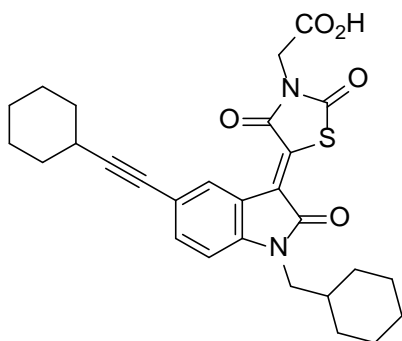
synthesized from **51c** and **40** as described in the preparation of **52a**. Yield: 47%. Amber crystals. ^1H NMR (400 MHz, DMSO) δ 13.53 (s, 1H), 9.24 (d, $J = 1.7$ Hz, 1H), 8.13 (s, 1H), 8.06 – 7.89 (m, 4H), 7.78 (dd, $J = 8.5, 1.6$ Hz, 1H), 7.58 – 7.50 (m, 2H), 7.35 (d, $J = 8.3$ Hz, 1H), 4.48 (s, 2H), 3.67 (d, $J = 7.2$ Hz, 2H), 1.88 – 1.50 (m, 6H), 1.20 – 0.95 (m, 5H). ^{13}C NMR (101 MHz, DMSO) δ 169.31, 167.93, 167.05, 164.95, 144.32, 137.23, 134.68, 133.28, 132.10, 131.69, 129.97, 128.68, 128.11, 127.54, 126.91, 126.54, 126.30,

126.09, 124.85, 124.66, 119.69, 110.44, 46.06, 42.01, 35.97, 30.22, 25.81, 25.22. HRMS (ESI+) m/z calcd for $C_{30}H_{25}N_2O_5S$ [M-H]⁻: 525.1490, found: 525.1530.



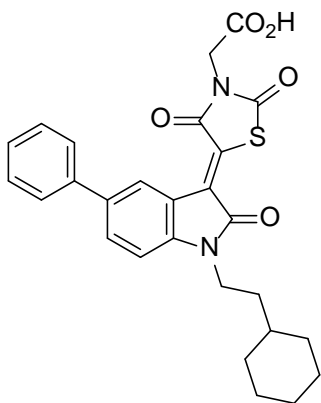
(Z)-2-(5-(1-(Cyclohexylmethyl)-2-oxo-5-(phenylethynyl)indolin-3-ylidene)-2,4-dioxothiazolidin-3-yl)acetic acid (52d).

Compound **52d** was synthesized from **51d** and **40** as described in the preparation of **52a**. Yield: 67%. Mahogany crystals. ¹H NMR (400 MHz, DMSO) δ 13.54 (s, 1H), 8.95 (d, J = 1.5 Hz, 1H), 7.69 (dd, J = 8.2, 1.6 Hz, 1H), 7.62 – 7.51 (m, 2H), 7.51 – 7.38 (m, 3H), 7.29 (d, J = 8.3 Hz, 1H), 4.47 (s, 2H), 3.64 (d, J = 7.2 Hz, 2H), 1.78 – 1.57 (m, 6H), 1.18 – 0.95 (m, 5H). ¹³C NMR (101 MHz, DMSO) δ 169.09, 167.87, 166.99, 164.85, 144.82, 135.92, 131.36, 130.83, 130.23, 128.78, 128.71, 125.97, 122.33, 119.27, 116.29, 110.41, 89.15, 88.50, 46.13, 42.03, 35.94, 30.19, 25.81, 25.21. HRMS (ESI+) m/z calcd for $C_{28}H_{23}N_2O_5S$ [M-H]⁻: 499.1333, found: 499.1373.

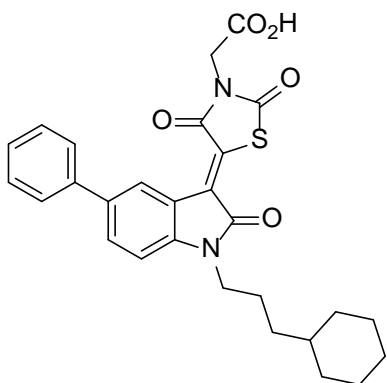


(Z)-2-(5-(5-(Cyclohexylethynyl)-1-(cyclohexylmethyl)-2-oxoindolin-3-ylidene)-2,4-dioxothiazolidin-3-yl)acetic acid (52e). Compound **52e** was synthesized from **51e** and **40** as described in the preparation of **52a**. Yield: 72%. Mahogany crystals. ¹H NMR (400 MHz, DMSO) δ 8.76 (s, 1H), 7.47 (d, J = 8.2 Hz, 1H), 7.16 (d, J = 8.3 Hz, 1H), 4.45 (s, 2H), 3.59 (d, J = 7.0 Hz, 2H), 2.67 – 2.58 (m, 1H), 1.89 – 1.78 (m, 2H), 1.72 – 1.42 (m, 11H), 1.38 – 1.06 (m, 6H), 1.03 – 0.90 (m, 2H). ¹³C NMR (101 MHz, DMSO) δ 169.15, 167.88, 166.94, 164.82, 144.11, 135.71, 130.45, 130.26, 126.16, 119.11,

117.43, 110.17, 93.48, 80.09, 46.06, 42.00, 35.92, 32.33, 30.19, 28.89, 25.81, 25.40, 25.22, 24.45. HRMS (ESI+) m/z calcd for $C_{28}H_{29}N_2O_5S$ $[M-H]^-$: 505.1803, found: 505.1853.



(Z)-2-(5-(1-(2-Cyclohexylethyl)-2-oxo-5-phenylindolin-3-ylidene)-2,4-dioxothiazolidin-3-yl)acetic acid (55a). Compound **55a** was synthesized from **54a** and **40** as described in the preparation of **52a**. Yield: 63%. Rust crystals. 1H NMR (400 MHz, DMSO) δ 9.11 (s, 1H), 7.78 (d, $J = 8.0$ Hz, 1H), 7.61 (d, $J = 7.6$ Hz, 2H), 7.48 (t, $J = 7.6$ Hz, 2H), 7.36 (t, $J = 7.3$ Hz, 1H), 7.21 (d, $J = 8.2$ Hz, 1H), 4.41 (s, 2H), 3.78 (t, $J = 7.3$ Hz, 2H), 1.80 – 1.46 (m, 7H), 1.33 – 1.09 (m, 4H), 0.98 – 0.85 (m, 2H). ^{13}C NMR (101 MHz, DMSO) δ 169.24, 167.86, 166.56, 164.94, 143.53, 139.68, 134.75, 131.23, 129.90, 129.05, 127.26, 126.88, 126.21, 126.08, 119.75, 109.86, 42.24, 37.91, 34.69, 34.22, 32.50, 26.02, 25.67. HRMS (ESI+) m/z calcd for $C_{27}H_{25}N_2O_5S$ $[M-H]^-$: 489.1490, found: 489.1546.

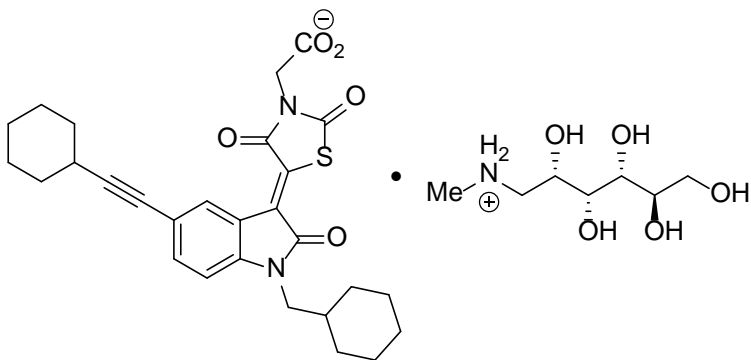


(Z)-2-(5-(1-(3-Cyclohexylpropyl)-2-oxo-5-phenylindolin-3-ylidene)-2,4-dioxothiazolidin-3-yl)acetic acid (55b). Compound **55b** was synthesized from **54b** and **40** as described in the preparation of **52a**. Yield: 58%. Sangria crystals. 1H NMR (400 MHz, DMSO) δ 13.51 (s, 1H), 9.09 (s, 1H), 7.76 (d, $J = 8.2$ Hz, 1H), 7.60 (d, $J = 7.7$ Hz, 2H), 7.48 (t, $J = 7.4$ Hz, 2H), 7.36 (t, $J = 7.3$ Hz, 1H),

from **54d** and **40** as described in the preparation of **52a**. Yield: 69%. Mahogany crystals. ^1H NMR (400 MHz, DMSO) δ 13.52 (s, 1H), 9.16 (d, $J = 1.6$ Hz, 1H), 7.74 (dd, $J = 8.3$, 1.7 Hz, 1H), 7.61 (d, $J = 7.4$ Hz, 2H), 7.54 – 7.32 (m, 7H), 7.17 (d, $J = 8.3$ Hz, 1H), 5.07 (s, 2H), 4.48 (s, 2H). ^{13}C NMR (101 MHz, DMSO) δ 169.08, 167.86, 167.01, 164.91, 143.20, 139.69, 135.18, 134.75, 132.27, 131.23, 130.37, 129.21, 129.06, 128.72, 127.33, 126.86, 126.28, 126.15, 119.90, 110.32, 42.63, 42.04. HRMS (ESI+) m/z calcd for $\text{C}_{26}\text{H}_{18}\text{ClN}_2\text{O}_5\text{S}$ $[\text{M}+\text{H}]^+$: 505.0619, found: 505.0621.

4.2.15 Preparation of the meglumine salt of **52e** (**52e-MEG**)

Preparation of the meglumine salt of (Z)-2-(5-(5-(Cyclohexylethynyl)-1-(cyclohexylmethyl)-2-oxoindolin-3-ylidene)-2,4-dioxothiazolidin-3-yl)acetic acid (52e-MEG**).** The protocol was slightly modified as described in the literature.^[92] The suspension of **52e** (1.85 g, 3.65 mmol, 1.00 equiv.) and meglumine (*N*-methyl-D-glucamine, 1.20 equiv., 4.38 mmol, 0.86 g) in EtOH (50 mL) was heated at reflux for 5 h with rigorous stirring. The reaction mixture was stood at room temperature overnight. The precipitate was filtered off, washed with cold EtOH (25 mL \times 3) and dried with infrared lamp and recrystallized from EtOH. The meglumine salt of **52e** (**52e-MEG**) was thus obtained as brick red solid (2.08 g, 2.96 mmol, 81% yield).



The meglumine salt of (Z)-2-(5-(5-(Cyclohexylethynyl)-1-(cyclohexylmethyl)-2-oxoindolin-3-ylidene)-2,4-dioxothiazolidin-3-yl)acetic acid (52e-MEG**).** Yield: 81%. Brick red solid. ^1H NMR (400 MHz, DMSO) δ 8.84 (d, $J = 1.6$ Hz, 1H), 7.46 (dd, $J = 8.2$, 1.6 Hz, 1H), 7.17 (d, $J = 8.3$ Hz, 1H), 5.27 (d, $J = 447.2$ Hz, 3H), 4.04 (s, 2H), 3.89 – 3.82 (m, 1H), 3.65 – 3.54 (m, 4H), 3.50 – 3.35 (m, 4H), 3.00 (dd, $J = 12.6$, 3.2 Hz, 1H), 2.89 (dd, $J = 12.5$, 9.3 Hz, 1H), 2.69

– 2.58 (m, 1H), 2.50 (s, 3H), 1.88 – 1.43 (m, 13H), 1.39 – 1.28 (m, 3H), 1.18 – 0.91 (m, 5H). ¹³C NMR (101 MHz, DMSO) δ 169.23, 168.09, 167.03, 165.27, 143.87, 135.26, 131.87, 130.28, 125.17, 119.21, 117.28, 110.01, 93.33, 80.17, 71.27, 70.31, 68.46, 63.35, 51.06, 45.97, 44.68, 35.88, 32.99, 32.29, 30.17, 28.85, 25.78, 25.36, 25.18, 24.41. HRMS (ESI+) *m/z* calcd for C₂₈H₃₁N₂O₅S [M+H]⁺: 507.1948, found: 507.1950. HRMS (ESI+) *m/z* calcd for C₇H₁₈NO₅ [M+H]⁺: 196.1179, found: 196.1184.

4.3 Crystallographic studies

Single crystals of compound **42** suitable for X-ray crystallographic analysis were obtained by slow recrystallization from DMSO solution of **42** in the fume hood at room temperature. Maroon single crystals of **42** were placed in dry and degassed polyisobutene oil and mounted on a fiber loop^[100] and used for X-ray diffraction analysis. Single crystal X-ray diffraction data were collected at 90.0 (2) K on a Bruker D8 Venture diffractometer with graded-multilayer focused Mo K_α X-rays. Raw data were integrated, scaled, merged and corrected for Lorentz-polarization effects using the APEX3 package.^[101] Corrections for absorption were applied using SADABS.^[102] The structure was solved by direct methods^[103] and refinement was carried out against F² by weighted full-matrix least-squares.^[104] Hydrogen atoms were found in difference maps, but subsequently placed at calculated positions and refined using a riding model. Non-hydrogen atoms were refined with anisotropic displacement parameters. Non-merohedric twinning was diagnosed with APEX3, but later handled by TwinRotMat in Platon^[105] as it gave a more complete dataset. Refinement progress was checked using Platon and by an *R*-tensor.^[106] The final model was further checked with the IUCr utility checkCIF. Atomic scattering factors were taken from the International Tables for Crystallography.^[107] Crystallographic data are collected in Table 1. All other details are included in the CIF, which is available free of charge from the CCDC, deposition code 1846371.

Table 4-1. Crystallographic data for compound **42**.

Compound	42
Moiety formula	C ₁₃ H ₈ N ₂ O ₅ S, C ₂ H ₆ OS

Sum formula	C ₁₅ H ₁₄ N ₂ O ₆ S ₂
Crystal size (mm)	382.03
Crystal system	Triclinic
Space group	P $\bar{1}$
<i>a</i> /Å	5.0022(10)
<i>b</i> /Å	11.119(4)
<i>c</i> /Å	14.996(5)
α /°	75.785(8)
β /°	86.220(8)
γ /°	85.097(8)
<i>Z</i>	2
<i>V</i> /Å ³	804.7(4)
<i>D</i> _{calcd} /g·cm ⁻³	1.578
<i>T</i> /K	90
<i>F</i> (000)	396
<i>h, k, l</i> _{max}	6, 14, 19
<i>R</i> (reflections)	0.0642
<i>wR</i> ₂ (reflections)	0.1790

4.4 *In vitro* experimental tests

4.4.1 Preparation of mPGES-1 enzymes

Cloning of mPGES-1 and the protein preparation were described in our previous reports.^[108] Briefly, FreeStyle Max Expression system was used to express wild-type human and mouse mPGES-1 enzymes separately. FreeStyle 293-F cells were cultured following manufacturer's manual in FreeStyle 293 expression medium on orbit rotate shaker in 8% CO₂ incubator at 37°C. Cells were transfected with 1.5 µg/mL of mPGES-1/pcDNA3 construct using FreeStyle Max reagent at a cell density of 1 × 10⁶ for 2 days. Transfected cells were collected, washed, and sonicated in TSES buffer (15 mM Tris-HCl, pH 8.0 plus 0.25 M sucrose, 0.1 mM EDTA and 1 mM DTT) on ice. The broken cells were first

centrifuged at $12,500 \times g$ for 10 min. The supernatant was further centrifuged at $105,000 \times g$ for 1 hr at 4°C . The pellet was washed and homogenized in PBS buffer. The crude microsomal mPGES-1 preparations were aliquoted and stored at -80°C before use.

4.4.2 Activity assays using a recombinant mPGES-1

The enzyme activity assays were performed according to our previous reports.^[76-77] Briefly, the mPGES-1-catalyzed reaction was carried out in 1.5 mL microfuge tubes with reaction mixture of 0.2 $\text{Na}_2\text{HPO}_4/\text{NaH}_2\text{PO}_4$, pH 7.2 (10 μL); 2.5 mM GSH (2.5 μL); diluted microsomal human or mouse mPGES-1 enzyme (80 $\mu\text{g}/\text{mL}$, 1 μL); inhibitor in DMSO solution (1 μL); 0.31 mM PGH_2 in DMF (5 μL) and distilled deionized water in a final volume of 100 μL . An inhibitor was incubated with enzyme for 15 min at ambient temperature followed by the addition of cold PGH_2 (stored in dry ice). The enzymatic reaction was initiated immediately upon adding PGH_2 . After 1 min of reaction, stop solution (40 mg/mL SnCl_2 in absolute ethanol, 10 μL) was added to cease the reaction by converting excess PGH_2 to $\text{PGF}_{2\alpha}$. The produced PGE_2 from the enzymatic reaction was quantified by the PGE_2 enzyme immunoassay.^[109]

4.4.3 Activity assays of COX-1/2

The inhibition of COX isoenzymes was determined by using COX (ovine/human) inhibitor screening assay kit purchased from Cayman Chemical Company (Ann Arbor, MI). We used a mixture of equal amount COX-1 and COX-2 instead of single enzyme and followed the recommended protocol.

4.5 *In vivo* experiments

4.5.1 Animals

Wild-type male CD-1 mice (28-35 g) were ordered from Harlan (Indianapolis, IN), and housed for a week prior to the experimental studies. All animals were allowed ad libitum access to food and water and maintained on a 12 h light/12 h dark cycle, with the lights on at 8:00 am at a room temperature of $21\text{--}22^{\circ}\text{C}$. Experiments were performed in a same

colony room in accordance with the Guide for the Care and Use of Laboratory Animals as adopted and promulgated by the National Institutes of Health. The animal protocol was approved by the IACUC (Institutional Animal Care and Use Committee) at the University of Kentucky.

4.5.2 Wild-type mice based air-pouch model of inflammation

Air-pouches (cavities) were produced by duplicate injections of 3 mL of sterile air under the skin on the backs of mice. Following the formation of the air-pouch, six days after the initial air injection, 1 mL of 1% (w/v) solution of λ -carrageenan dissolved in sterile saline was injected directly into the pouch to produce an inflammatory response. Then, the mice treated with the test compound, celecoxib, or vehicle administered orally. 24 hours later, the mice were sacrificed by carbon dioxide (compressed gas) inhalation until visible respiration has ceased, followed by thoracotomy, and the air-pouch fluid and other tissues (including kidney) were collected. The collected samples were analyzed for their PGE₂ concentrations by using the PGE₂ enzyme immunoassay.

Chapter 5 Concluding Remarks

5.1 Overall conclusion

Generally, a traditional typical drug discovery and development process is largely focused on identifying ligands of human enzyme targets. The species distinction is not specifically taken into consideration during the early stage of drug design and discovery. Actually, some ligands identified *in vitro* turn out to be inactive in the *in vivo* mouse/rat models.

Our study described in this thesis has demonstrated that it is a more effective strategy to rationally design a dual inhibitor of human and mouse target enzymes. We successfully designed and developed two series of compounds, substituted benzylidenebarbituric acid derivatives and (Z)-5-(2-oxoindolin-3-ylidene)thiazolidine-2,4-dione derivatives, as inhibitors potent against both human and mouse mPGES-1 enzymes. A number of these synthesized compounds were not only potent in *in vitro* assays, selective for mPGES-1 over COX isozymes, but also effective *in vivo* using wild-type mouse carrageenan air-pouch model. The results demonstrated that by focusing on the conserved region at the active site of both human and mouse enzymes, it is possible to design and discover dual inhibitors targeting enzymes in multiple species. The general strategy of our presented structure-based rational design of dual inhibitors of both human and mouse mPGES-1 enzymes might also be employed for other drug targets with species difference in the ligand-enzyme bindings.

5.2 Future directions

The results shown in Fig. 2-4 and Fig. 3-4 indicated the effectiveness of compounds **25b** and **52e** in reducing PGE₂ levels in both air-pouch fluid and kidney extract samples in mouse carrageenan air-pouch model. However, to further elucidate the *in vivo* activity and the pharmacological effects of these compounds, more animal experiments should be conducted. For the evaluation of anti-inflammatory effects, rat carrageenan-induced paw edema model and adjuvant arthritis model are frequently used. In addition, we may also evaluate the analgesic effects with these candidate compounds by performing carrageenan-

induced hyperalgesia experiment, formalin test, and acetic acid-induced writhing experiment.

Compounds **25b** and **52e** were identified as potent inhibitors against both human and mouse mPGES-1 enzymes, and these two compounds can be used as new leads for the design of inhibitors with the same scaffolds. In order to maintain the similar binding modes with human and mouse mPGES-1 enzymes, minor structural modification can be made on the original structures. We may pay particular attention in the improvement of aqueous solubility by introducing hydrophilic groups. In addition, virtual screening has emerged as a powerful approach widely employed in modern rational drug design. Using the recently disclosed human mPGES-1 structure and mouse mPGES-1 structure (derived by using human mPGES-1 crystal structure as a template), our group is able to screen compounds with a wide range of chemical scaffolds. Based on the binding modes, the identified hits with novel scaffolds are subjected to structural optimization *via* organic synthesis. The synthesized compounds are screened at single concentration (*i.e.* 10 μ M) and those caused significant inhibition ($\geq 70\%$) are further tested for their IC₅₀ values. As described in Chapters 2 and 3, the selectivity of mPGES-1 over COX isozymes will be also tested. Similarly, mouse carrageenan air-pouch model can be used as the initial investigation of the *in vivo* activity of the inhibitors.

References

- [1] C. D. Funk, *Science* **2001**, *294*, 1871-1875.
- [2] T. A. Samad, A. Sapirstein, C. J. Woolf, *Trends Mol. Med.* **2002**, *8*, 390-396.
- [3] D. Wang, R. N. Dubois, *Gut* **2006**, *55*, 115-122.
- [4] a) W. L. Smith, *Biochem. J* **1989**, *259*, 315-324; b) Y. Sugimoto, S. Narumiya, *J. Biol. Chem.* **2007**, *282*, 11613-11617.
- [5] J. K. Norberg, E. Sells, H. H. Chang, S. R. Alla, S. Zhang, E. J. Meuillet, *Pharm Pat Anal* **2013**, *2*, 265-288.
- [6] R. M. Garavito, D. L. DeWitt, *Biochim. Biophys. Acta* **1999**, *1441*, 278-287.
- [7] I. Kudo, M. Murakami, *J. Biochem. Mol. Biol.* **2005**, *38*, 633-638.
- [8] B. Samuelsson, R. Morgenstern, P. J. Jakobsson, *Pharmacol. Rev.* **2007**, *59*, 207-224.
- [9] a) Y. S. Bakhle, *Drugs Today (Barc)* **1999**, *35*, 237-250; b) C. J. Hawkey, *Best Pract. Res. Clin. Gastroenterol.* **2001**, *15*, 801-820.
- [10] K. D. Rainsford, *Subcell. Biochem.* **2007**, *42*, 3-27.
- [11] M. Murakami, Y. Nakatani, T. Tanioka, I. Kudo, *Prostaglandins Other Lipid Mediat.* **2002**, *68-69*, 383-399.
- [12] K. Scholich, G. Geisslinger, *Trends in pharmacological sciences* **2006**, *27*, 399-401.
- [13] F. Buttgerit, G. R. Burmester, L. S. Simon, *Am. J. Med.* **2001**, *110 Suppl 3A*, 13S-19S.
- [14] P. McGettigan, D. Henry, *JAMA* **2006**, *296*, 1633-1644.
- [15] I. Tegeder, G. Geisslinger, *Naunyn Schmiedebergs Arch. Pharmacol.* **2006**, *373*, 1-17.
- [16] D. P. Hajjar, K. B. Pomerantz, *FASEB J.* **1992**, *6*, 2933-2941.
- [17] A. Hamza, X. Zhao, M. Tong, H. H. Tai, C. G. Zhan, *Bioorg. Med. Chem.* **2011**, *19*, 6077-6086.
- [18] T. Tanioka, Y. Nakatani, N. Semmyo, M. Murakami, I. Kudo, *J. Biol. Chem.* **2000**, *275*, 32775-32782.
- [19] P. J. Jakobsson, S. Thoren, R. Morgenstern, B. Samuelsson, *Proc. Natl. Acad. Sci. U. S. A.* **1999**, *96*, 7220-7225.
- [20] C. E. Trebino, J. L. Stock, C. P. Gibbons, B. M. Naiman, T. S. Wachtmann, J. P. Umland, K. Pandher, J. M. Lapointe, S. Saha, M. L. Roach, D. Carter, N. A. Thomas, B. A. Durtschi, J. D. McNeish, J. E. Hambor, P. J. Jakobsson, T. J. Carty, J. R. Perez, L. P. Audoly, *Proc. Natl. Acad. Sci. U. S. A.* **2003**, *100*, 9044-9049.
- [21] M. Wang, A. M. Zukas, Y. Hui, E. Ricciotti, E. Pure, G. A. FitzGerald, *Proc. Natl. Acad. Sci. U. S. A.* **2006**, *103*, 14507-14512.
- [22] D. Engblom, S. Saha, L. Engstrom, M. Westman, L. P. Audoly, P. J. Jakobsson, A. Blomqvist, *Nat. Neurosci.* **2003**, *6*, 1137-1138.
- [23] Y. Kihara, T. Matsushita, Y. Kita, S. Uematsu, S. Akira, J. Kira, S. Ishii, T. Shimizu, *Proc. Natl. Acad. Sci. U. S. A.* **2009**, *106*, 21807-21812.
- [24] R. W. Friesen, J. A. Mancini, *J. Med. Chem.* **2008**, *51*, 4059-4067.
- [25] M. Westman, M. Korotkova, E. af Klint, A. Stark, L. P. Audoly, L. Klareskog, A. K. Ulfgren, P. J. Jakobsson, *Arthritis Rheum.* **2004**, *50*, 1774-1780.
- [26] M. Korotkova, S. B. Helmers, I. Loell, H. Alexanderson, C. Grundtman, C. Dorph, I. E. Lundberg, P. J. Jakobsson, *Ann. Rheum. Dis.* **2008**, *67*, 1596-1602.
- [27] F. Cipollone, M. Fazia, A. Iezzi, G. Ciabattini, B. Pini, C. Cuccurullo, S. Uchino,

- F. Spigonardo, M. De Luca, C. Prontera, F. Chiarelli, F. Cuccurullo, A. Mezzetti, *Arterioscler. Thromb. Vasc. Biol.* **2004**, *24*, 1259-1265.
- [28] K. Subbaramaiah, K. Yoshimatsu, E. Scherl, K. M. Das, K. D. Glazier, D. Golijanin, R. A. Soslow, T. Tanabe, H. Naraba, A. J. Dannenberg, *J. Biol. Chem.* **2004**, *279*, 12647-12658.
- [29] a) K. Gudis, A. Tatsuguchi, K. Wada, T. Hiratsuka, S. Futagami, Y. Fukuda, T. Kiyama, T. Tajiri, K. Miyake, C. Sakamoto, *Hum. Pathol.* **2007**, *38*, 1826-1835; b) T. Seo, A. Tatsuguchi, S. Shinji, M. Yonezawa, K. Mitsui, S. Tanaka, S. Fujimori, K. Gudis, Y. Fukuda, C. Sakamoto, *Virchows Arch.* **2009**, *454*, 667-676.
- [30] U. A. Chaudhry, H. Zhuang, B. J. Crain, S. Dore, *Alzheimers Dement* **2008**, *4*, 6-13.
- [31] C. Jegerschold, S. C. Pawelzik, P. Purhonen, P. Bhakat, K. R. Gheorghe, N. Gyobu, K. Mitsuoka, R. Morgenstern, P. J. Jakobsson, H. Hebert, *Proc. Natl. Acad. Sci. U. S. A.* **2008**, *105*, 11110-11115.
- [32] T. Sjogren, J. Nord, M. Ek, P. Johansson, G. Liu, S. Geschwindner, *Proc. Natl. Acad. Sci. U. S. A.* **2013**, *110*, 3806-3811.
- [33] D. Li, N. Howe, A. Dukkipati, S. T. Shah, B. D. Bax, C. Edge, A. Bridges, P. Hardwicke, O. M. Singh, G. Giblin, A. Pautsch, R. Pfau, G. Schnapp, M. Wang, V. Olieric, M. Caffrey, *Cryst. Growth Des.* **2014**, *14*, 2034-2047.
- [34] a) T. Yamada, J. Komoto, K. Watanabe, Y. Ohmiya, F. Takusagawa, *J. Mol. Biol.* **2005**, *348*, 1163-1176; b) T. Hammarberg, M. Hamberg, A. Wetterholm, H. Hansson, B. Samuelsson, J. Z. Haeggstrom, *J Biol Chem* **2009**, *284*, 301-305.
- [35] a) M. D. AbdulHameed, A. Hamza, J. Liu, X. Huang, C. G. Zhan, *J. Chem. Inf. Model.* **2008**, *48*, 179-185; b) A. Hamza, M. D. Abdulhameed, C. G. Zhan, *J. Phys. Chem. B* **2008**, *112*, 7320-7329; c) X. Huang, W. Yan, D. Gao, M. Tong, H. H. Tai, C. G. Zhan, *Bioorg. Med. Chem.* **2006**, *14*, 3553-3562.
- [36] O. Quraishi, J. A. Mancini, D. Riendeau, *Biochem. Pharmacol.* **2002**, *63*, 1183-1189.
- [37] D. Riendeau, R. Aspiotis, D. Ethier, Y. Gareau, E. L. Grimm, J. Guay, S. Guiral, H. Juteau, J. A. Mancini, N. Methot, J. Rubin, R. W. Friesen, *Bioorg. Med. Chem. Lett.* **2005**, *15*, 3352-3355.
- [38] B. Cote, L. Boulet, C. Brideau, D. Claveau, D. Ethier, R. Frenette, M. Gagnon, A. Giroux, J. Guay, S. Guiral, J. Mancini, E. Martins, F. Masse, N. Methot, D. Riendeau, J. Rubin, D. Xu, H. Yu, Y. Ducharme, R. W. Friesen, *Bioorg. Med. Chem. Lett.* **2007**, *17*, 6816-6820.
- [39] D. Xu, S. E. Rowland, P. Clark, A. Giroux, B. Cote, S. Guiral, M. Salem, Y. Ducharme, R. W. Friesen, N. Methot, J. Mancini, L. Audoly, D. Riendeau, *J. Pharmacol. Exp. Ther.* **2008**, *326*, 754-763.
- [40] A. Giroux, L. Boulet, C. Brideau, A. Chau, D. Claveau, B. Cote, D. Ethier, R. Frenette, M. Gagnon, J. Guay, S. Guiral, J. Mancini, E. Martins, F. Masse, N. Methot, D. Riendeau, J. Rubin, D. Xu, H. Yu, Y. Ducharme, R. W. Friesen, *Bioorg. Med. Chem. Lett.* **2009**, *19*, 5837-5841.
- [41] T. Y. Wu, H. Juteau, Y. Ducharme, R. W. Friesen, S. Guiral, L. Dufresne, H. Poirier, M. Salem, D. Riendeau, J. Mancini, C. Brideau, *Bioorg. Med. Chem. Lett.* **2010**, *20*, 6978-6982.
- [42] J. Wang, D. Limburg, J. Carter, G. Mbalaviele, J. Gierse, M. Vazquez, *Bioorg. Med.*

- Chem. Lett.* **2010**, *20*, 1604-1609.
- [43] D. P. Walker, G. B. Arhancet, H. F. Lu, S. E. Heasley, S. Metz, N. M. Kablaoui, F. M. Franco, C. E. Hanau, J. A. Scholten, J. R. Springer, Y. M. Fobian, J. S. Carter, L. Xing, S. Yang, A. F. Shaffer, G. M. Jerome, M. T. Baratta, W. M. Moore, M. L. Vazquez, *Bioorg. Med. Chem. Lett.* **2013**, *23*, 1120-1126.
- [44] M. Peters-Golden, W. R. Henderson, Jr., *N. Engl. J. Med.* **2007**, *357*, 1841-1854.
- [45] a) O. Radmark, B. Samuelsson, *J. Intern. Med.* **2010**, *268*, 5-14; b) D. Wang, R. N. Dubois, *Nat. Rev. Cancer* **2010**, *10*, 181-193.
- [46] A. Koeberle, E. M. Haberl, A. Rossi, C. Pergola, F. Dehm, H. Northoff, R. Troschuetz, L. Sautebin, O. Werz, *Bioorg. Med. Chem.* **2009**, *17*, 7924-7932.
- [47] M. G. Chini, R. De Simone, I. Bruno, R. Riccio, F. Dehm, C. Weinigel, D. Barz, O. Werz, G. Bifulco, *Eur. J. Med. Chem.* **2012**, *54*, 311-323.
- [48] M. Elkady, R. Niess, A. M. Schaible, J. Bauer, S. Luderer, G. Ambrosi, O. Werz, S. A. Laufer, *J. Med. Chem.* **2012**, *55*, 8958-8962.
- [49] S. He, C. Li, Y. Liu, L. Lai, *J. Med. Chem.* **2013**, *56*, 3296-3309.
- [50] A. Bruno, L. Di Francesco, I. Coletta, G. Mangano, M. A. Alisi, L. Polenzani, C. Milanese, P. Anzellotti, E. Ricciotti, M. Dovizio, A. Di Francesco, S. Tacconelli, M. L. Capone, P. Patrignani, *Biochem. Pharmacol.* **2010**, *79*, 974-981.
- [51] a) T. Shiro, K. Kakiguchi, H. Takahashi, H. Nagata, M. Tobe, *Bioorg. Med. Chem.* **2013**, *21*, 2068-2078; b) T. Shiro, H. Takahashi, K. Kakiguchi, Y. Inoue, K. Masuda, H. Nagata, M. Tobe, *Bioorg. Med. Chem. Lett.* **2012**, *22*, 285-288.
- [52] S. Terracciano, G. Lauro, M. Strocchia, K. Fischer, O. Werz, R. Riccio, I. Bruno, G. Bifulco, *ACS Med. Chem. Lett.* **2015**, *6*, 187-191.
- [53] P. Leclerc, S. C. Pawelzik, H. Idborg, L. Spahiu, C. Larsson, P. Stenberg, M. Korotkova, P. J. Jakobsson, *Prostaglandins Other Lipid Mediat.* **2013**, *102-103*, 1-12.
- [54] A. Koeberle, H. Northoff, O. Werz, *Mol. Cancer Ther.* **2009**, *8*, 2348-2355.
- [55] A. Koeberle, F. Pollastro, H. Northoff, O. Werz, *Br. J. Pharmacol.* **2009**, *156*, 952-961.
- [56] A. Koeberle, A. Rossi, J. Bauer, F. Dehm, L. Verotta, H. Northoff, L. Sautebin, O. Werz, *Front. Pharmacol.* **2011**, *2*, 7.
- [57] A. Koeberle, H. Northoff, O. Werz, *Biochem. Pharmacol.* **2009**, *77*, 1513-1521.
- [58] J. Bauer, A. Koeberle, F. Dehm, F. Pollastro, G. Appendino, H. Northoff, A. Rossi, L. Sautebin, O. Werz, *Biochem. Pharmacol.* **2011**, *81*, 259-268.
- [59] a) T. Hanke, F. Dehm, S. Liening, S. D. Popella, J. Maczewsky, M. Pillong, J. Kunze, C. Weinigel, D. Barz, A. Kaiser, M. Wurglics, M. Lammerhofer, G. Schneider, L. Sautebin, M. Schubert-Zsilavec, O. Werz, *J. Med. Chem.* **2013**, *56*, 9031-9044; b) M. Hieke, C. Greiner, M. Dittrich, F. Reisen, G. Schneider, M. Schubert-Zsilavec, O. Werz, *J. Med. Chem.* **2011**, *54*, 4490-4507; c) K. Lee, V. C. Pham, M. J. Choi, K. J. Kim, K. T. Lee, S. G. Han, Y. G. Yu, J. Y. Lee, *Bioorg. Med. Chem. Lett.* **2013**, *23*, 75-80; d) A. J. Liedtke, P. R. Keck, F. Lehmann, A. Koeberle, O. Werz, S. A. Laufer, *J. Med. Chem.* **2009**, *52*, 4968-4972; e) M. A. Schiffler, S. Antonysamy, S. N. Bhattachar, K. M. Campanale, S. Chandrasekhar, B. Condon, P. V. Desai, M. J. Fisher, C. Groshong, A. Harvey, M. J. Hickey, N. E. Hughes, S. A. Jones, E. J. Kim, S. L. Kuklish, J. G. Luz, B. H. Norman, R. E. Rathmell, J. R. Rizzo, T. W. Seng, S. J. Thibodeaux, T. A. Woods, J. S. York, X. P. Yu, *J. Med. Chem.* **2016**, *59*, 194-205;

- f) E. Shang, Y. Wu, P. Liu, Y. Liu, W. Zhu, X. Deng, C. He, S. He, C. Li, L. Lai, *Bioorg. Med. Chem. Lett.* **2014**, *24*, 2764-2767; g) T. Shiro, K. Kakiguchi, H. Takahashi, H. Nagata, M. Tobe, *Bioorg. Med. Chem.* **2013**, *21*, 2868-2878; h) A. Wiegard, W. Hanekamp, K. Griessbach, J. Fabian, M. Lehr, *Eur. J. Med. Chem.* **2012**, *48*, 153-163.
- [60] Y. Jin, C. L. Smith, L. Hu, K. M. Campanale, R. Stoltz, L. G. Huffman, Jr., T. A. McNearney, X. Y. Yang, B. L. Ackermann, R. Dean, A. Regev, W. Landschulz, *Clin. Pharmacol. Ther.* **2016**, *99*, 274-284.
- [61] C. N. Serhan, B. Levy, *Proc. Natl. Acad. Sci. U. S. A.* **2003**, *100*, 8609-8611.
- [62] a) O. Radmark, B. Samuelsson, *J. Intern. Med.* **2010**, *268*, 5-14; b) H. Hanaka, S.-C. Pawelzik, J. I. Johnsen, M. Rakonjac, K. Terawaki, A. Rasmuson, B. Sveinbjornsson, M. C. Schumacher, M. Hamberg, B. Samuelsson, P.-J. Jakobsson, P. Kogner, O. Rådmark, *Proc. Natl. Acad. Sci. USA* **2009**, *106*, 18757-18762; c) A. Koeberle, O. Werz, *Biochem. Pharmacol.* **2015**, *98*, 1-15.
- [63] I. Kudo, M. Murakami, *J. Biochem. Mol. Biol.* **2005**, *38*, 633-638.
- [64] H. Fahmi, *Curr. Opin. Rheumatol.* **2004**, *16*, 623-627.
- [65] Y. Cheng, M. Wang, Y. Yu, J. Lawson, C. D. Funk, G. A. FitzGerald, *Journal of Clinical Investigation* **2006**, *116*, 1391-1399.
- [66] a) D. Engblom, S. Saha, L. Engstrom, M. Westman, L. P. Audoly, P. J. Jakobsson, A. Blomqvist, *Nat. Neurosci.* **2003**, *6*, 1137-1138; b) C. E. Trebino, J. L. Stock, C. P. Gibbons, B. M. Naiman, T. S. Wachtmann, J. P. Umland, K. Pandher, J. M. Lapointe, S. Saha, M. L. Roach, D. Carter, N. A. Thomas, B. A. Durtschi, J. D. McNeish, J. E. Hambor, P. J. Jakobsson, T. J. Carty, J. R. Perez, L. P. Audoly, *Proceedings of the National Academy of Sciences of the United States of America* **2003**, *100*, 9044-9049.
- [67] a) H. Sandler, J. Kreth, H. T. Timmers, G. Stoecklin, *Nucleic Acids Res.* **2011**, *39*, 4373-4386; b) F. P. Marchese, A. Aubareda, C. Tudor, J. Saklatvala, A. R. Clark, J. L. Dean, *J. Biol. Chem.* **2010**, *285*, 27590-27600.
- [68] F. Bollig, R. Winzen, M. Gaestel, S. Kostka, K. Resch, H. Holtmann, *Biochem. Biophys. Res. Commun.* **2003**, *301*, 665-670.
- [69] M. Murakami, K. Nakashima, D. Kamei, S. Masuda, Y. Ishikawa, T. Ishii, Y. Ohmiya, K. Watanabe, I. Kudo, *J. Biol. Chem.* **2003**, *278*, 37937-37947.
- [70] a) Y. Ikeda-Matsuo, A. Ota, T. Fukada, S. Uematsu, S. Akira, Y. Sasaki, *Proc. Natl. Acad. Sci. U. S. A.* **2006**, *103*, 11790-11795; b) R. W. Friesen, J. A. Mancini, *J. Med. Chem.* **2008**, *51*, 4059-4067.
- [71] D. Xu, S. E. Rowland, P. Clark, A. Giroux, B. Cote, S. Guiral, M. Salem, Y. Ducharme, R. W. Friesen, N. Methot, J. Mancini, L. Audoly, D. Riendeau, *The Journal of pharmacology and experimental therapeutics* **2008**, *326*, 754-763.
- [72] A. Hamza, X. Zhao, M. Tong, H.-H. Tai, C.-G. Zhan, *Bioorg. Med. Chem.* **2011**, *19*, 6077-6086.
- [73] G. A. FitzGerald, C. Patrono, *N. Engl. J. Med.* **2001**, *345*, 433-442.
- [74] Y. Cheng, M. Wang, Y. Yu, J. Lawson, C. D. Funk, G. A. Fitzgerald, *J. Clin. Invest.* **2006**, *116*, 1391-1399.
- [75] a) K. Ding, Z. Zhou, S. Hou, Y. Yuan, S. Zhou, X. Zheng, J. Chen, C. Loftin, F. Zheng, C. G. Zhan, *Sci. Rep.* **2018**, *8*, 5205; b) K. Ding, Z. Zhou, S. Zhou, Y. Yuan, K. Kim, T. Zhang, X. Zheng, F. Zheng, C.-G. Zhan, *Bioorg. Med. Chem. Letters*

- [76] a) P. Limpachayaporn, M. Schafers, O. Schober, K. Kopka, G. Haufe, *Bioorg. Med. Chem.* **2013**, *21*, 2025-2036; b) C. Wu, C. Du, J. Gubbens, Y. H. Choi, G. P. van Wezel, *J. Nat. Prod.* **2015**, *78*, 2355-2363; c) P. Limpachayaporn, S. Wagner, K. Kopka, O. Schober, M. Schafers, G. Haufe, *J. Med. Chem.* **2014**, *57*, 9383-9395; d) M. D. Hall, K. R. Brimacombe, M. S. Varonka, K. M. Pluchino, J. K. Monda, J. Li, M. J. Walsh, M. B. Boxer, T. H. Warren, H. M. Fales, M. M. Gottesman, *J. Med. Chem.* **2011**, *54*, 5878-5889; e) B. Yu, S. Q. Wang, P. P. Qi, D. X. Yang, K. Tang, H. M. Liu, *Eur. J. Med. Chem.* **2016**, *124*, 350-360.
- [77] C.-P. Lo, E. Shropshire, *The Journal of Organic Chemistry* **1957**, *22*, 999-1001.
- [78] R. Murugan, S. Anbazhagan, Lingeshwaran, S. Sriman Narayanan, *Eur. J. Med. Chem.* **2009**, *44*, 3272-3279.
- [79] M. O. Shibinskaya, S. A. Lyakhov, A. V. Mazepa, S. A. Andronati, A. V. Turov, N. M. Zholobak, N. Y. Spivak, *Eur. J. Med. Chem.* **2010**, *45*, 1237-1243.
- [80] D. Chaturvedi, S. Ray, A. K. Srivastava, R. Chander, *Bioorg. Med. Chem.* **2008**, *16*, 2489-2498.
- [81] N. Sin, B. L. Venables, K. D. Combrink, H. B. Gulgeze, K. L. Yu, R. L. Civiello, J. Thuring, X. A. Wang, Z. Yang, L. Zadjura, A. Marino, K. F. Kadow, C. W. Cianci, J. Clarke, E. V. Genovesi, I. Medina, L. Lamb, M. Krystal, N. A. Meanwell, *Bioorg. Med. Chem. Lett.* **2009**, *19*, 4857-4862.
- [82] P. P. Kattimani, R. R. Kamble, M. Y. Kariduraganavar, A. Dorababu, R. K. Hunnur, *Eur. J. Med. Chem.* **2013**, *62*, 232-240.
- [83] H. Singh, J. V. Singh, M. K. Gupta, A. K. Saxena, S. Sharma, K. Nepali, P. M. S. Bedi, *Bioorg. Med. Chem. Lett.* **2017**, *27*, 3974-3979.
- [84] a) N. Kaila, K. Janz, A. Huang, A. Moretto, S. DeBernardo, P. W. Bedard, S. Tam, V. Clerin, J. C. Keith, Jr., D. H. Tsao, N. Sushkova, G. D. Shaw, R. T. Camphausen, R. G. Schaub, Q. Wang, *J. Med. Chem.* **2007**, *50*, 40-64; b) Y. Yamamoto, M. Yohda, T. Shirai, H. Ito, N. Miyaura, *Chem. Asian J.* **2012**, *7*, 2446-2449.
- [85] a) B. R. Ambler, S. Peddi, R. A. Altman, *Org. Lett.* **2015**, *17*, 2506-2509; b) B. Xu, J. A. Gartman, U. K. Tambar, *Tetrahedron* **2017**, *73*, 4150-4159.
- [86] a) A. Hamza, M. Tong, M. D. AbdulHameed, J. Liu, A. C. Goren, H. H. Tai, C. G. Zhan, *J Phys Chem B.* **2010**, *114*, 5605-5616; b) Z. Zhou, Y. Yuan, S. Zhou, K. Ding, F. Zheng, C.-G. Zhan, *Biorg. Med. Chem. Letters* **2017**, *27*, 3739-3743.
- [87] O. Trott, A. J. Olson, *J. Comput. Chem.* **2010**, *31*, 455-461.
- [88] M. Ohno, Y. Tanaka, M. Miyamoto, T. Takeda, K. Hoshi, N. Yamada, A. Ohtake, *Bioorg. Med. Chem.* **2006**, *14*, 2005-2021.
- [89] D. B. Duarte, M. R. Vasko, J. C. Fehrenbacher, *Curr. Protoc. Pharmacol.* **2012**, Chapter 5, Unit5 6.
- [90]
- [91] a) U. Consortium, *Nucleic Acids Res.* **2008**, *36*, D190-D195; b) C. UniProt, *Nucleic Acids Res.* **2008**, *36*, D190-195.
- [92] a) A. Sali, L. Potterton, F. Yuan, H. van Vlijmen, M. Karplus, *Proteins* **1995**, *23*, 318-326; b) A. Nayeem, D. Sitkoff, S. Krystek, Jr., *Protein Sci.* **2006**, *15*, 808-824.
- [93] D. Studio, *Accelrys Inc.: San Diego, CA, USA* **2009**.
- [94] M. y. Shen, A. Sali, *Protein Sci.* **2006**, *15*, 2507-2524.

- [95] G. M. Morris, R. Huey, W. Lindstrom, M. F. Sanner, R. K. Belew, D. S. Goodsell, A. J. Olson, *J. Comput. Chem.* **2009**, *30*, 2785-2791.
- [96] A. A. Nagle, S. A. Reddy, H. Bertrand, H. Tajima, T. M. Dang, S. C. Wong, J. D. Hayes, G. Wells, E. H. Chew, *ChemMedChem* **2014**, *9*, 1763-1774.
- [97] S. Parkin, H. Hope, *J. Appl. Crystallogr.* **1998**, *31*, 945-953.
- [98] Bruker-AXS (2016). APEX3 Bruker-AXS Inc., Madison, WI, USA.
- [99] L. Krause, R. Herbst-Irmer, G. M. Sheldrick, D. Stalke, *J. Appl. Crystallogr.* **2015**, *48*, 3-10.
- [100] G. Sheldrick, *Acta Crystallographica Section A* **2015**, *71*, 3-8.
- [101] G. M. Sheldrick, *Acta Crystallographica. Section C, Structural Chemistry* **2015**, *71*, 3-8.
- [102] A. Spek, *Acta Crystallographica Section D* **2009**, *65*, 148-155.
- [103] S. Parkin, *Acta Crystallographica Section A* **2000**, *56*, 157-162.
- [104] Wilson, A. J. and Geist, V. (1993), *International Tables for Crystallography. Volume C: Mathematical, Physical and Chemical Tables*. Kluwer Academic Publishers, Dordrecht/Boston/London 1992
- [105] A. Hamza, M. Tong, M. D. AbdulHameed, J. Liu, A. C. Goren, H. H. Tai, C. G. Zhan, *J. Phys. Chem. B* **2010**, *114*, 5605-5616.
- [106] L. Harding, Z. Wang, H. H. Tai, *Biochim. Biophys. Acta* **1996**, *1310*, 48-52.

Vita

Personal Information

Name	Kai Ding
Place of Birth	China
Nationality	China

Education

Degree	Year	University	Major
PhD	2018 (expected)	University of Kentucky	Chemistry
MS	2009	Zhejiang University of Technology	Medicinal Chemistry
BE	2006	Zhejiang University of Technology	Pharmaceutical Engineering

Research/Work Experience

Time	Job Title	Research/Work Experience
16-18	Research Assistant	Development of a long-acting cocaine hydrolase for addiction therapy
13-18		Design, synthesis and evaluation of mPGES-1 inhibitors
14-16	Teaching Assistant	Organic chemistry lab: teaching, troubleshooting & grading
12-14	Assistant	General chemistry lab: teaching, office hours & grading
10-12	Lecturer	Zhejiang New Century College of Economy & Trade
09-10	Foreign Trader	Zhejiang Medicines and Health Products Imp & Exp Co., Ltd
06-09	MS Student	Metal triflate and functionalized ionic liquid catalysis
		Sucralose synthesis using BTC as chlorinating reagent

Professional Publications

- (1) **Ding, K.***; Zhou, Z.*; Hou, S.; Yuan, Y.; Zhou, S.; Zheng, X.; Chen, J.; Loftin, C.; Zheng, F.; Zhan, C. G. Structure-based discovery of mPGES-1 inhibitors suitable for preclinical testing in wild-type mice as a new generation of anti-inflammatory drugs. *Sci. Rep.* **2018**, 8 (1), 5205.
- (2) **Ding, K.***; Zhou, Z.*; Zhou, S.*; Yuan, Y.; Kim, K.; Zhang, T.; Zheng, X.; Zheng, F.; Zhan, C. G. Design, synthesis, and discovery of 5-((1,3-diphenyl-1*H*-pyrazol-4-yl)methylene)pyrimidine-2,4,6-(1*H*,3*H*,5*H*)-triones and related derivatives as novel

inhibitors of mPGES-1. *Bioorg. Med. Chem. Lett.* **2018**, 28 (5), 858.

- (3) Zhou, Z.; Yuan, Y.; Zhou, S.; **Ding, K.**; Zheng, F.; Zhan, C. G. Selective inhibitors of human mPGES-1 from structure-based computational screening. *Bioorg. Med. Chem. Lett.* **2017**, 27 (16), 3739.
- (4) Chen, X.; Zheng, X.; **Ding, K.**; Zhou, Z.; Zhan, C. G.; Zheng, F. A quantitative LC-MS/MS method for simultaneous determination of cocaine and its metabolites in whole blood. *J. Pharm. Biomed. Anal.* **2017**, 134, 243.
- (5) Chen, Z.; **Ding, K.**; Su, W. Basic Ionic Liquid as Catalyst for the Efficient and Green Synthesis of 2-Amino-3-nitrobenzonitriles in Ethanol. *Synth. Commun.* **2011**, 41 (10), 1410.
- (6) Su, W.; **Ding, K.**; Chen, Z. Cu(OTf)₂/Et₃N-promoted cyclocondensation of activated α -methylene alkenes and nitroolefins: a novel one-pot synthesis of polysubstituted benzenes. *Tetrahedron Lett.* **2009**, 50 (6), 636.